Master Thesis

TVVR20/5014

Long-term morphological evolution of Cua Lo inlet, Central Vietnam

A process-based, numerical approach

Nikita Tegenfeldt
Orio Johansson

Division of Water Resources Engineering

Department of Building and Environmental Technology

Lund University

Long-term morphological evolution of Cua Lo inlet, Central Vietnam

A process-based, numerical approach

By:
Nikita Tegenfeldt
Orio Johansson

Master Thesis

Division of Water Resources Engineering
Department of Building & Environmental Technology
Lund University
Box 118
221 00 Lund, Sweden

Water Resources Engineering
TVVR-20/5014
ISSN 1101-9824

Lund 2020
www.tvrl.lth.se

Master Thesis
Division of Water Resources Engineering
Department of Building & Environmental Technology
Lund University

English title:	< Long-term morphological evolution of Cua Lo inlet, Central Vietnam>
Swedish title:	<Långsiktig morfologisk utveckling av Cua Lo mynning i centrala Vietnam>
Author(s):	<Nikita Tegenfeldt> <Orio Johansson>
Supervisor:	<Magnus Larson>
Examiner:	<Hans Hanson>
Language	<English>
Year:	2020
Keywords:	<Inlet morphology; Sand spit; Water exchange; Numerical modelling; Cua Lo river mouth; Sediment transport>

Acknowledgements

Many people have contributed to the completion of this Master´s thesis. Professor Nguyen Trung Viet, Doctor Dinh Nath Quang, PhD student Nguyen Quang Duc Anh, and the rest of the research team at Thuyloi University in Vietnam welcomed us with open arms at arrival, integrated us into the research team, presented relevant previous research performed in the area, and provided us with necessary data. Much appreciation for their availability and for always being only one wave away. Special thanks to PhD student Dien Duong for performing essential ocean water level simulations, keeping us from being swept away by the tides. Also, thanks to Doctor Dinh Nhat Quang for performing MIKE simulations. Without them we would be drowned in the flood. We would also like to thank Professor Ho Sy Tam, Professor Nguyen Trung Viet, and Dr Quang for taking us on culinary trips and for their endless hospitality, making our stay in Hanoi memorable.

Extraordinary gratitude to Professor Magnus Larson for his engagement, faith in our abilities, and his availability. He kept our heads above the water at all times. PhD student Almir Nunes have also been available for discussions and advices. Finally, we would also like to thank Professor Hans Hanson for offering his time and is knowledge on the topic to finalize the project.

The project, which was performed as a Minor Field Study, MFS, was founded by the Swedish International Development Cooperation Agency, SIDA. Without this support, the study would not have been possible to perform. Thank you for giving us this opportunity.

Local field-site data used in this project was collected by the research team at Thuyloi University with support from a bilateral program between Vietnam and Japan (code: HNQT/SPĐP/16.19) and partly by a Research Environment Links grant, ID 527612186, under the Newton Programme Vietnam partnership. The grant is funded by the UK Department of Business, Energy and Industrial Strategy (BEIS) and delivered by the British Council. For further information, visit www.newtonfund.ac.uk. The authors would like to express their gratitude for this support.

Abstract

Cua Lo river mouth is a coastal inlet connected to an estuary at the central coast of Vietnam. The area is valuable for maritime trade, fishing industries, and tourism development. Natural disasters during the monsoon period are a problem, causing seasonal flooding. In connection to the inlet lies an elongating sand spit which causes erosion and destruction of residential areas on one side of the inlet. The objective was therefore to investigate the dynamics of the sand spit and the inlet, and to describe their long-term morphological development using a fast and simple, yet accurate model. Modelling was done using a process-based numerical approach, where both inlet migration and changes in inlet width were considered. The model base compared the longshore and inlet sediment transport, and exhibited satisfactory performance. A seasonal pattern related to the dry- and monsoon season was observed for the longshore sediment transport. Longshore transport was much larger compared to the inlet transport during the monsoon period. The sediment transport in the inlet had a clear connection to tidal variation. Two scenarios were considered for predicting inlet migration and width evolution. Migration and width evolution were modelled separately due to model limitations, over the period 2020-2049. Scenario 2 allowed for 2000 m migration, with the endpoint being a hard rock boundary. The boundary was not reached during the modelled period as the migration was only 1350 m. Scenario 1 allowed for 980 m of migration before the inlet reached the boundary limited either by longshore sediment transport changes, or a rock boundary. By 2041 the inlet was estimated to reach the boundary if the LST remained unchanged. A very narrow (4-20 m) equilibrium state took place rapidly after the width model was initiated, pointing towards seasonal or permanent closure. A sensitivity analysis on the LST and its effect on the morphological evolution suggested that the inlet could stop migrating before the 980 m boundary and that the inlet width could reach a dynamical equilibrium at that point. Actions are needed if the properties in the migration path are to be kept safe.

Table of contents

1. Introduction

1.1 Background

Out of the vast stretches of land in connection to water bodies, the places where rivers meet oceans are perhaps most attractive for human development and settlement. The intersection is often characterized by an inlet, a connecting water body such as an estuary, and associated rivers. Inlets act as hubs for both national and international maritime trade, as well as centres for fishing industries and societies. Rivers provide freshwater to the cities, industries, and agriculture, boosting economic growth and development. Coasts serve as recreational areas for local citizens and are important for tourism development giving an, often significant, economical contribution to the area (Pernetta and Milliman, 1995; Turner et al., 1996).

Although popular for permanent settlements, the river-ocean intersection can be a highly variable and dynamic system that can take on several forms. From straight, deep inlets that are subject only to small changes even over longer time periods, to vast lagoons and river deltas that undergo changes on a both seasonal and long-term basis. It is indeed a complex system governed by processes that might be seemingly simple, but of which many are hard to predict and describe. In general, over longer time scales, the main contributing factors for the dynamics are variations in river flows, and ocean waves and currents, which in turn depend on climatological changes and variations (Van de Kreeke, 2017).

A characteristic of an inlet is that it interrupts the coastline, and thus also the flow of sand along the coast. It not only interrupts but also captures some sand, which can cause erosion of the beach. As a result of sand accumulation, one feature commonly found in connection to inlets that are associated to lagoons or rivers are sand spits. These are long sand formations, that often elongate and shorten at inlet entrances (Schwartz, 1972). For long, they have been known to contribute to morphological changes in inlets and affect water exchange characteristics of upstream water bodies. In a natural state these changes do not generally have a negative effect on the surrounding environment, but when anthropogenic structures come into play the situation becomes different.

Only about 16% of the land area in Vietnam is coastal area, but it harbours more than 18 million of the roughly 100 million inhabitants. 23% of these are

living in urban areas. The majority of the population in the coastal areas are still employed within the primary sector, working with agri- and aquaculture, and fishing (Tung, 2011). However, Vietnam has over the recent decades experienced, and still is experiencing, a fast-socio-economic development, with annual growth rates on up to 10% per year (Tang et al., 2016). This applies especially to the central coastal areas, which are less developed compared to the Northern and Southern parts of Vietnam (Nauditt and Ribbe, 2017). Accompanying the rise in economy, a shift is seen towards the secondary (industry and construction) and tertiary (service) sectors, together with urbanization. Tourism is also increasing in the area. The well-known cuisine, pristine white sandy beaches, predictable weather, and excellent conditions for water sports draw international attention from both Asia and the rest of the world. Many of the coastal cities are growing, and some villages are experiencing a tourist surge with a following establishment of coastal tourist resorts (Nauditt and Ribbe, 2017).

The Cua Lo area in the Quang Nam province, central Vietnam (Figure 1, right), is one of the areas experiencing socio-economic growth. Together with the economic expansion, an increasing pressure on maintaining development of infrastructure and industrial areas is seen. The ability to meet the pressure is complicated by natural disasters affecting the area-associated coastal lagoon and coastal plains.

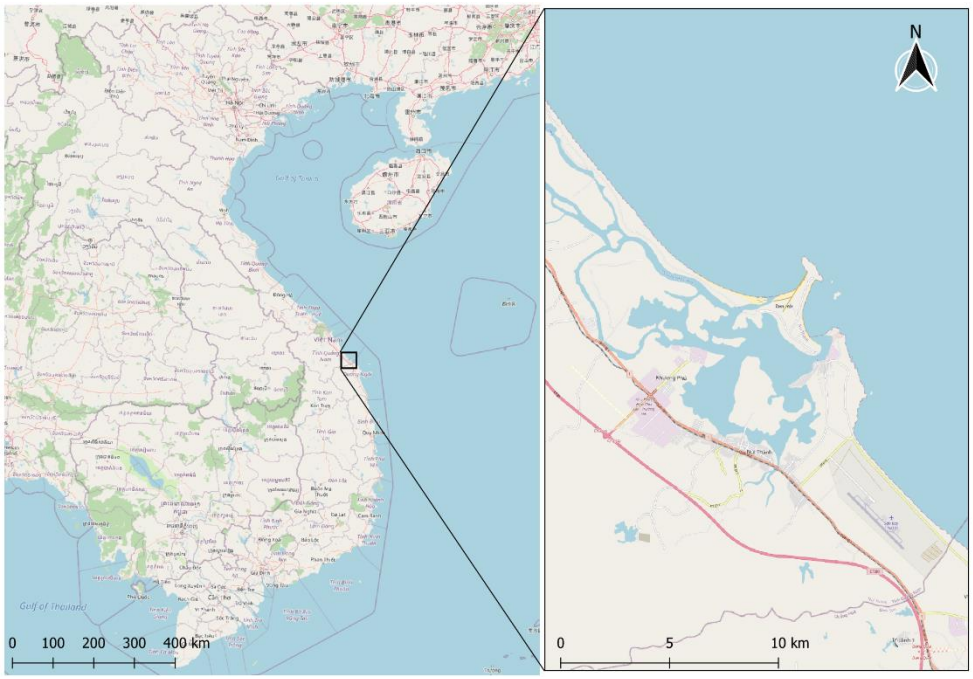

Figure 1. Map of Vietnam (left side), and the Cua Lo area (right side) (OpenStreetMap QGIS, 2019).

Every year Typhoons pass through, causing rough ocean conditions and releasing large amounts of rain over the catchment, flooding the rivers and lowlands. Discharge of the flood volumes is mostly restricted through the inlets in the estuary due to the low-lying nature of Cua Lo. Sediment accumulation in and around the inlets can restrict water exchange to the ocean, increasing flood risk. The decreased water exchange can also lead to negative effects on the water quality in the upstream water bodies due to extended residence times in the estuary. Sediment accumulation in the inlet can also hinder maritime transport and local fishermen from passing through.

Even if the inlet remains open, issues can arise. Erosion due to inlet migration is perhaps one of the largest concerns. On the northern side of the inlet, sand spit development is causing erosion on the downdrift side of the spit elongation, inflicting damage on existing infrastructure such as fishponds and houses. Inlet migration and development thus complicates flood protection and management, as well as infrastructure development plans. (Nauditt and Ribbe, 2017; Tung, 2011).

A few studies regarding the morphological changes of the Cua Lo inlet have been published. Duy et al. (2018) conducted a satellite image analysis of the Cua Lo inlet with images dating from 1973 to 2017. Inlet width, as well as right and left inlet bank evolution was analyzed graphically. It was concluded in their analysis that the sand spit elongation will eventually close the inlet, directing the flow towards the second (southeastern) lagoon inlet. A similar conclusion was made by Nguyen et al. (2018 (a)) after making simulations of short term (75 days) morphological changes in the inlet using Delft 3D simulations, an open source modeling software. Their results showed a tendency of flow divergence towards an alternative water course through the lagoon over time. Both studies also suggest that the inlet migration will continue until the inlet reaches the rocky boundary of An Hoa Cape. However, to the best of the authors' knowledge, the future long-term morphological development of the Cua Lo inlet has not been investigated through any modeling. Neither has a time scale been proposed for when closure could occur, or the inlet reaches the rocky boundary of An Hoa Cape.

The two main scientific tools for studying inlet processes and morphology are process-based models (Van de Kreeke, 1996; Ranasinghe et al., 1999; Stive and Wang, 2003), and empirical models (Jarrett, 1976; Hughes, 2002). Empirical models rely on the assumption that the system will always move towards a dynamical equilibrium state after a perturbation of the system. The dynamical equilibrium state is characterized by empirical relationships between the size of the different parts of the system, and the flow through it during a tidal cycle. After perturbation, the shift towards equilibrium is described by empirical equations. These models have been proven to be of use for characterizing the long-term equilibrium area and position of inlets, but they may not be adequate to account for changes in the input parameters such as sea level, wave climate, and river flow (van de Wegen et al., 2010).

The basis for process-based simulation models is simple physics which can describe the behaviour of natural systems, or if complex, in at least a schematized way. In order to solve the process-based model, a numerical approach is often required. Although the result is realistic if the model is well-calibrated, it is often not sufficient to outline the interactions giving rise to the end result (Murray, 2003). Another drawback of this kind of modelling is that some important physical processes are disregarded or, if included, developed to a level of complexity that requires several large input data series. Vast input data requires a larger computational effort and limits the time and thus also the ability to run many scenarios or to combine models (Nunes et al., 2020).

Another aspect is that such quantities are seldom available in developing countries, where economy and priorities have set restrictions on data collection (Van de Kreeke, 1996; Cayocca, 2001).

1.2 Objectives

The objective of the project is to investigate the morphological dynamics of the sand spit and the Cua Lo inlet in the central parts of Vietnam and describe its long-term development, the subsequent effects from inlet-associated erosion and possible water exchange effects in the connecting estuary. A numerical modeling approach will be employed, where both inlet migration and changes in inlet width are considered. Modeling theory and derivations will largely be based on the work of previous studies and well-known equations governing the hydrodynamics. As available data might be scarce or hard to obtain the governing equations will be kept rather simple in terms of input data requirements. This is motivated since it has been concluded that for smaller projects, simplified models can still be sufficient to describe the governing processes of inlet morphodynamics and provide a robust result (Kraus, 2010; Larson et al., 2020; Nunes et al., 2020). In addition, by using a rather simple numerical approach to model water exchange, sediment transport and morphological changes, computational process times can be kept at a lower level (Larson et al., 2020).

Model results could be used for further research topics or as guidance for infrastructure development and flood management plans at the field site. Although there are indications of how the system will behave in the future in the mentioned studies, the present model will add further certainties with regards to the time aspect of the evolution. Finally, it will also motivate why long-term simulations can be of particular interest in planning decisions (Dissanayake et al., 2009; Yin et al., 2019).

In order to fulfill the objectives of the project, the following tasks are performed:

- Formulation of a water exchange model for the coastal lagoon connected to the inlet. The model should only use ocean water levels as input parameter and be capable of describing the water levels in the lagoon.

- Calculation of the general offshore wave climate and consequently the nearshore longshore sediment transport in the area. Historical offshore wave data will be used as input.

- Construction of a morphological model capable of simulating realistic predictions of the inlet migration over a decadal perspective based on the longshore sediment transport and the inlet sediment transport. Computational efforts are to be kept low.

- Construction of a morphological model capable of simulating the inlet width variation once the inlet reaches a boundary position. This model should use the same input data as the "migration model".

- Calibration and validation of the models towards collected data and previously conducted research.

Over a decadal perspective, climate change could affect the outcome of the model results. It has been described that a rise in water levels can affect the dynamics of a lagoon system. In addition, changes in climatological events such as storms can also affect the inlet evolution. These aspects were however excluded in the study. Their effect could be incorporated into future similar studies in order to increase the accuracy of the model.

1.3 Procedure

A comprehensive literature review of previously conducted research in and around the field area initialized the project in Sweden. Papers about local wave climate, coastal erosion, hydro dynamics, the geological setting and land use were in focus, to get a picture of the area and understand the problems in the area. Studies regarding water exchange models, sediment transport models, morphological models, sand spits and numerical mathematical modelling were also of interest for the modelling part.

Upon arrival in Vietnam, meetings were held with the research group at Thuyloi University in Hanoi. The thesis proposal and needed input data for the project was discussed. It emerged that data collections had already been done over two periods during 2019 and measuring stations which frequently uploaded some data online existed. No more data on the project were to be collected. Thus, the project focus shifted from collecting data to processing and sorting the already collected data and the six following weeks were spent

in Hanoi, processing collected raw data. The water exchange model and longshore sediment transport model were developed in Python (Appendix A7), in parallel with the data processing. Report writing was also conducted during the stay in Hanoi.

Towards the end of the stay in Vietnam a field visit to the Cua Lo area was arranged in order to get an overview of the study area and to evaluate some features of the area. Pictures and notes were taken of all features in the area which were of interest.

Back in Sweden, development and calibration of the water exchange model and calculations of the longshore sediment transport continued. Development of the models for calculating the inlet sediment transport, the migration of the sand spit and changes in the inlet cross sectional area was initiated. Different features, factors and assumptions were discussed and taken into consideration during development of the models. Calibration and validation of the models was performed until the result coincided with measured values and the models were considered to represent a realistic future, or historical, scenario. Report writing continued during the whole time.

1.4 Report disposition

This section works as a guide, containing information and descriptions of the content in each chapter.

Chapter 1 introduces the report via background information to the research topic. Relevant areas in coastal processes and modelling are touched upon and the purpose and objectives of the project are explained. A project procedure gives some background of how the project has been conducted.

Chapter 2 contains theoretical background to the research topic by introducing and thoroughly going through relevant coastal processes, river dynamics, coastal erosion, and protective measures needed to paint up the whole picture. The subsection coastal processes include waves, currents, sand spits, estuaries, and tidal inlets.

Chapter 3 introduces the studied geographical area of which the formulated models are applied to. The hydrology and climate, the current socio-economic situation and development, problems related to the area are described, as well as relevant detailed information on the field sight, and a general description of the offshore wave climate outside the field site.

Chapter 4 describes the physics, governing equations and approaches which are the mathematical base of the models. The equations are combined and developed into general models which are used to describe the water level variations in the water exchange model, how the longshore sediment transport and the inlet sediment transport are calculated, and the equations describing the movement of the sand spit and change of the inlet width.

Chapter 5 describes the used model input and the resulting models previously described in chapter 4. The equations from chapter 4 are in chapter 5 motivated and developed in more detail by implementing the general equations to the specific case at the field site.

Chapter 6 contains results from the simulations, represented as graphs, together with descriptions of the results. The model results were divided into subsections of water exchange model, sediment transport, inlet morphology, and sensitivity analysis. In the section "Sensitivity analysis", the effect of model sensitive parameters on the model results was investigated and motivated with graphs.

Chapter 7 contains an analysing section with motivations and discussion of the results. The discussion was divided into model aspects and input data, water exchange model, sediment transport, spit migration and inlet morphology, and effects on the estuary.

Chapter 8 contains the conclusion. The purpose, objectives, the model performance, results, and the most important analysis on the results is discussed in this section.

Chapter 9 contains references in alphabetical order.

Appendix contains more detailed information on some equations, descriptions of some calculated parameters in model input, tidal constituents used in the simulations of ocean water level, bathymetry of the channels and estuary, lagoon water levels, figures and graphs of the morphological models, and the code behind the programs.

2. Theory

2.1 Coastal processes

2.1.1 The Beach and Nearshore Zone

At the shoreline, the intersection between land and the sea, the land becomes subject to forces from waves, winds, and tides. The land responds to these forces by measures to dissipate the energy from the sea.

Material constituents on beaches usually range from fine sand to cobbles. Some of the beach sediment originates several kilometres inland, where weathering of rock into fragments, and transport via rivers has resulted in deposition of the material on the beaches. Beach sediment also originates from erosion of coastal formations via wave action and currents. Some of the material is transported to the beach by onshore movement from offshore deep water. Altogether, the beach characteristics in terms of sediment is usually described as the median sand particles making up the beach, termed "D_{50}". Other factors that are taken into account when describing the beach characteristics are the sand composition, the range of particle sizes, width and elevation of the berm, the slope of the foreshore, the existence of a bar, and the average slope of the zone in front of the beach (Figure 2). Some of these characteristics are interdependent, e.g. the size of the grains and the slope of the beach. Larger sand particles generate a steeper slope of the beach, while smaller sand particles generate a milder slope (US Army Corps of Engineers, 1984).

Wave action on the foreshore causes sorting of beach sediment which results in a selective distribution of larger sediment particles at the shoreline and finer particles when moving offshore, perpendicular to the beach. This profile perpendicular to the shoreline, directed offshore, is called a beach profile.

The surf zone (see Figure 2) is defined as the part of the coastal area of wave action which extends from the water line, out to the most seaward point of the zone at which waves initiate breaking.

In beach terminology, the littoral zone extends from the shoreline, seaward to just offshore of the breaking point. In Figure 2, the littoral zone is defined as the same area as the surf zone (US Army Corps of Engineers, 1984).

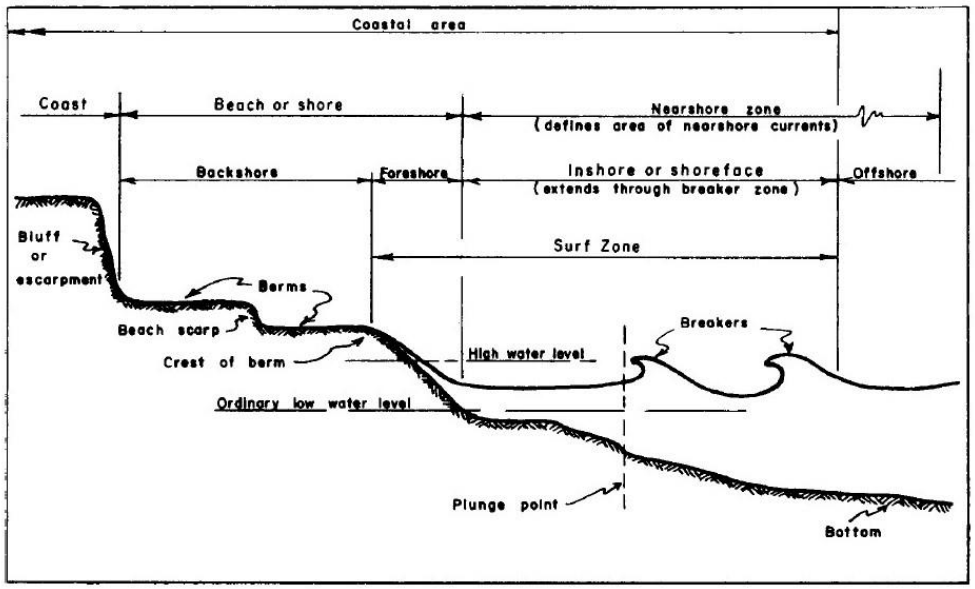

Figure 2. A schematic sketch defining the different zones in the coastal area (US Army Corps of Engineers, 1984).

2.1.2 Waves

Ocean waves are formed by numerous processes, from great gravitational pulls of celestial bodies, winds and storms, to small capillary forces acting between small objects. Constantly affecting coasts, they constitute the largest factor of beach formation and evolution. Offshore waves formed in the open ocean approach the coastline and break in the surf zone where much of their energy is expended, disturbing sediments, creating currents, eroding coasts, and creating recreational areas. Although waves might seem to move water forward, as will be explained, this is only the case in shallow water where the waves are affecting the entire water column. Waves outside the surf zone simply transport energy, not matter (US Army Corps of Engineers, 1984).

Waves can take on many forms. Under windy conditions the ocean sometimes seems chaotic and waves are hard to distinguish from each other. In contrast, during calm days waves can roll into shore in seemingly perfect patterns with distinct wave forms. To describe how wave patterns will behave and predict their appearance has for long been a challenge for scientists, and it is still a large area of research. On an open ocean surface, it is still, even with advanced modelling software, very difficult and complex to describe wave interactions and dynamics in a mathematical way. Due to this complexity, a few simplified

models are commonly used to describe waves. Of these, the linear Airy theory (1845) is perhaps the most fundamental, but also one of the more commonly used due to its simplicity and good accuracy under the right conditions. It is most suited for deep water waves where depth is large relative to wavelength. For shallow water close to where the waves are breaking, solitary wave theory can instead describe wave behaviour in a satisfactory way (US Army Corps of Engineers, 1984).

2.1.1.1 Fundamentals of Airy wave theory

When broken down into solitary units, water waves can be described as sinusoidal patterns with an amplitude "*A*", a wavelength "*L*", and a period "*T*". In addition, depth "*d*" from the still-water level is also an important factor. With these definitions, the free surface water level at a point when a wave passes by can be described by the following equation:

$$\eta = \frac{H}{2}\cos\left(\frac{2\pi x}{L} - \frac{2\pi t}{LT}\right) \quad (1)$$

Where η is the water level relative to the still-water level and x represents the direction of movement of the wave.

2.1.1.2 Celerity, shoaling and refraction

The speed of propagation of a wave is commonly termed wave celerity "C". When related to wave period and length, C is given by:

$$C = \frac{L}{T} \quad (2)$$

Celerity can also be expressed with inclusion of water depth, resulting in the equation:

$$C = \sqrt{\frac{gL}{2\pi}\tanh\frac{2\pi d}{L}} = \frac{gT}{2\pi}\tanh\left(\frac{2\pi d}{L}\right) \quad (3)$$

In Equation 3, celerity depends on the water depth the wave is traveling over. If the water is shallow enough the wave will have contact with the bottom and change some characteristics accordingly. The border between shallow and deep water is termed transitional depth and the respective depths are classified in Table 1.

Table 1. Classification of water depths (US Army Corps of Engineers, 1984).

Classification	*d/L*
Deep water	>1/2
Transitional water	1/25 to 1/2
Shallow water	<1/25

As d/L approaches 0.5 the equation for wave celerity can be simplified to:

$$C_o = \sqrt{\frac{gL_o}{2\pi}} = \frac{L_o}{T} \tag{4}$$

Where the subscript "o" represents deep water. Deep water wave speed is thus only dependent on the wavelength and the wave period. In transitional water the equation cannot be simplified, but for shallow water (d/L < 1/25) it simply becomes:

$$C = \sqrt{gd} \tag{5}$$

It is worth noting that wave celerity is strongly dependent on water depth in shallow water. Waves will travel faster close to the shallow water limit, and slow down when they approach the shoreline. Since wave motion is more or less dissipation-free, another parameter of wave dynamics must change in order to maintain the conservation of energy. This parameter is the wave amplitude and the process is often termed "shoaling". When waves approach a shore their amplitude increases, a phenomenon well observed by frequent beach visitors and surfers. Mathematically, the change in amplitude (A) can be expressed as:

$$A = A_0\sqrt{\frac{C_0}{C}} \tag{6}$$

Shoaling as an isolated process affecting wave height only occurs when waves are approaching shore from a perpendicular angle relative to the shoreline. When waves approach the shoreline at an angle another phenomenon called *refraction* occurs in shallow water. Refraction describes the way incoming waves are changing direction and "turns" to a more perpendicular angle relative to the shoreline when approach it. It has a significant influence on the individual wave height and overall energy distribution along the coastline. From here on it will be assumed that the bottom contours are straight and parallel to the shoreline. Refraction can be calculated in either way, but it is not necessary for basic understanding of the phenomenon (US Army Corps of Engineers, 1984).

Snell's law (Equation 7), describes how the angle and speed of a wave changes over an instant change in depth:

$$\frac{\sin \alpha}{C} = \frac{\sin \alpha_0}{C_0} \tag{7}$$

α and α_0 are the outgoing and incoming wave angles in relation to a line perpendicular to the wave propagation, respectively. Snell's law can then be combined with Equation 6 to express the change in wave amplitude:

$$A = A_0 \sqrt{\frac{C_0}{C}} \sqrt{\frac{\cos \alpha_0}{\cos \alpha}} \tag{8}$$

Commonly, waves do not travel as individual entities but rather as groups or "wave trains". The celerity for these wave trains is in general different from that of the individual waves within it. For any given wave group and water depth, the group celerity "C_g" can be expressed as:

$$C_g = \frac{1}{2}\frac{L}{T}\left(1 + \frac{\frac{4\pi d}{L}}{\sinh\left(\frac{4\pi d}{L}\right)}\right) \tag{9}$$

Which is commonly rewritten:

$$C_g = nC = \frac{1}{2}\left(1 + \frac{\frac{4\pi d}{L}}{\sinh\left(\frac{4\pi d}{L}\right)}\right)C \qquad (10)$$

In deep water the "*n*" simplifies to 0.5 and the equation thus becomes $C_g = 0.5C_0$. For shallow water the group velocity is approximated as $C_g = \sqrt{gd}$, hence the wave train travels with the same speed as the individual waves (US Army Corps of Engineers, 1984).

2.1.1.3 Tides

Gravitational pulls between the rotating Moon, Sun and Earth, causes forces which give rise to periodic water level changes in large water bodies. These vertical changes in the water level caused by these forces is termed tide, or astronomical tide. The horizontal water movements generated by these tides are termed tidal currents. Tides vary significantly between different locations on Earth. Minas Basin in Canada, with its impressive 15 meters of tidal range belongs to some of the larger ranges, while almost enclosed seas like the Mediterranean and the Baltic varies around 1 meter.

With rather high accuracy, the tidal response can be forecasted over many years. A method termed harmonic analysis is the base of the predictions. Water level measurements at a specific location performed over a couple of years can be used in such an analysis to extract the different tidal constituents. Tidal constituents are the separate sinusoidal wave patterns from tidal forces that make up the complete tidal range (Parker, 2007).

The tidal range, from ebbtide to floodtide constitutes the tidal cycle. Tidal cycles vary depending on the location on Earth, but three general patterns can be distinguished. If the cycle takes about 24h to complete and has only one high and one low, it is termed *diurnal*. A *semi-diurnal* cycle exists when two highs and two lows occur during a day. Finally, the *mixed tidal cycle* is as the name implies, a mixture of the two preceding types. Of these, the semi-diurnal is the most common (US Army Corps of Engineers, 1984).

The period of a tidal range is the time from one high water to the next high water. A period is usually 12.42 h for most water areas world-wide, but for

some areas is it 24.48 h. The tidal frequency is the inverse of the tidal period, referred to a solar day, resulting in 1.932 cycles per solar day. The cycles can also be expressed in lunar days, which is 2.0 cycles per lunar day, where a lunar day is 24.84 hours long. Other tidal variations exist as well. Due to changing distance between the moon and Earth, or due to changes in the angle of the plane of the moon-Earth orbit relative to the Earth´s equatorial plane, both fortnightly, monthly and annual variations are also occurring. Variations between years also occurs throughout the 18.6 year long lunar nodal cycle, these variations are in the order of 5 to 10 % of the average tidal range (Parker, 2007).

2.1.3 Nearshore currents

Wind and wave action are the two dominant factors affecting nearshore currents. These currents, simply water in motion, can be initiated when the water depth is shallow enough for the waves to affect the bottom, this depth is termed the wave base. The circular motion of water particles as a wave passes by then becomes elliptical, and the deepest portion of water mass can start to move horizontally. These elliptical circular movements are not fully closed, and particles can thus move in the direction of the wave propagation each time a wave passes. Although there is a net transport of water in the shoreward direction, it is slow and rather weak as long as the waves are not breaking.

Breaking waves are the largest cause of currents in the nearshore area. The decreased momentum flux of energy in the direction of propagation of a breaking wave needs to be compensated by a force in the opposite direction, according to Newton's third law. If the incident wave angle is perpendicular to the shoreline, this force generates a setup at the shoreline and thus also a hydrostatic force acting "against" the wave. In other words, this hydrostatic force creates a cross-shore current in the seaward direction. Rip currents are perhaps the most well-known example of cross-shore currents. These jets of water in the seaward direction are sometimes prominent and can be strong enough to cause risks for swimmers (US Army Corps of Engineers, 1984).

If the incoming waves instead have an angle in relation to the shoreline, a longshore water movement is generated. In this case, the reduction in momentum energy flux is directly translated into a current since there is no direct obstacle in the longshore direction. Wave incident angle is the most important factor in determining current velocity for longshore currents and breaker wave height mainly governs the volumetric flow rate. The longshore

current reaches its highest values when the incident wave angle is 45 degrees (US Army Corps of Engineers, 1984).

2.1.4 Sediment dynamics

Transport of sediments in the nearshore area can be classified into two processes which follow the same principles as nearshore currents: longshore sediment transport (LST) and cross-shore sediment transport. LST refers to sediment transport with a net direction parallel to the shoreline, whereas cross-shore sediment transport occurs perpendicular to the shoreline. In the surf zone both the longshore and cross-shore components of sediment transport are of significant magnitude. Fluid motions at wave breaking initiates most of the sediment transport in the littoral zone. The large forces of breaking waves stir up sediment which would otherwise not be moved by the less powerful nearshore currents. Although, once suspended, sediments can be transported by other weaker currents.

Grain size, wave steepness and beach slope are the main factors affecting the magnitude of the cross-shore sediment transport. This process mainly changes the beach profile on a seasonal basis. Stormy winter or rain season weather with large steep waves predominantly moves sediment offshore, while calmer seasons with low and less steep waves move sediment onshore (US Army Corps of Engineers, 1984).

LST is mainly affected by wave energy, incident wave angle and duration. These factors can vary even over short time periods, which makes it difficult to predict short-term LST. A common way to classify transport, and to facilitate analysis, is instead to look at the total amount of sediment moving in one direction past a given point over a year. This is called “net transport”. Net transport is then compared to the total amount of sediment moving past that same point in either direction, called the “gross transport”. Over time the general direction and magnitude of transport may change, but knowing these two parameters for a coastal area can be very helpful when developing shore protection plans as it gives a rough estimate of how the shoreline will behave (US Army Corps of Engineers, 1984). The LST is most efficient when the waves reach a straight or very gently curved shoreline without headlands or inlets and with a smooth nearshore sea-floor profile (Siegle et al., 2007).

For both longshore and cross-shore processes, sediment transport occurs in three different modes, or levels, in the water column: bed load, sheet flow and

suspended load. Bed load transport occurs along the bottom, suspended load refers to transport of sediment supported by uplift fluid motion, and sheet flow is when sediment move collectively as a sheet along the bottom. Initiation of movement for bed load occurs when the bed shear stress reaches the threshold of motion. Usually more than one of the modes occur at the same time, and it can be hard to distinguish between the boundaries. Thus, for modelling the three modes are simply grouped together (US Army Corps of Engineers, 1984).

2.1.5 Sand spits

Sand spits are pointy formations that usually develop outside inlets, down-drift of barrier islands and on outskirts of bays. A common way of sand spit development and growth is through accumulation of sediment transported to the site via longshore sediment transport. Following this mode of deposition, sand spits usually consist of material in the grain size range between sand and gravel. Kraus (1999) describes the main factors affecting spit geometry and evolution in Table 2.

Table 2. Main factors affecting sand spit evolution and geometry. Modified table based on Kraus (1999).

Parameter	*Short term change*	*Long term change*
Length	LST rate; proximity to inlet; strength of channel current	Sediment supply; breaching; geologic controls; cyclic and intermittent forcing
Width	Run-up; tidal range; depth-contour gradients perpendicular to spit	Dunes and other blocking features; depth of bay/lagoon on shoreward side
Elongation speed	LST rate; grain size; proximity to inlet; beach slope and depth-contour gradients parallel to spit	Cyclic and intermittent forcing

Long term evolution is largely dependent on changes in sediment supply to the site. Such changes can involve construction of hard coastal protection measures on the up-drift side, sand mining, and changes in ocean currents. For spits in connection to river mouths construction of hydroelectric dams,

dredging and flood protection measures can also affect sediment supply. Annual fluctuations in wave climate, winds and storms, as well as inter-annual changes in water levels and climate variations also has a long-term effect on sand spit evolution (Kraus, 1999).

Five principal shapes of sand spits exist: linear, recurved, compound, complex, and serpentine (Johnson, 1919). The linear configuration is suggested to evolve when the longshore sediment transport is much more dominant compared to the cross-shore counterpart (e.g. by river inlets). A recurved spit can start to form e.g. if the cross-shore component is stronger or similar to the longshore component, or as a result of wave refraction on the tip of the spit (Johnson, 1919; Evans, 1942).

Depending on the environment around it, spits can either grow in an unrestricted or a restricted way. When unrestricted, the spit has little or no influence from other currents than the wave-generated longshore current. Restricted growth then prevails when spit growth is influenced by other currents (Kraus, 1999). For this mode of growth, the spit can enter a dynamic equilibrium where the sediment supply and removal become equal and the spit length remains constant. Equally, if either of the sediment supplying components are stronger the spit can retract or propagate. When in connection to an inlet this can result in inlet widening or narrowing, with the ultimate state of total inlet closure (Tanaka et al., 1996; Larson et al., 2009).

Breakthrough of sand spits at undesired locations may occur due to inlet closure during a major river flood event or during coastal flooding. The breakthrough may threaten local people which, due to pressure from dense population in the coastal region, have settled on the sand spit. It can isolate local communities and destroy infrastructure in the zone of breaking. Long term consequences can be disturbance and changes in the environment and ecology of the estuary or the lagoon behind the inlet. The creation of a new inlet may disturb the hydrologic system and cause the system to become unstable (Tung, 2011).

2.1.6 Estuaries

Estuaries or coastal lagoons are shallow coastal water bodies that are separated from the ocean by a barrier, intermittently connected to the ocean by one or more restricted inlets, and are usually parallel to the shore. The water depth is usually between one and three meters and is always less than five meters,

except in the inlet channel and in isolated relict holes or channels. Inorganic sediment and organic matter are in general trapped in estuaries, making them serve as sinks and/or material filters. The primary and secondary biomass production is usually very high, which is valuable for coastal farming, agriculture and sometimes for salt extraction. In a geological time-perspective, they are short-lived landscape features, often changing in both appearance and water exchange properties. Estuaries are affected and altered by forces from river input, wind stress, precipitation to evaporation balance changes, tides, and subsurface heat balance (Kjerfve, 1994).

2.1.6.2 Water exchange in estuaries

Water exchange between seas and estuaries occurs through connected narrow inlet channels. Water and salt balances, eutrophication and water quality depend on water exchange with the sea, lagoon circulation, dispersion of salt and material, turn-over time, and residence time. In terms of planning and implementation of coastal management strategies in estuaries it is important to understand their physical, chemical, ecological, and geological dynamics (Kjerfve, 1994). Of the factors affecting water exchange in estuaries, the main factors are tides, river flow, surface runoff, circulation caused by wind, currents driven by waves, and evaporation. It is very common that the tidal flow and the river flow are the most important components affecting the water exchange and water quality in an estuary. A commonly used term to describe the quantity of the water exchange due to tides is the tidal prism *(P)*. It is defined as the total volume of water exchanged during a tidal cycle, in other words the volume of water that flows in during flood tide and out during ebb tide (Jarret, 1976; Walton and Adams, 1976). O´Brien (1969) found that the size of the throat cross-sectional area of a tidal inlet is related to the tidal prism. It is also depending on the delivery of sediment to the inlet channel. A larger inlet cross-sectional area leads to a larger tidal prism in a linear dependency. Similarly, a large tidal prism leads to a larger delivery of sediment to the inlet channel.

Coastal lagoons can be divided into three different morphologic types related to differences in water exchange with the sea; choked-, restricted-, and leaky coastal lagoons. Choked systems usually consists of one long and narrow inlet and generally occur in areas that are subject to high wave energy and strong longshore sediment transport. Restricted systems generally have two or more inlets and usually do not show any vertical stratification. Leaky systems are

generally long and thin shaped with unlimited water exchange passes. They are usually located in tide dominated areas in littoral drift. The three different morphological types of coastal lagoons are illustrated in Figure 3 (Kjerfve, 1994).

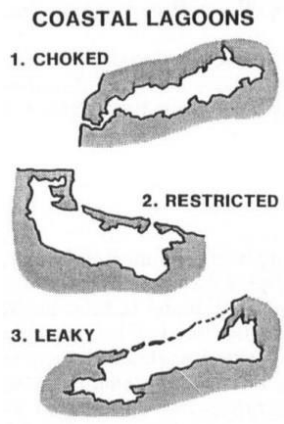

Figure 3. Three different morphological types of coastal lagoons, sub-divided based on the degree of water exchange with the sea (Kjerfve, 1994).

In estuaries connected to the ocean via two inlets, spatial variations in the water level may occur within the basin. The barrier which restricts the exchange between the parts of the estuary may be seen as a topographic high which in nature could be a tidal flat. A tidal flat is where the tides which are entering the inlets meet, resulting in low velocities and sedimentation. Tidal flats allow for exchange between the estuaries at a certain degree depending on the height and extent (van de Kreeke, 2017).

2.1.6.3 Estuarine sedimentation

When the sediment carrying capacity in an aquatic system is exceeded, sediment will deposit. This typically occurs in areas with lower energy fluxes like sand bars or mudflats. The water becomes shallower as the sedimentation increases, further decreasing energy flux and increasing deposition. This can have an impact on local industries, maritime transport, navigation, and the ecology of the estuary.

Estuarine sedimentation can be described as the erosion, transport and deposition of sediment and material from the water column. Natural sources contributing to siltation are erosion of soils and redistribution of soil within

the estuary due to storms, tides, and movement within the estuary itself. Due to the grain size distribution, deposition of sediment is not expected to behave uniformly. Finer materials can remain in suspension for longer periods and be carried with the flow until the velocity is decreasing, e.g. after a decrease in the channel cross-sectional area. During storms or high tides, larger-sized sediment discharged into the estuary can be deposited close to the upstream source. Sediments that have deposited in the estuary can also be re-suspended due to tidal action and storms. The coarse-grained sediment transported in the estuary can also cause shoaling problems through bedload transport leading to development of sand waves and shoals. This can result in more pronounced deposition in certain regions. Human activities can increase the sedimentation in receiving waters. This can occur due to increased runoff from urban impervious surfaces. As the cities develop and the land-use changes, the impervious areas are also increasing, resulting in an increased runoff and addition of sediment to the receiving waters. Other sources of sediment arising from human activities are construction sites, agricultural lands, forestry operations and transportation related infrastructure (State of New Hampshire, 2010).

2.1.7 Tidal inlets

A tidal inlet is a narrow opening between an associated tidal basin and the ocean where the opening is maintained by tidal action. The inlet-basin combination is termed “tidal system”. Such systems are commonly found at several locations along barrier island chains and serve as passages to the ocean if they are wide- and deep enough (Escoffier, 1940; Glaeser, 1978). Human activities such as fishing, aquaculture, navigation, sand mining and recreation are facilitated by tidal inlet systems which make them economically valuable to coastal nations like Vietnam. Apart from the human perspective tidal systems are also important ecosystems, serving as nurseries and resting grounds for many aquatic and semi aquatic species (Stive et al., 2006). Further, inlets can have considerable effects on nearby shores and shoreline evolution since they disturb the LST and trap the cross-shore transport. Thereby, tidal inlets are storing sediment and reduces the sediment supply to adjacent shores (US Army Corps of Engineers, 1984).

2.1.7.1 Inlet formation

Inlet systems are usually dynamic and develop over time. Formation processes can include flooding of coastal plains, aeolian transport processes, and/or sand spit growth followed by breaching. A common requirement is usually an embayment which becomes partially closed off. Formation by sand spit development is often fed with sediment from LST or other nearby sediment sources. When the spit elongates across a bay, flow velocities in the inlets increases in order to keep the water exchange volumes constant. Eventually the inlet reaches an equilibrium width as the erosive powers of the water flow limits narrowing. Breaching of narrow or low sand spits can occur during storm surges and high wave action, or during high discharges in associated rives (Leatherman, 1988). Changing morphology such as migration, narrowing, widening, closure and opening of new inlets may occur both during and after the system development (Bruun et al., 1978). New inlets may be formed in the spit or barrier island due to action of storm waves. Inlets enable beach sediment lost at storms to enter an estuary and deposit there. Tidal currents may carry bottom sediment from the estuary to the sea and transport it along the shore via longshore currents (US Army Corps of Engineers, 1984).

2.1.7.2 Inlet migration

Inlet migration occurs when LST adds sediment to the updrift side of the inlet. This causes narrowing of the inlet channel, resulting in higher flow velocities, and thus also increased scouring to maintain the water exchange. Sediment scouring occurs more on the downdrift side of the inlet and as the process continues the inlet migrates towards the downdrift side (Johnson, 1919). Migration will continue until the LST properties no longer favour deposition, or until the side of erosion reaches a fixed boundary such as a bedrock formation (De Alteris and Byrne, 1975). The rate at which an inlet migrates is also highly dependent on the LST, combined with riverine currents and ebb tidal current velocity. Riverbank composition is also affecting inlet migration rate, where highly consolidated material slows down migration (Fitzgerald, 1988).

2.1.7.3 Sediment bypassing

Not all the LST is deposited on the updrift side of an inlet. A process called sediment bypassing enables sediment to return to the normal littoral drift zone on the downdrift side of an inlet, or similar interruption (Bruun, 2005). The mechanisms of how this process occurs have been described by several models, of which the first was made by Bruun and Gerritsen (1959). The work

of Bruun (1966), and Fitzgerald (1982, 1988) added more conceptual models. Fitzgerald et al. (2000) summarized the combined work on sand bypassing into six conceptual models, of which five are presented here (Figure 4 and 5).

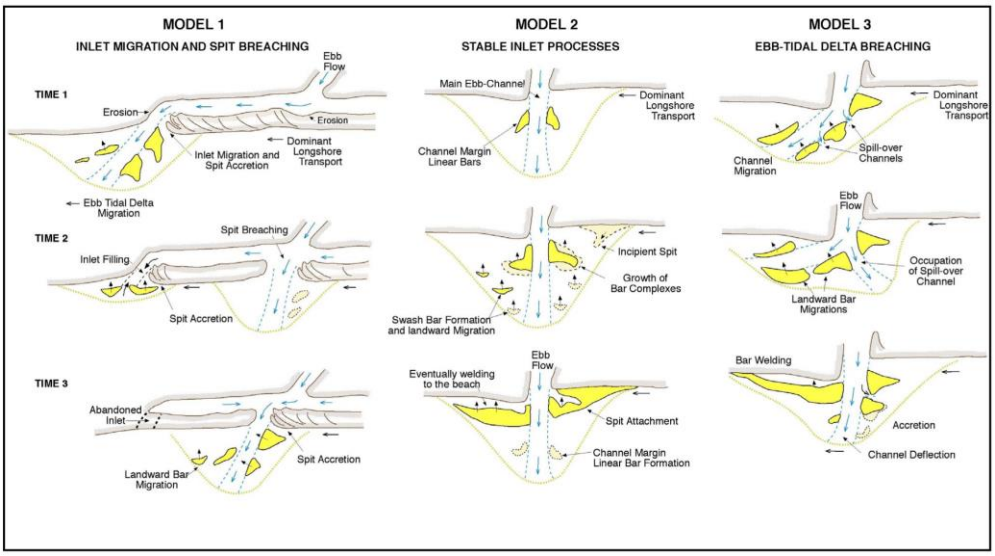

Figure 4. Different processes for sediment bypassing an inlet as summarized by Fitzgerald et al. (2000).

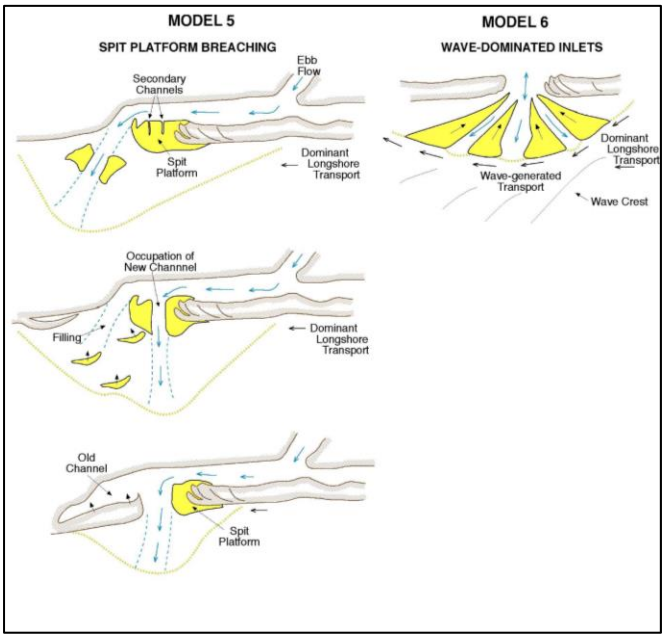

Figure 5. Different processes for sediment bypassing an inlet as summarized by Fitzgerald et al. (2000).

1. **Inlet migration and spit breaching:**
   This model is largely described by the mechanisms mentioned in "2.1.7.2 Inlet migration". Breaching can occur if the upstream river or ebb-tidal flow occurs at an angle compared to the spit elongation. The flow can initiate erosion on the spit which eventually will lead to spit breaching. Such an event usually occurs during a storm surge or riverine flooding event.

2. **Stable inlet processes:**
   Inlets that are anchored in an erosion resistant substrate and/or have deep channels are usually not migrating. The mechanism of bypassing instead depends on the formation of bar complexes outside the inlet. Due to cross-shore transport the bars will move in the landward direction, eventually reaching shore. Longshore currents shift the bar accretion towards the downdrift side, making these bars bigger. A cycle from bar complex formation to attachment can take between 4 and 10 years.

3. **Ebb-tidal delta breaching:**
   If the inlet position remains fixed over time but the ebb channels migrate, ebb-tidal delta breaching can occur. LST deflects the ebb-channels towards the downdrift side of the inlet, usually causing erosion on the downdrift side. The hydraulic efficiency of the flow eventually becomes too low and the flow is diverted to a more direct seaward path. The old channel will become filled with sediment from tidal and wave-generated currents. The cycling period of this mechanism is about 5-10 years.

5. **Spit platform breaching:**
   At an inlet which exhibits migration, large intertidal platforms are often formed. These are often submerged and can be several hundred meters long. As accretion occurs on the updrift side the inlet channel becomes longer. The flow efficiency is then lowered and flow across the platform can become channelized. Deepening of the newly formed channel can then cut off a part of the platform, completely redirecting the ebb-tidal flow.

Large sediment volumes can be transported via this mechanism as it is not only the cut off spit platform which is transported to the downdrift zone. A majority of the old ebb-tidal delta sediment is also transported to the downdrift shore.

6. **Wave-dominated inlets:**
   Outside wave-dominated inlets sand bypassing occurs continuously rather than episodically, as for the other conceptual models. Characterizing for this kind of inlet is a narrow opening (<200 m) and a depth shallower than 6 m. Shallow sand shoals are formed close to the inlet throat, allowing sediment to be transported past outside the shoals by longshore currents.

2.1.7.4 Seasonal evolution and morphological stability

Both river flow, tidal variations and LST often exhibit seasonal variations. During e.g. monsoon periods the ebb-tidal flow is larger due to heavy rainfall and river flooding. Stronger wave action during monsoon conditions, with more wind and different wind directions, can also affect the ebb-tidal flow in both a counteracting and enhancing way. At the same time, the gross LST can increase due to a stronger wave climate, enabling more or less deposition at the inlet. This is particularly the case for areas that have a monsoon period and where trade winds shift during the year (Bruun et al., 1978). Cycling of tidal variations are mostly detached from the climatological events. Instead the fortnightly spring-neap tide cycle is the strongest parameter (Parker, 2007).

Inlets are rarely static but widen and narrow dynamically over short time periods in response to changes in the tidal prism, changing wave energy, storms, and other factors. Seasonal fluctuations during monsoon periods, floods, strong currents, and larger tidal prisms may increase the channel scouring and enlarge the inlet cross-sectional area. Changes in the inlet cross-sectional area over a long-time perspective are related to inlet migration, morphological changes of the ebb-tidal delta, sedimentation in the back barrier and human activities (Jarret, 1976; Walton and Adams, 1976).

If the conditions affecting inlet cross-sectional area are drastically changed to favour inlet narrowing, closure can occur. Across the world, it is a well-documented phenomenon observed on many locations e.g. USA (Elwany et al., 1998) Brazil (Bruun et al., 1978), and Vietnam (Tung et al., 2007).

Inlet closure occurs simply as a consequence of insufficient flow capacity to keep the inlet free from being filled up with sediment. It can occur gradually or as an episodic event from a storm which causes the closure. Inlet shoaling may lead to inlet closure and it can occur due to elongation of a sandspit, or due to extreme deposition of littoral drift material during storms (Bruun and Gerritsen, 1960). Inlet shoaling can also occur due to splitting up of the main channel into two or more channels, or formation of new channels from artificial or natural causes. It can also be due to opening of a new inlet or due to change in the lagoon area or by growth of marshlands. It is common that inlets with small cross-sectional area and small tidal prism may close seasonally during short periods, or to close during severe conditions. The sand bypass via bar or flow bypassing mechanisms might be unable to handle the large volumetric flows of sediment which can occur during storms. In this case the inlet channel may become overloaded with sediment and eventually close (Fitzgerald, 1988). An inlet may become unstable and close as a consequence of several breakthroughs of the sand barrier during extreme storms. The inlets become unstable since both the old inlet and the new inlets created after the storm have the same tidal prism. As a consequence, they will shoal up, become unstable and one or many of them will close (Tung, 2011).

Closure of a tidal inlet or entrance shoaling may affect the local fishing communities negatively since they are using the entrances as navigation channels to the sea. Also, many fishermen are using lagoons and estuaries as fishing boat shelters during typhoons, and closure or shoaling of inlets may block the entrance to these and force the men to store their boats at less safe places which may result in damages on the boats. Closure of estuary inlets may also result in blocking of the exchange of water between the estuary and the sea, which restricts the circulation of water in the estuary and it may affect the water quality. A consequence of this is that the local farmers which cultivate in the estuary are threatened by water pollution and the animals are threatened by the change of environment (Tung, 2011).

2.2 River dynamics

Rivers are systems in dynamic equilibrium considering water flow and sediment transport. Equilibrium tends to be reached by a process of erosion at one site, balanced by deposition at another. The energy of a river must be in balance with the size and the volume of the carried sediment. The system is striving for balance between sediment load and transport capacity of the water. If the quantity of sediment exceeds the flow-capacity, the stream channel

becomes aggregated with sediment. Equally, a sediment deficiency results in degradation of the stream channel (Couture, 2008).

River channels which have been altered by humans or nature must readjust to return to its former equilibrium. The adjustments are made with respect to dimensions of the river, as well as the river profile and pattern. Many rivers are changing fast due to land development and changing land use in certain susceptible areas. River channels can also enlarge rapidly if they receive larger volumes of stormwater. Global climate shifts and cycles can also affect the rivers. Rivers are also affected if traditional management of them are not supporting the natural hydrology. These factors result in that high flows are kept in the channel which generates high erosive powers, instead of allowing the energy in the waterflow to dissipate onto the floodplain. Adjustments of channels caused by large water events may involve catastrophic economic outcomes for societies (Couture, 2008).

2.3 Coastal erosion

Erosion arises when less sediment enters an area compared to the sediment leaving the area. This causes the area, such as a beach, to lose sediment and thereby change in appearance. It can be caused either by nature or by human activities (US Army Corps of Engineers, 1984). The rate of erosion depends on the type of soil, beach slope, precipitation, and water velocity. Erosion often becomes a problem when humans are not taking into consideration that rivers, coastlines, and water bodies are systems in dynamic equilibrium. Erosion also becomes an issue when structures are built too close to eroding banks, which can eventually result in structural damage. It also becomes a problem when natural or human activities accelerate the natural rate of erosion, or when riparian buffers are not maintained (Couture, 2008).

A natural factor causing erosion is sea-level rise, a slow process that affects over long time perspectives. The effect of erosion caused by sea level rise depends on the relation between sea level rise and land uplift. If the sea level is rising faster than the land a slow recession of the shoreline will occur. While the profile is adjusting to the higher water level, flooding may occur. Another factor is variability in sediment supply to the littoral zone. This can be caused by climate variability, where droughts may result in reduction of flow in rivers which in turn causes a reduction in the supply of sediment to the coastal zone. Storms are the largest cause of temporary erosion. As described under “2.1.4 Sediment dynamics” waves from storms transport sand offshore where it is

stored temporary in a sandbar or a shoal. With time the beach recovers by natural transport of the material. Some material is permanently lost offshore in deep water. Wave and surge overwash are phenomenon where waves and overflowing water is eroding the beach, transporting, and depositing the material shoreward of the beach. The material can also be deposited as an overwash fan on low-lying barrier islands, on the bay side. Overwash is occurring during storm surges and severe wave action. Deflation or aeolian transport is also contributing to beach erosion. It is the process where loose material is transported from the beach by wind actions. Longshore sediment transport is contributing to coastal erosion by transporting sediment alongshore via waves. This is occurring if the waves are breaking at an angle to the shore. Sorting of beach sediment caused by wave actions results in movement of sediment and redistribution of the sediment particles along a beach profile. Finer particles move offshore, and more course particles move onshore. These processes are also contributing to coastal erosion (US Army Corps of Engineers, 1984).

Land removal of subsurface resources like gas, oil, coal, and groundwater can induce land subsidence. Material in transport interrupted by human activities is a significant cause of erosion. This interruption is caused by improvement of inlets by channel dredging, channel control and harbour structures. Use of structures like groins causes realignment of the shoreline by trapping and thus reducing the material reaching downcoast. Another man-induced cause of erosion is when the supply of sediment to the littoral zone is reduced. This can occur if the supply of material to the coast by rivers is interrupted by human activities (2.2 River dynamics).

Navigation inlets like harbour or bay entrances are widened and deepened, enabling larger waves to enter the inlet, and making the harbour or bay more exposed and more vulnerable to erosion. This results in an increase in water level fluctuations in the area in question. If the natural coastal protection is interfered and changed the dissipated wave energy increases. Following this, the rate of erosion at that location will increase. Interference can be due to dredging of the nearshore bars and shoals, or destruction of onshore protection like sand dunes and beach vegetation. Removal of material from the beach causes a direct loss of available material for support. Addition of material may add support by increasing the amount of sediment available for transport, but erosion can still occur (US Army Corps of Engineers, 1984).

2.4 Protective measures

When waves are shoaling and approaches the beach, the beach slope and the beach berm are forming an outer line which is defending the beach against the wave energy. If overtopping of the berm occurs, the beach dunes protects and reduces the rate of erosion. Depending on the current situation, different protective measures are necessary to protect the beach from erosion. Three different categories of coastal protection exist: soft, intermediate, and hard structures (US Army Corps of Engineers, 1984).

Soft nourishment, or sand nourishment, is a quasi-natural method where mechanical deposition of sand is done in the nearshore zone to widen the shoreline or to maintain the volume of sand in the nearshore zone. This method is protective, preserves the recreational value of the beach and leaves the coastal area in a more natural way compared to hard structures. Shoreface nourishment is when the sediment is placed at the seaward flank of the outer sandbar. It is usually used at wide beaches with high dunes, with the purpose to maintain the volume of sand in the littoral zone by in the long term nourish the littoral zone via natural processes. Beach nourishment refers to an anthropogenic deposition of sediment on the beach in order to widen it. It is usually used in areas with narrow beaches, low sand dunes and where the beach is too narrow for tourism and recreational purposes (Rijn, 2011).

Intermediate coastal protection is a combination of soft and hard structures to prevent beach erosion. Sandbags and geotextile tubes are examples of an intermediate structure, where geotextile tubes are filled with dredged or local material to prevent beach erosion. The tubes become sensitive to different wavelengths of the sun after a certain time, which then can damage the tubes. A solution is to protect the geotextiles with a layer of cemented sand on the exposed surface (Imran, et al., 2017). The tubes can be used as a submerged bar if longshore currents are not of any concern. The submerged bars should be combined with groins, submerged or not, if longshore currents are present. They can also be used as revetments (Montanari, 2017).

Hard structures are usually built in urban areas to reduce beach erosion and to preserve a small beach for recreation. Sea walls, groynes, detached breakwaters, and artificial reefs are examples of these hard structures. Sea walls are built to stop shoreline recession at a certain location, to protect urban areas. Groynes and detached breakwaters are built to trap sediment between the groins or at the detached breakwaters, at locations where longshore transport is a problem. But these kinds of structures increase the variability of

the shoreline with the largest recession compared to the initial recession of the shoreline when the waves have one dominant direction. Straight groins are not protecting against cross-shore sediment transport since nothing is hindering the transport parallel to the shoreline (Rijn, 2011). These hard shore protection measures may accelerate the total amount of erosion which the measure was intended to alleviate. Another consequence may be that material in transport may be interrupted or altered by the construction of a hard protection. This may reduce the amount of sediment reaching downcoast beaches via entrapment, resulting in an increased erosion rate downcoast (US Army Corps of Engineers, 1984).

3. Area description

3.1 Hydrology and climate

Typical hydrological characteristics for the coast of central Vietnam is high seasonal geomorphologic variations of tidal inlets and river mouths. From narrowing, shoaling or complete closure of the inlet during the dry seasons, to widening or breaching during the monsoon period. It is prioritized to work with stabilization of inlets at the central coast to milder the potential risks and effects of natural disasters like floods on low-lying coastal plains. Stabilization of inlets is also prioritized since it promotes safe and more stable conditions for socio-economic development in the area. The most destructive and common water-related disaster in the central coast is river flooding. It is caused by upstream deforestation, steep coastal landforms, intense rainfall and/or the fast blockage of river mouths or estuary inlets during dry seasons due to littoral sedimentation. Typhoons, monsoon rains and storm surges are big threats causing flooding. Usually river mouths and lagoon inlets are the only outlets for flood release. Therefore, migration of channel inlets, shoaling and closure of inlet entrances can cause problems for flood protection management for the low-lying coastal plains. This since the flood discharge capacity is reduced and the risk of flooding increases (Tung, 2011).

The province, or more specifically the Vu Gia Thu Bon (VGTB) lowlands, has a tropical monsoon climate. The precipitation for one year has an approximate magnitude of 2400 mm. The monsoon period occurs between September and December, when 65% to 80% of the precipitation falls. Flooding is very common during these months. The dry season spans from February to August and water shortage is a common problem during this period (Nauditt et.al, 2017).

3.2 Socio-economic development

The province of Quang Nam is located along the coast in the central parts of Vietnam. The region is undergoing a change from agriculture to development of industry and service. The average annual growth rate of the region has been 10 % during the last decade, and the percentage of the population working with agriculture is decreasing. The primary sector consisting of agriculture, fishery, forestry, and handicrafts is changing, and the secondary and tertiary sectors are growing strongly. Vietnam is one of the world leaders in terms of export of agricultural commodities. Among many commodities, shrimp farming is a big industry in the coastal areas and the deltas. The total area of

coastal and marine agriculture in Vietnam almost doubled between year 1991 and year 2001. In Quang Nam province, there are many shrimp farms in the coastal areas and in the deltas (Nauditt et.al, 2017).

Regarding the bigger economic areas in the region, the vast majority is located in the lowlands. The dense population, industries, services, and intensive agriculture is supporting the dynamic growth. Both hydropower generation and forestry are major activities contributing to economic growth in the midlands. Quang Nam is a province with high potential to develop marine economy, especially the coastal area along the Truong Giang river which is an economic zone named Chu Lai. This economic zone is currently being planned to become an urban centre of tourism, industry, and service. Dien Nam-Dien Ngoc Industrial Park, as it is named, is the first coastal economic zone of multi-sectoral engagement in Vietnam (Nauditt et.al, 2017).

3.3 Area-related concerns

The land-use in the province of Quang Nam is not used in an economic beneficial manner. This is due to inefficient exploitation of the Cua Lo area (Figure 6), and it is also due to natural disasters. The natural disasters occurring along the coast of central Vietnam are caused by meteorological and oceanographical factors which are intensified by human activities like damming of rivers or deforestation to create agricultural lands. Many rivers are steep and have naturally temporally varying flows which are seasonally prone to flood large areas since the coastal plains are very low lying. However, during rest of the year the rivers may be almost completely dry. Frequent natural disasters are hindering development efforts and risk to trap the local population in poverty (Tung, 2011). A big problem is the high level of sedimentation in the Truong Giang river and Cua Lo estuary. The shallow river bottom and low water level brings many problems to the local inhabitants. Amongst others, it obstructs boats from going to sea, affecting the local fishing industry. As mentioned before there are many shrimp farms in the province, and more specifically in the Truong Giang river and the Cua Lo estuary area. The shrimp farms are also affected by the low water level, but they are also hindering the economic development of the area in terms of tourism. The shallow water level also results in increased risk of flooding in the area. All these factors contribute to a bad tourist economy for the area (H. S. Tam, personal conversation, 2020).

3.4 Cua Lo estuary and its vicinity

The Cua Lo River mouth is a tidal inlet and is located at around 15° 29'51.4" N Latitude and 108° 39'33.9" E Longitude. This is about 650 km south of Hanoi, in the Núi Thành district, province of Quang Nam (Figure 6). The river mouth is connected via a channel to the Cua Lo estuary, which in turn is connected to Cua Dai inlet (Tung, 2011). Cua Lo is part of the littoral system extending from Da Nang to An Hoa Cape. Sediment is supplied from Thu Bon river to Cua Dai river mouth and alongshore to An Hoa cape. The main river connected to Cua Lo estuary is the Truong Giang river, which is a tributary to the larger Thu Bôn river (Duy et.al, 2018). North of the Cua Lo inlet lies a sand spit, southeast of the inlet exists an island named Tam Hái island with a rocky formation at the top named An Hoa Cape. On the southeast side of Tam Hái island exists another inlet which also is connected to the Cua Lo estuary, this inlet is named Ký Hà. The south side of Ký Hà inlet is called Chu Lai. An Hoa cape and the northern part of Chu Lai Peninsula consists of hard rock which includes some stratified older sediment and some volcanic material (Inman, 1966).

The inlet at Ky Ha (Inlet 2) had a cross-sectional area of about 2 415 m^2, in year 1966. This year, when the inlet area was measured and calculated from satellite images and bathymetry data, the area was calculated to 2 500 m^2. This indicates that the inlet at Ky Ha is rather stable. In year 1966 a plan was developed to facilitate for boats to enter through the inlet by creating an entrance channel and a turning basin. This was performed by dredging. The dredging activities had to be done annually since waves and tide caused a gradual refill to its natural conditions. Approximately 190 000 m^3 had to be dredged annually in the inlet channel and 120 000 m^3 in the turning basin to maintain a depth of 6 m at both locations. The dredging was performed between April and October, in the dry period (Inman, 1966).

Figure 6. Overview map of Cua Lo area including the two inlets Cuo Lo and Ký Hà, the rivers Truong Giang river and Song Cho river and Tam Hái island with An Hoa Cape (OpenStreetMaps, 2019).

The tidal inlet and the estuary are in a micro-tidal environment with the influence of episodic river flooding. Along the Vietnamese coastline, the tidal patterns are varying. Some parts have diurnal, some have semi-diurnal and some have a mixed tide. The province of Quang Nam has a mixed tide, predominantly diurnal (Tung, 2011).

The beach morphology at the river mouth is changing and the result is further development of the sand spit on the northern side and severe erosion on the sand bank on the downdrift side (Duy et. al, 2016). The average sand spit migration alongshore towards southeast has been estimated to 40 meters per year. Since 1973 the sand spit has elongated about 1.7 km towards southeast (Nguyen et.al, 2018 (a)). The LST causing the elongation of the sand spit is mainly originating from sediment from Cua Dai, the river mouth of Thu Bon river. Thu Bon river is transporting about 520 000 m^3 of sediment per year through Cua Dai and about 450 000 m^3 of sediment is transported south of Cua Dai inlet, towards Cua Lo (Nguyen et. al, 2018 (b)). Scientists and local

authorities are giving attention to the situation since it results in issues for the local people by disturbing e.g. agriculture and tourism (Duy et.al, 2016). The hydrodynamic conditions at the Cua Lo inlet is dominated by tidal currents and during the northeast monsoon season by waves. The elongation of the sand spit north of the Cua Lo inlet is caused by reduced hydraulic efficiency in the inlet mouth, which also is causing erosion and land loss at the downdrift side of the inlet. Dune erosion and shoreline retreat is occurring.

In 2008 regulatory works were performed to protect Cua Lo area from the occurring erosion. Six geotubes were placed perpendicular to the beach, but in year 2012 the constructions were damaged, and the protection was lost (Tam, 2020). Countermeasures which included cross-shore hard structures, groins, were implemented between 2010 and 2011 with the purpose to sustain erosion and protect the shrimp ponds. The construction of the groins was not enough to withstand the erosion and maintain the shoreline and erosion is still occurring following the elongation of the updrift sand spit. In 2015 dredging activities were performed to prevent the infilling of the inlet, and according to the locals dredging activities are performed frequently after every monsoon period (Nguyen et.al, 2018 (a)). It is observed that the eroded material is transported and trapped by the An Hoa cape which is a solid boundary hindering further sediment transport (Duy et.al, 2018).

3.5 Offshore wave climate

Generally, along the coast of the province Quang Nam the main offshore wave direction is ENE and SE, but NE is the overall dominant direction. The most dominant wave direction from June to August is SE, the wave direction during the rest of the year is dominated by NE. The waves during the period from September to May are dominantly originating from NE. The largest wave heights occur from December to February, wave heights above 4 m have been recorded. Among all incoming offshore wave heights, 25 % are higher than 3 m and originates from ENE and 35 % are 0.75 m and larger and originates from ENE. Only 10 % of all wave heights originates from SE and are larger than 0.75 m. The waves originating from E and SE are hindered by An Hoa cape. Therefore, is the influence of the waves originating from NE more pronounced, both regarding duration and wave height. This causes the sediment transport from NE to have a larger effect on the littoral zone compared to the more limited sediment transport from SE (Nguyen et al., 2018 (a) and (b)).

4. Modelling theory

A conceptual model of the modelled area can be seen in Figure 7. The model includes the two estuaries, the interconnecting inlet, the two inlets which are connected to the ocean and the sediment transport in the inlet (m_{I1}) and alongshore (m_L).

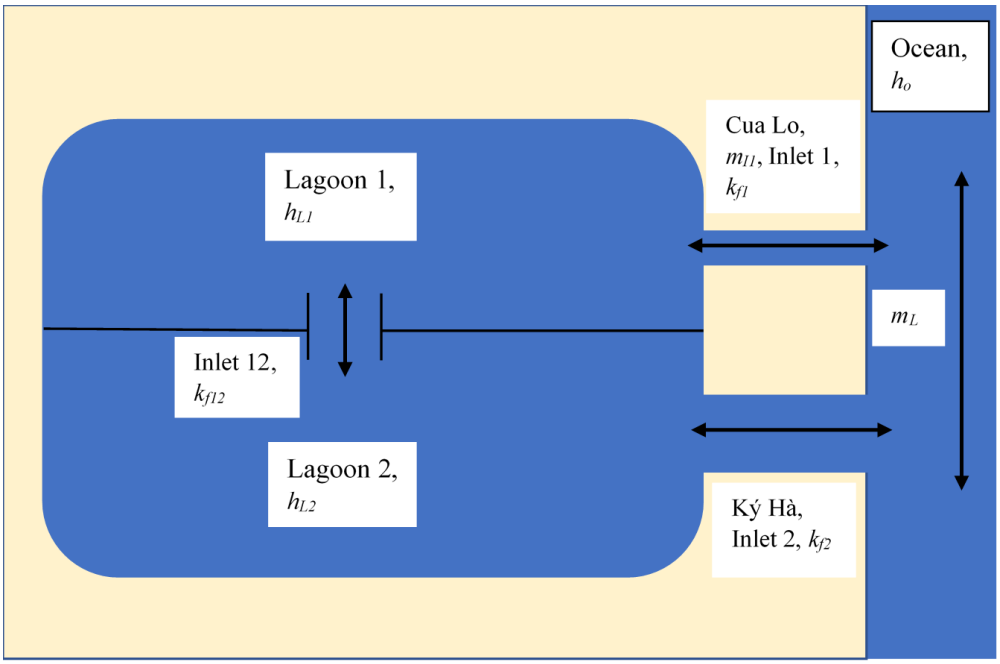

Figure 7. Conceptual model of Cua Lo area, including the estuaries, the two inlets connected to the sea, the inlet for exchange between the estuaries, the sediment transport in inlet 1 and the sediment transport alongshore.

4.1 Water exchange model

A simple mathematical model for water exchange between water bodies was developed by Keulegan (1967) which includes only river and tidal flow. The simplicity derives from that spatial water level differences in the water body and changes in area are not accounted for. The model is governed by two equations: the water volume conservation equation for the water body, and conservation of energy equation for connected inlets.

For water bodies with multiple inlets and river connections, the volume conservation equation can be expressed as:

$$\frac{d(A_L h_L)}{dt} = \sum_{i=1}^{n} \left(Q_{I,i} + Q_{R,i}\right) \tag{11}$$

A_L is the surface area of the estuary (assumed constant), h_L is the water level in the estuary, $Q_{I,i}$ and $Q_{R,i}$ are the volumetric flows in the inlets and rivers, respectively. Water velocities ($u_{I,i}$) in the inlets can be obtained by using the energy equation between each inlet and the ocean, resulting in the equation:

$$h_o = h_L + k_{f,i} \frac{u_{I,i}|u_{I,i}|}{2g} \tag{12}$$

The pressure-term is excluded on both sides of the equation since it is assumed that the pressure is the same in the ocean and the lagoon. The velocity-term is neglected since it is assumed that it is small in comparison with the other terms. "h_o" represents the ocean water level and $k_{f,i}$ is a loss coefficient which includes entrance, exit and friction losses for each inlet, respectively. The velocity in the inlet is a vector and has a direction, but in the calculations is it always considered to be positive since both directions are scouring the inlet and causes sediment transport. With this assumption, Equation 12 can be expressed as below (Equation 13):

$$u_{I,i} = \sqrt{\frac{2g(h_o - h_L)}{k_{f,i}}} \tag{13}$$

To include the situations where $h_o < h_L$ an implicit expression for flow direction is used, resulting in:

$$u_{I,i} = \sqrt{\frac{2g}{k_{f,i}}} * \frac{(h_o - h_L)}{\sqrt{|h_o - h_L|}} \tag{14}$$

Rewriting the volumetric inflow at the inlet into $A_{I,i}\, u_{I,i}$ and inserting the expression for $u_{I,i}$, and dividing each term by A_L Equation 14 can be written as:

$$\frac{d(h_L)}{dt} = \sum_{i=1}^{n} \frac{A_{I,i}}{A_L}\left(\sqrt{\frac{2g}{k_{f,i}}} * \frac{(h_o - h_L)}{\sqrt{|h_o - h_L|}} + \frac{Q_{R,i}}{A_L}\right) = \sum_{i=1}^{n}\left\{\left(\frac{A_{I,i}}{\sqrt{k_{f,i}}}\right)\left(\frac{\sqrt{2g}}{A_L} * \frac{(h_o - h_L)}{\sqrt{|h_o - h_L|}}\right) + \frac{Q_{R,i}}{A_L}\right\} \quad (15)$$

For an estuary with two inlets, where the water levels are varying spatially different, it is also possible to describe the exchange within the estuary by dividing it into two estuaries with an interconnecting inlet between the estuaries (Van de Kreeke, 2017). Each estuary has an inlet for the water exchange with the ocean and one common inlet in between which is taking into consideration that water is exchanged between the estuaries. The flow between the inlets is assumed to be continuous, implying that the continuity equation is applied. The flow in one estuary is the same in the other, but the lagoon area and the velocity differs. The continuity equation states that the flow is continuous from one point to another, expressed as the velocity (u_L) times the area (A_L).

$$Q_{L1} = Q_{L2}$$
$$u_{L1}A_{L1} = u_{L2}A_{L2} \quad (16)$$

The exchange between lagoon 1 and 2 is described with the energy equation from a point in lagoon 1 to a point in lagoon 2. The velocity term in the energy equation is neglected since the velocity is assumed to be small in comparison with the other terms. Index 12 denotes the position in the inlet in between the estuaries.

$$h_{L1} = h_{L2} + \frac{k_{f12}|u_{12}|u_{12}}{2g} \quad (17)$$

The velocity in the interconnected inlet can be expressed in terms of the flow (Q_{12}) and the area (A_{12}) in the inlet and rearranged into Equation 18.

$$Q_{12} = \sqrt{\frac{A_{12}^2}{k_{f12}}(h_{L2} - h_{L1})2g} \tag{18}$$

To take the sign into consideration and avoid that the denominator becomes negative, Equation 18 is expressed as:

$$Q_{12} = A_{12}\sqrt{\frac{2g}{k_{f12}}}\frac{h_{L2} - h_{L1}}{\sqrt{|h_{L2} - h_{L1}|}} \tag{19}$$

The volume conservation equation can be expressed according to Equation 20a. The equation describes the change in volume with time for lagoon 1 when the change in volume only depends on the in- and outflows to and from the estuary. This is the case if lagoon 1 has three inflows, from the ocean (Q_{I1}), from a connected river (Q_R) and exchange with the other lagoon (Q_{12}).

$$\frac{d(A_{L1}h_{L1})}{dt} = Q_{I1} + Q_R + Q_{12} \tag{20a}$$

Equation 20a can be expressed as Equation 21a when a numerical approach is applied and the expression for each flow are inserted.

$${h_{L1}}^{k+1} = {h_{L1}}^{k} + \frac{\Delta t}{A_{L1}}\left\{\begin{array}{l}\left(A_{I1}\sqrt{\frac{2g}{k_{f1}}}\right)\left(\frac{({h_o}^{k} - {h_{L1}}^{k})}{\sqrt{|{h_o}^{k} - {h_{L1}}^{k}|}}\right) + Q_R + \\ A_{12}\sqrt{\frac{2g}{k_{f12}}}\left(\frac{({h_{L2}}^{k} - {h_{L1}}^{k})}{\sqrt{|{h_{L2}}^{k} - {h_{L1}}^{k}|}}\right)\end{array}\right\} \tag{21a}$$

The same approach is applied to describe the water level in lagoon 2. The volume conservation equation includes the flow through inlet 2 (Q_{I2}) and the flow between the lagoons (Q_{12}).

$$\frac{d(A_{L2}h_{L2})}{dt} = Q_{I2} + Q_{12} \tag{20b}$$

The water level in lagoon 2 is described in Equation 21b. A numerical approach is used, the expression for each volumetric flow is inserted and the direction is taken into consideration.

$$h_{L2}{}^{k+1} = h_{L2}{}^{k} + \frac{\Delta t}{A_{L2}} \left\{ \begin{array}{l} \left(A_{I2} \sqrt{\frac{2g}{k_{f2}}} \right) \left(\frac{(h_o{}^{k} - h_{L2}{}^{k})}{\sqrt{|h_o{}^{k} - h_{L2}{}^{k}|}} \right) + \\ A_{12} \sqrt{\frac{2g}{k_{f12}}} \left(\frac{(h_{L2}{}^{k} - h_{L1}{}^{k})}{\sqrt{|h_{L2}{}^{k} - h_{L1}{}^{k}|}} \right) \end{array} \right\} \tag{21b}$$

4.2 Inlet sediment transport

Watanabe et al, (1991) developed a formula describing the sediment transport in an inlet channel (m_I). The formula includes the bottom shear stress of the inlet channel (τ_I), the critical shear stress for the sediment transport in the channel (τ_{cr}), the water density (ρ), an empirical transport coefficient (k_w), the width of the inlet channel (W_{I1}) and the velocity in the inlet (u_I). If the shear stress in the inlet is less than the critical shear stress ($\tau_I < \tau_{cr}$) then the sediment transport in the inlet is considered to be zero. The inlet sediment transport is always considered to be positive since both directions of the inlet sediment transport are scouring the inlet and causes sediment transport.

$$m_I = k_w \left(\frac{\tau_I - \tau_{cr}}{\rho g} \right) u_I W \tag{22}$$

The shear stress in the channel (τ_I) is obtained from the Darcy-Weisbach equation for shear stress in open channels, Equation 23. The equation includes the water density (ρ), the Darcy bottom friction factor (f_D) and the velocity in the channel (u_I).

$$\tau_I = \left(\frac{1}{8} \right) \rho f_D u_I^2 \tag{23}$$

The critical shear stress in the channel (τ_{cr}) is obtained from the Shield relation, Equation 24. The specific weight of water is denoted γ_w, the specific weight of the sediment particles is denoted γ_s, Θ_{cr} is Shield´s coefficient and D_s is the median particle diameter.

$$\tau_{cr} = \Theta_{cr}(\gamma_s - \gamma_w)D_s \tag{24}$$

Shield´s coefficient (Θ_{cr}) is calculated by using Equation 25, the empirical formula of Soulsby and Whitehouse (1997).

$$\Theta_{cr} = \frac{0{,}3}{1 + 1.2D_*} + 0.055(1 - e^{-0.02D_*}) \tag{25}$$

D_* is defined according to Equation 26.

$$D_* = \left(\frac{g(s-1)}{\nu^2}\right)^{\frac{1}{3}} \mathrm{D_s} \tag{26}$$

g is the gravitational constant, s is the specific weight of the sediment ($\frac{\rho_s}{\rho}$), D_s is the median grain size diameter referred to as D_{50}, and ν is the kinematic viscosity.

In an estuary with two inlets, the velocity in the two inlets can be described by the continuity equation for each inlet and by applying the energy equation from the ocean to the estuary via each inlet.

$$u_{I1} = \frac{Q_{I1}}{A_{I1}}$$

$$u_{I1} = \sqrt{(h_o - h_L)\frac{2g}{k_{f1}}}$$

$$u_{I2} = \frac{Q_{I2}}{A_{I2}}$$

$$u_{I2} = \sqrt{(h_o - h_L)\frac{2g}{k_{f2}}} \tag{27}$$

The volume conservation equation for lagoon 1 in the case with two connected lagoons (Equation 11), combined with the continuity equation for the inlet yields Equation 28. Q_R denotes the flow in the river and Q_{12} denotes the flow in the inlet which connects the two estuaries.

$$\frac{d(A_{L1}h_{L1})}{dt} = A_{I1}u_{I1} + Q_R + Q_{12} \tag{28}$$

If the velocity in inlet 1 is of interest and the area in estuary 1 (A_{L1}) is assumed to be constant, Equation 28 can be rearranged to Equation 29.

$$u_{I1} = \frac{dh_{L1}}{dt}\frac{A_{L1}}{A_{I1}} - \frac{Q_R}{A_{I1}} - \frac{A_{12}}{A_{I1}}\sqrt{\frac{2g}{k_{f12}}}\sqrt{h_{L2} - h_{L1}} \tag{29}$$

In order to solve the equation above, a numerical approach is used where the expression is discretized with a time step Δt. Both the lagoon water level, the water level in the sea and the flow in the river varies with time.

$$u_{I1}^{k+1} = \frac{(h_{L1}^{k+1} - h_{L1}^{k})}{\Delta t}\frac{A_{L1}}{A_{I1}} - \frac{Q_R}{A_{I1}} - \frac{A_{12}}{A_{I1}}\sqrt{\frac{2g}{k_{f12}}}\sqrt{h_{L2}^{k} - h_{L1}^{k}}$$

This equation can be rewritten in a similar way as the water exchange model, to include negative values of $h_o^k - h_L^k$, resulting in Equation 30.

$$u_{I1}^{k+1} = \frac{\left(h_{L1}^{k+1} - h_{L1}^{k}\right)}{\Delta t}\frac{A_{L1}}{A_{I1}} - \frac{Q_R}{A_{I1}} - \frac{A_{12}}{A_{I1}}\sqrt{\frac{2g}{k_{f12}}}\frac{\left(h_{L2}^{k} - h_{L1}^{k}\right)}{\sqrt{\left|h_{L2}^{k} - h_{L1}^{k}\right|}} \tag{30}$$

Inserting the expressions for the shear stresses into Equation 20 yields the final sediment transport formula in the inlet channel:

$$m_I = \frac{k_w u_{I1} W_{I1}}{\rho g}\left(\frac{1}{8}\rho f_D u_{I1}^2 - \theta_{cr} D_s(\gamma_s - \gamma_w)\right) \tag{31}$$

4.3 Longshore sediment transport

When estimating the LST, offshore wave height is a common input parameter to the calculation regime. Offshore waves can be represented in a couple of ways, but it is generally considered that their wave height can be described by a Rayleigh distribution curve. The root mean square (rms) wave height (H_{rms}) represents the wave heights in such a Rayleigh distribution and can be used to determine the design wave for LST. The significant offshore wave height (H_{so}) represents the average height of the one-third highest waves from measured waves and is a common design wave height. The significant wave height is defined in Equation 32.

$$H_{so} = \sqrt{2} H_{rms} \tag{32}$$

The wave energy flux conservation equation originates from the assumption that no energy is lost from an offshore point to the breaking point. The equation is developed from setting the energy flux at the offshore point equal to the energy flux at the breaker point. Equation 33 defines the energy flux, P, and Equation 34 shows the wave energy flux conservation equation from an arbitrary offshore point *"m"* to the breaking point.

$$P = \frac{1}{8}\rho g H^2 C_g \cos(\theta) \tag{33}$$

$$H_m^2 C_{gm} cos\theta_m = H_{sb}^2 C_{gb} cos\theta_b \tag{34}$$

The significant wave height at the breaker line (H_{sb}) and the angle between the wave crest and the shoreline (θ_b) describes the wave properties at the breaker line. The breaking wave properties are input parameters for computing the LST (US Army Corps of Engineers, 1984). These quantities are obtained by

using the wave energy flux conservation equation and Snell´s law (Equation 35).

$$\frac{sin\theta_m}{C_m} = \frac{sin\theta_b}{C_b} \tag{35}$$

H_s is the significant wave height, C_g is the group velocity, θ is the incident angle and C the velocity. The subscript m and b represents an arbitrary offshore point and breaking point, respectively.

Several assumptions are made when using Snell´s law. The wave energy between wave rays or orthogonals are assumed to remain constant. In the direction of the orthogonals, the wave advance is assumed to be perpendicular to the wave crest. At a given period and a specific location, the speed of the wave is only dependent on the depth at the location. It is also assumed that changes in the bottom topography are gradual. The waves are long-crested, has a constant period, a small amplitude and are monochromatic. The effects of winds, currents, reflections from beaches and variations in the underwater topography are assumed negligible (US Army Corps of Engineers, 1984).

The energy flux conservation equation and Snell´s law can be merged into one equation, Equation 36. The unknown angle in Snell´s law, the angle at breaking, is substituted into the energy flux conservation equation. Here, the breaking depth h_b is the unknown parameter (Larson et al., 2010).

$$H_m^2 C_{gm} cos\theta_m = \gamma_b^2 h_b^2 \sqrt{g h_b} \cos\left\{arcsin\left(sin\theta_m \frac{C_b}{C_m}\right)\right\} \tag{36}$$

$$\gamma_b = \frac{H_b}{h_b}$$

The breaker depth ratio γ_b is included in the equation. When the breaker depth ratio reaches its maximum value for which the waveform can remain stable, the waves start to break. This occurs at a breaker depth ratio of 0.78 (Bayram et.al, 2007; Nunes et.al, 2020). The parameter λ (Equation 37), introduced into Equation 36, yields Equation 38 (Larson et al., 2010).

$$\lambda = \frac{g h_b}{C_m^2} \tag{37}$$

$$\lambda^{\frac{5}{2}}\left(\frac{C_m}{\sqrt{gH_m}}\right)^4\frac{C_m}{C_{gm}}\frac{\gamma_b^2}{cos\theta_m}\cos\{arcsin(sin\theta_m\sqrt{\lambda}\,)\}=1 \qquad (38)$$

The parameter (α) is also introduced, and is defined as:

$$\alpha=\left(\frac{C_m}{\sqrt{gH_m}}\right)^4\frac{C_m}{C_{gm}}\gamma_b^2$$

Introducing the parameter α together with a trigonometric relationship yields:

$$\lambda^{\frac{5}{2}}\frac{\alpha}{cos\theta_m}\sqrt{1-\sin^2\theta_m\,\lambda}=1 \qquad (39)$$

If it is assumed that the angle of a breaking wave is small, the term including the square root will approach 1, this results in Equation 40. The subscript *a* denotes that it is an approximate solution in comparison with the linearized case where deep-water conditions are assumed at the offshore point, of the input parameters.

$$\lambda_a=\left(\frac{cos\theta_m}{\alpha}\right)^{\frac{2}{5}} \qquad (40)$$

Equation 38 can now be expressed as the following:

$$\left(\frac{\lambda}{\lambda_a}\right)^{\frac{5}{2}}\sqrt{1-\varepsilon\frac{\lambda}{\lambda_a}}=1 \qquad (41)$$

Where the parameter ε is defined according to:

$$\varepsilon=\frac{sin^2\theta_m(cos\theta_m)^{\frac{2}{5}}}{\alpha^{\frac{2}{5}}}=sin^2\theta_m\lambda_a \qquad (42)$$

When applied, this equation is solved with different values of ε by using the input wave angles. The correction factor delta (δ), defined as $\delta = \frac{\lambda}{\lambda_a}$ is then predicted from ε. Delta (δ) is multiplied with lambda (λ_a) to obtain the depth corrected lambda.

Once λ is obtained, h_b can be found from the definition of lambda (Equation 37). γ_b can then be used to obtain the breaking wave height (H_b).

When H_b is known, the breaking wave angle θ_b can be found from Equation 38 (the combination of energy flux conservation equation and Snell´s law), the definition can be seen below. The breaking wave properties act as input parameters to the CERC equation (Larson et al., 2010).

$$\theta_b = arcsin\left(sin\theta_m\sqrt{\lambda}\,\right)$$

The CERC equation, developed by the Coastal Engineering Research Centre of the US Army Corps of Engineers, describes the volume of sediment transported per unit time alongshore (m_L in m^3/s). The longshore transport rate includes both bed load and suspended load. The CERC equation is based on the principle that the longshore sediment transport (LST) is proportional to the longshore wave power (P) per beach length unit; $LST = K * P$, where K is a calibration coefficient (van Rijn, 2002). The CERC equation is only taking the sediment into consideration through the sediment density ρ_s and the porosity p. The grain size distribution and the slope are not taken into consideration. Regarding the factors influencing and generating the LST is the CERC equation (Equation 43) only taking the wave-generated currents into consideration (Bayram et.al, 2007). In the LST calculations, cross-shore processes like overwash of the barriers and berm-bar exchange, as well as effects from wave-current interactions are neglected.

$$m_L = k_L\left(\frac{\rho\sqrt{g}}{16\sqrt{\gamma_b}(\rho_s-\rho)(1-p)}\right)H_{br}^{2.5}\sin(2\theta_{br}) \qquad (43)$$

The flow of sediment is defined as m_L, k_L is a dimensionless empirical coefficient, ρ and ρ_s are the density of water and the sediment respectively, and p is the porosity of the sediment.

4.4 Inlet morphology

If an inlet is located in connection to a sand spit, the changes and dynamics of the sand spit in terms of elongation, migration and widening has to be taken into consideration when describing changes of the inlet in a model. Kraus (1999) derived a mathematical model to describe sand spit evolution. Equation 44 describes how the volume of the sand spit, defined as the cross-sectional area (A_s) times a small change in distance (x) integrated over a distance ($x = 0\ to\ x = x_s$), changes with time (t). This equals the inflow of sediment at the foot of the spit (Q_{IN}), minus the outflow of sediment at the head or tip of the spit (Q_{OUT}).

$$\frac{\delta}{\delta t}\left(\int_0^{x_s} A_s dx\right) = Q_{IN} - Q_{OUT} \tag{44}$$

In the case of spit growth at an inlet or river mouth, the spit growth is restricted, and cross-shore transport may erode the head or tip of the spit. In this case (Q_{OUT}) differs from zero and varies with time. For an elongating, growing sand spit is the sediment supplied via longshore transport and the contribution to the cross-sectional shape of the spit is caused by cross-shore transport. The response of the cross-shore transport is faster than the response of the longshore transport. Therefore, in a long-time perspective is it reasonable to assume that the cross-sectional area of a sand spit has reached an equilibrium and do not change ($A_s = A_e$) (Larson et.al, 2015).

Equation 44 may be developed by integrating the left side and by applying an approach where small changes in the spit morphology occurs during a short time perspective (dt).

$$\frac{d}{dt}\, A_s x_s = Q_{IN} - Q_{OUT} \tag{45}$$

By using a numerical approach, Equation 45 is developed into Equation 46. The current position of the sand spit is calculated for each time step Δt, where

"*k*" denotes a particular time step so that *k+1* is the index for x_s after one time step.

$$\frac{(A_s x_s^{k+1} - A_s x_s^k)}{\Delta t} = Q_{IN} - Q_{OUT} \tag{48}$$

The cross-sectional area of a sand spit (A_s), which has the shape of a trapezoid, can be described with Equation 47. B is the berm height, D_c is the depth of closure, W_s is the width of the sand spit, K_α is defined as $K_\alpha = \frac{1}{tan\alpha_s} + \frac{1}{tan\alpha_L}$. α_s and α_L are the slopes of the sand spit on the seaside and the land side, respectively. These quantities are all assumed to be constant.

$$A_s = (B + D_c)W_s\left(1 + \frac{K_\alpha(D_c - B)}{2W_s}\right) \tag{49}$$

Q_{IN} is the same as the longshore sediment transport (m_L) and Q_{OUT} is the same as the sediment transport through the inlet (m_I).

The numerical model can be developed into Equation 48.

$$\frac{(A_s x_s^{k+1} - A_s x_s^k)}{\Delta t} = m_L - m_I \tag{48}$$

To solve for the current position of the sand spit (migration), Equation 48 is rearranged to Equation 49.

$$x_s^{k+1} = \frac{m_L \Delta t}{A_s} - \frac{m_I \Delta t}{A_s} + x_s^k \tag{49}$$

Morphological changes of inlets are caused by the exchange of sediment through it. The exchange of sediment consists of the flow of sediment in the inlet due to river flows and tidal flows (m_I), and the flow of sediment alongshore due to nearshore breaking waves which generates a longshore sediment transport (m_L). The morphological changes in the inlet cross-sectional area with time is caused by the exchange of sediment which occurs both inside, and in the vicinity of the inlet. This relation is described in

Equation 50 below. The purpose of this model is to predict changes in the inlet width with time. The width is included in both the inlet cross-sectional area (A_{I1}) and in the inlet sediment transport (m_I). The longshore sediment transport (m_L) and the spit width (W_s) are assumed to be constant over a long-time perspective.

$$\frac{d}{dt}(A_{I1}W_s) = m_I - m_L \tag{50}$$

From the model it is possible to analyze evolution of the inlet in terms of narrowing, widening and closure of the inlet. When the sediment transport in the inlet (m_I) is larger than the sediment transport alongshore (m_L), the cross-sectional area (A_{I1}) is increasing through scouring of the inlet channel. When the transport alongshore is larger than the transport in the inlet channel, the cross-sectional area is decreasing due to accumulation of sediment in the channel (Nunes et.al, 2020).

It is assumed that the side slopes are constant and that the geometrical shape of the inlet channel remains as the width is changing. In this case is the inlet width and the area related via a shape coefficient (α). The value of α depends on the shape of the cross-section (Stive et al., 2010). The relation can be seen below:

$$W_{I1} = \alpha\sqrt{A_{I1}} \tag{51}$$

To model the width evolution over time, a numerical approach is applied to Equation 50:

$$\frac{\left(A_{I1}^{k+1} - A_{I1}^{k}\right)}{\Delta t} W_s = m_I^k - m_L$$

In order to solve for the inlet area, the equation is rearranged:

$$A_{I1}^{k+1} = \frac{\Delta t}{W_s}\left(m_{I1}^k - m_L\right) + A_{I1}^k$$

The expression for m_I is then inserted, which yields:

$$A_{I1}^{k+1} = \frac{\Delta t}{W_s}\left(\frac{k_w u_{I1}^k W_{I1}^k}{\rho g}\left(\frac{1}{8}\rho f_D u_{I1}^{k^2} - \theta_{cr} D_s(\gamma_s - \gamma_w)\right) - m_L\right) + A_{I1}^k$$

The shape factor is included to express the inlet cross-sectional area (A_{I1}) in terms of the inlet width (W_{I1}), resulting in Equation 52. The velocity in the inlet (u_{I1}) as well as the water level in lagoon 1 (h_{L1}^{k+1}) are affected by changes in the inlet cross sectional area. This is taken into consideration when deriving the final formula which describes the change in the inlet width with time. The expression which includes the shape factor and the inlet width (Equation 51) is inserted at all locations where the inlet area (A_{I1}^k) is present. See Appendix A1 for complete formula.

$$W_{I1}^{k+1} = \sqrt{\left(\frac{\alpha^2 \Delta t}{W_s}\left(\frac{k_w u_{I1}^k W_{I1}^k}{\rho g}\left(\frac{1}{8}\rho f_D u_{I1}^{k^2} - \theta_{cr} D_s(\gamma_s - \gamma_w)\right) - m_L\right) + W_{I1}^{k^2}\right)} \quad (52)$$

5. Modelling methods

5.1 Model input

A data collection survey performed by the Thuyloi University in Hanoi took place during one week in August (11th to 18th) and one week in November (12th to 19th) during 2019. Several measurements were performed in the Cua Lo area, both in the Cua Lo inlet, in the ocean outside Cua Lo inlet, in the Cua Lo estuary and in the Truong Giang river. Amongst the collected data, water levels in the lagoon, volumetric flows in the river, bathymetry in the area and sediment samples were used in the project. The locations of the measurement stations can be seen in Figure 8.

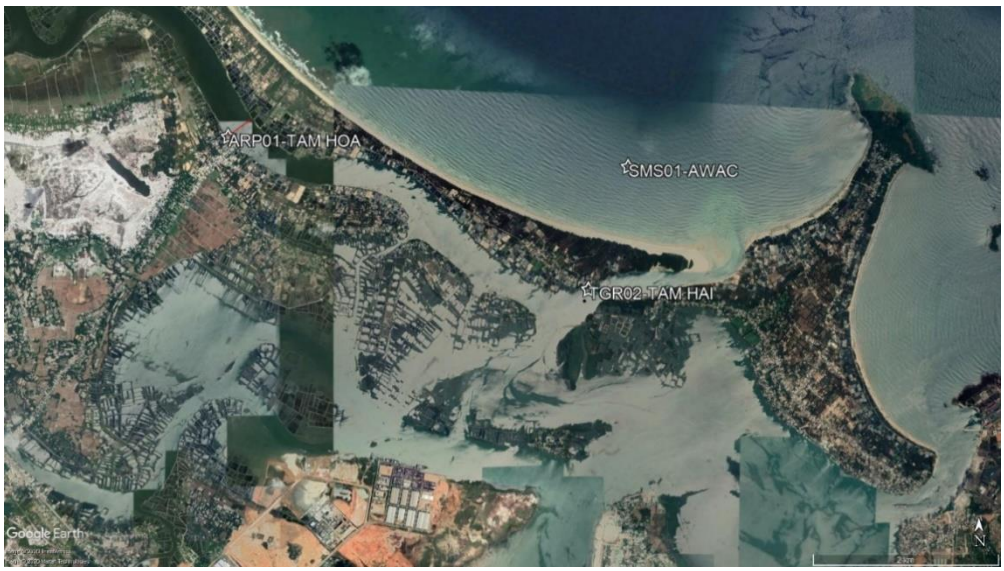

Figure 8. A map of the Cua Lo estuary and its vicinity including locations of the measuring stations from the survey in 2019, marked as stars. The red line at ARP01 defines the cross-section over which the flow was measured (Google Earth, 2020).

5.1.1 River analysis

River discharges were measured at an ARP (Across River Profiling) station (ARP01) in Truong Giang river (Tam Hoa) during the field survey in August and November (Figure 38 and 39, Appendix A2). The mean and median values in August were -41 m^3/s and -104 m^3/s, with a negative value meaning that water flows in the upstream direction. In November, the mean and median values were 50 m^3/s and 30 m^3/s. In addition to these measurements, data of

the discharge further upstream in the Truong Giang river (Q_{R1}) and at Song Cho river (Q_{R2}) based on precipitation measurements from 2017 were generated in the modelling program MIKE11 (see Figure 6 for river locations).

Initially a rainfall-runoff model was run in the program MIKE Nam to obtain the runoff from 2017. The output was then used as input to the hydraulic model in MIKE11, which generated flow data each hour for 2017 at the two locations. The river flow in Truong Giang (blue bars) and in Song Cho (orange bars) are shown in Figure 9. The y-axis shows flows in m^3/s, the x-axis shows time in days. Inflow during flood tide equals outflow during ebb tide during most of the year. In November and December, there is a net daily mean flow of 40 m^3/s in the rivers into lagoon 1. For some days in November the flow reaches above 100 m^3/s. The flow in Truong Giang is larger than the flow in Song Cho.

Spatial flow variations in MIKE21 during 2017 were also performed by Quang (2020) and showed that the river connecting the inlets has a zero-flow node along the channel. During flood tide, water is flowing from the ocean, into the estuaries, into the river, and flows a certain distance into the channel. During ebb tide, the reversed situation occurs. This is a consequence of flood tide and ebb tide from both directions, resulting in that Truong Giang river is acting more like a prolonged part of the estuary which contributes to the water exchange in the estuary (Figure 40 and 41, Appendix A2). Earlier studies in the area have assumed the section to be a river and included it as such, with a flow of 40 m^3/s (Nguyen et al., 2018 (a)). Indeed, the mean flow in Nov-Dec was also here found to be within the same range, but not for the rest of the year. With this background, the river inflows were excluded from the modelling process and some of the river network was included in the lagoon area.

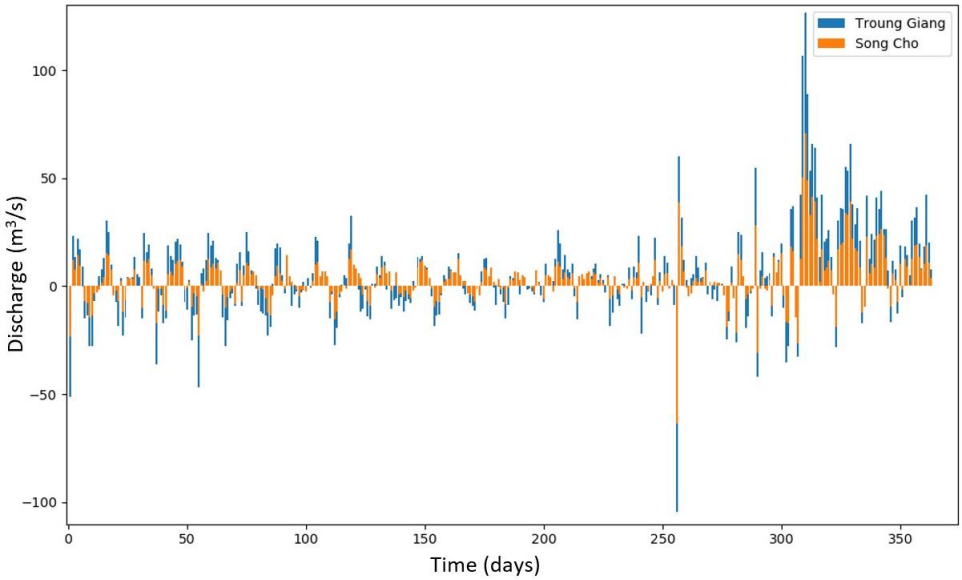

Figure 9. Simulated river flows in Truong Giang (blue bars) and in Song Cho (orange bars), using MIKE 11. The y-axis shows the mean daily flow in m3/s and the x-axis show time in days.

5.1.2 Water exchange model

Water levels in the estuary were recorded using a Tide Gauge Recording (TGR) at Tam Hai (TGR02) at an hourly interval. Ocean water levels were also recorded at an hourly interval, using a Seabed Mooring Station (SMS). An AWAC (Acoustic Wave and Current profiler) instrument was used at the station SMS01 to record water levels. Both of these water level measurements were performed simultaneously during the two measuring campaigns. These measurements were therefore chosen for model calibration.

A station at the same location as TGR02 was set up in August 2019, recording water levels every hour up until March 2020. Water levels recorded from this station, combined with simulated ocean water levels were used to validate the water exchange model results. The ocean water level data was generated from simulations performed using the Delft 3D Tide module. Input data for this simulation were harmonic constants (Table 7, Appendix A3) derived from long term measured water level data at Cua Dai inlet in Hoi An, about 50km north of Cua Lo. Ocean water levels were simulated from year 1988 to year 2049 at an hourly interval. Levels for 1988-2017 were used to calibrate the inlet migration, levels for 2019-2020 were used to validate the water exchange

model. The simulated predicted water levels in the ocean (2020-2049) were used as input to the model when the purpose was to predict future morphology.

The cross-sectional area for each inlet was determined from bathymetry measurements collected in November 2019. The bathymetry data points were processed in QGIS by using an IDW interpolation to create a Digital Elevation Model. A profile was drawn for each inlet at the narrowest part (Figure 42 and 43, Appendix A2) and cross-sectional areas were approximated with trapezoidal shapes.

Two satellite images (LANDSAT/Google Earth), one taken at a high and one at a low lagoon water level, were used for the lagoon area approximation. Polygon layers were drawn for each image and the mean surface area of the two polygons were used as area approximation. The land-water interface was estimated visually. After the entire area was estimated it was split into two subsections (Figure 44, Appendix A2) based partially on the bathymetry (Figure 45, Appendix A4), but also on the water exchange model results.

5.1.3 Inlet sediment transport

The sediment samples collected during the survey in 2019 consisted of both bottom and suspended sediment samples. The sediment in the Cua Lo area is, according to the 100 bottom sediment samples, characterized by a predominance of fine sand in the range of 0.1 to 0.25 mm in diameter. In the river, Truong Giang, D_{50} was about 0.16 mm, in the inlet and in the estuary D_{50} was 0.15 mm, and in the nearshore zone 0.17 mm. The grain size present in the area is clearly dominated by sand. The sediment diameter (D_s) was chosen as the median diameter (D_{50}) to be 0.15 mm.

The specific weight of the sediment (γ_s) was 2.66, and the value 1 was chosen for the specific weight of water (γ_w). The density of water (ρ) and the gravitational constant (g) were assumed to be 1000 kg/m^3 and 9.81 m/s^2 respectively. The initial width of the inlet channel (W) in 2019 was measured to be 165 m based on satellite imagery from 2019 in QGIS. Although the inlet has exhibited some width variation historically, a constant width was assumed for when the inlet is migrating (further discussed in section 5.3.3). The left and right limits of the width were defined as the section without possible tidal flats.

The empirical transport coefficient (k_w) was initially assumed to be 0.75. The Darcy friction factor (f_D) was assumed to be 0.03. k_w was later used to

calibrate the model by comparing the modelled and calculated spit migration with satellite images.

5.1.4 Longshore sediment transport model

The input wind data was obtained from the Japanese Meteorological Agency, measured at a meteorological station located at latitude 16 and longitude 108.625 in the East Vietnam sea (Figure 10). The offshore wave data was hindcasted based on the wind data by using the model SWAN. The offshore wave data included significant wave heights, wave periods and direction of the incoming waves in relation to true north. The data was collected from 1998 until the end of 2014 at three-hour intervals, and every hour for the consecutive three years, from 2015 till the end of year 2017 (Asplund and Malmström, 2018).

If offshore wave breaking was neglected, a Rayleigh distribution was suitable to represent the offshore wave heights (data not shown). The root mean square (rms) wave height (H_{rms}) represented the wave heights in the Rayleigh distribution. The significant offshore wave height (H_{so}) was then calculated from H_{rms} and used, as it is a common design wave height. The significant wave height represents the average height of the one-third highest waves from measured waves (US Army Corps of Engineers, 1984).

A point along the Cua Dai – Cua Lo littoral cell with a well-defined shoreline orientation of 56° was chosen to be the reference point for the LST calculation. North of Cua Lo inlet the Cham Islands are located (top middle in Figure 10). South of Cua Lo the An Hoa cape is located. Both Cham islands and An Hoa cape are shadowing the offshore waves which are entering the area and generates the longshore current (Asplund and Malmström, 2018). Measured relative to the point on the shore, the angles (-2° and 123°) to these structures were included to restrict the valid waves giving rise to the LST (Figure 10). In the figure the red line is representing true north, the blue line to the left of true north and the blue line second left of true north are marking the angles of shadowing. The first blue line to the right of true north represents the shoreline orientation, the line has an angle of 90 degrees to the shoreline. All lines are measured relative to true north.

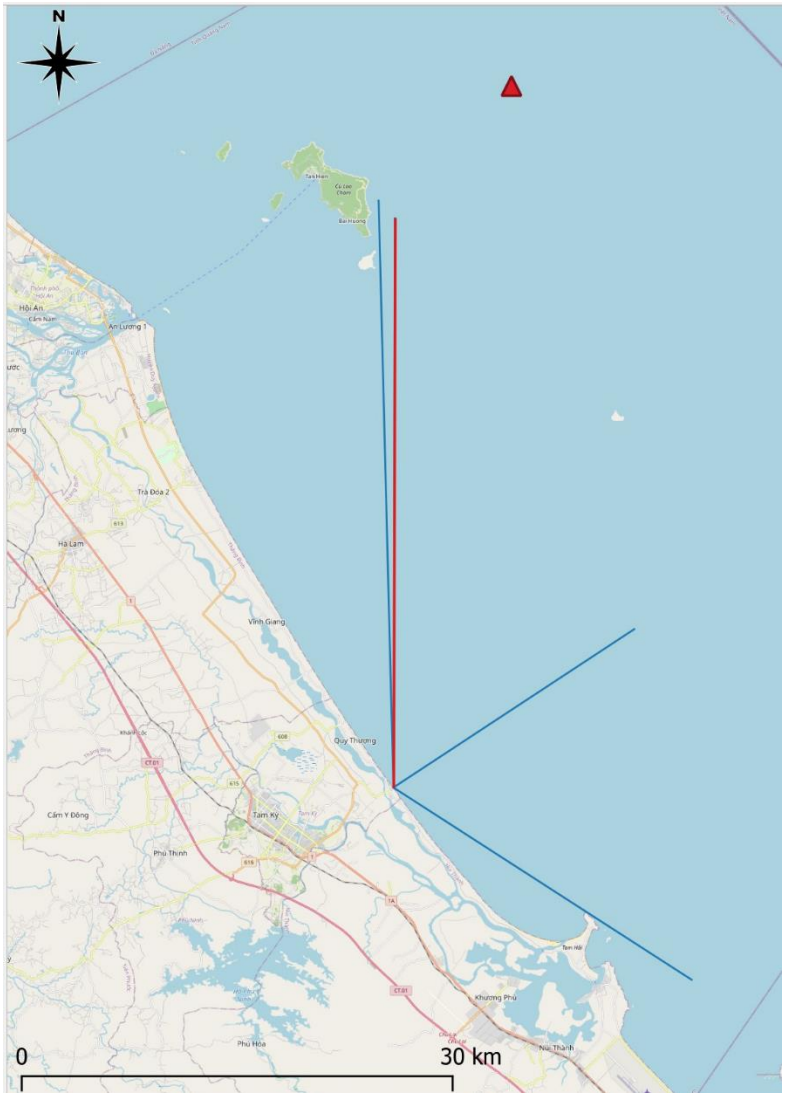

Figure 10. Map of the stretch between Cua Dai and Cua Lo, showing the location of the offshore wave bouy (red triangle) and the LST calculation point. The red line represents true north. The blue line to the left of true north (-2°) and the blue line second left of true north (123°) marks the angles of shadowing. The first blue line to the right of true north (56 degrees) represents the shoreline orientation.

In the calculation of the LST (Equation 32), k_L is a dimensionless empirical coefficient which range from 0.2 to about 2.2, depending on the study. It is recommended to use a value of 0.77 when using the root-mean-square wave height at breaking (Komar and Inman, 1970; Nunes et.al, 2020; van Rijn, 2002). When using the significant wave height (H_s) for the breaking wave height (H_b), the shore protection manual recommends a k_L value of 0.39. This

value was derived from the original field study year 1970 where tracers were used (Bayram et.al, 2007). With the significant wave height as input parameter for CERC, Schoonees and Theron (1993, 1996) have recommended a value of approximately 0.2 for k_L. The consultancy company Halcrow recommends a value of 0.195, which also coincides with modelled (M. Larson, personal conversation, 2020). The value of 0.195 was used in the calculations.

The sediment porosity (p) was assumed to be 40% (0.4), this is a common assumption in terms of sediment porosity (Nunes et.al, 2020; van Rijn, 2002). The sediment density (ρ_s kg/m^3) is equivalent to the sediment specific weight, which is defined as the mass per volume unit. The specific gravity of a sediment sample is the specific weight related to the density of water. In this study the water density ρ was assumed to be 1000 kg/m^3 when calculating the specific gravity of the sampled bedload sediment. This assumption was motivated as the samples were taken both in the river with fresh water and in the sea with saltwater. This causes the specific gravity of the sediment to be equivalent to the density and the specific weight of the samples. The 100 collected bedload sediment samples were collected in the area of Cua Lo, including the estuary, the river mouth, the inlet, Truong Giang river and in the nearshore zone in the sea. The specific gravity representing the bedload sediment in the area was determined by calculating the specific gravity of the 100 collected bedload samples. Then, a mean value was calculated which resulted in an average specific weight of 2,66 and a sediment density of 2660 kg/m^3.

5.1.5 Inlet morphology

For the cross-sectional area of the sand spit, Equation 48 (section 4.4) was used and a trapezoidal cross-sectional shape was assumed. Duy et al. (2017) found the depth of closure in the area to be 6 m, which was also used here. The berm height was estimated based on the bathymetry measurements in Cua Lo to 1.4 m; and α_s, α_L to 2.3° and 1.8°, respectively. Spit width was estimated from satellite imagery to 280 m. With these parameters, the resulting spit cross-sectional area was calculated to 3000 m^2.

5.1.6 Modelled scenarios

Two scenarios were considered in the modelling of the sand spit migration and the evolution of the inlet width. This first scenario assumes that the spit

migration stops after migrating a distance of 980 m past the current position. The spit and inlet are assumed to migrate along the blue line in Figure 12 and stop at the location where the blue and red line meet. This point was chosen for two reasons. Firstly, as a visual estimation of where the rocky boundary could begin as no information of where it actually starts could be found. Secondly, as an estimated distance after which the LST calculation model was no longer considered valid.

At the curvature along Tam Hai the spit migration is no longer directed towards SE, but more towards NE. As the beach curves and the wave shadowing of the An Hoa cape increases, LST validity is assumed to decrease. The chosen LST model does not consider processes governing interaction between inlet and the LST, refraction phenomena around the cape, or cross-shore dynamics etc.

Knowing that the LST value becomes less valid along the curvature, LST was still estimated in the 980 m point to give a ballpark indication of how realistic the scenario is. The resulting transport can be seen in Figure 11. LST is much smaller compared to the transport calculated at the point north of the inlet, and only negative transport is observed. The angles used were -38 degrees for shoreline orientation, -15 degrees for left limit of shadowing and 11 degrees for right limit of shadowing, the angles were measured from true north. Indeed, the values are significantly lower, with a net annual LST of -30 000 m^3. If the LST in Figure 11 was to be used, all values would be disregarded in the model since all values are negative. The model in turn is not adapted to handle a situation without any LST. In fact, the LST was calculated at some positions along the migration path between 1988 and 2017. None of these resulted in an LST in the realistic range compared to the migration rate, as the model predicted very low values and mainly negative LST. The 980 m point was therefore chosen and kept as an approximated location of where the LST becomes reduced enough to cause the spit migration to decrease enough to assume that the migration stops. LST was decided to be kept constant as the uncertainties in the LST values along the curvature were considered too high. When the inlet reaches the boundary only width variations are taken into consideration.

In order to introduce some indication of what such a scenario could look like, the sub-scenario of an LST-equilibrium somewhere along the migration path was investigated in the sensitivity analysis (section 6.4).

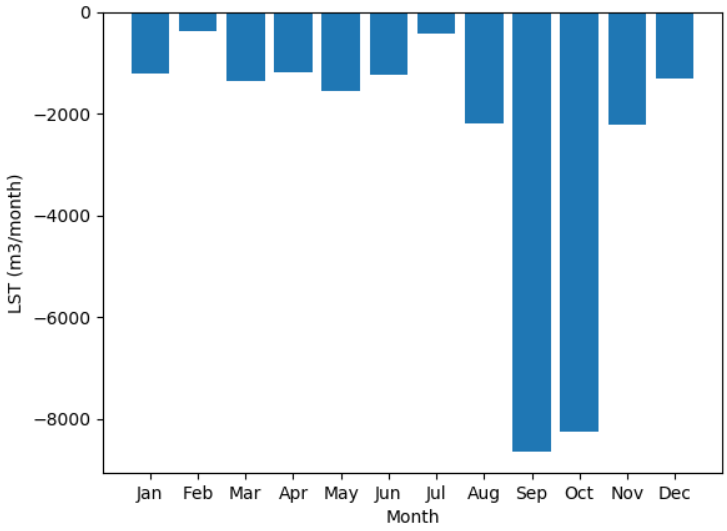

Figure 11. LST calculated at the point used in scenario 1, where the inlet migration is assumed to stop. The graph shows mean LST for each month based on data from 1988 to 2017.

The second scenario assumes that the sand spit together with the inlet continues to migrate towards a hard boundary at the An Hoa cape. The spit is assumed to migrate along the green line and stop at the cape (end of the green line) (Figure 12). The possible total migration distance (the distance along the green line) is 2000 m from the current position. Here, the preceding argument on LST validity is disregarded and the entire formation attached to An Hoa Cape is assumed to consist of sand only. As stated for Scenario 1, the validity of the assumption of non-changing LST is crude, and this should be considered a worst-case scenario for the inhabitants on the migration path.

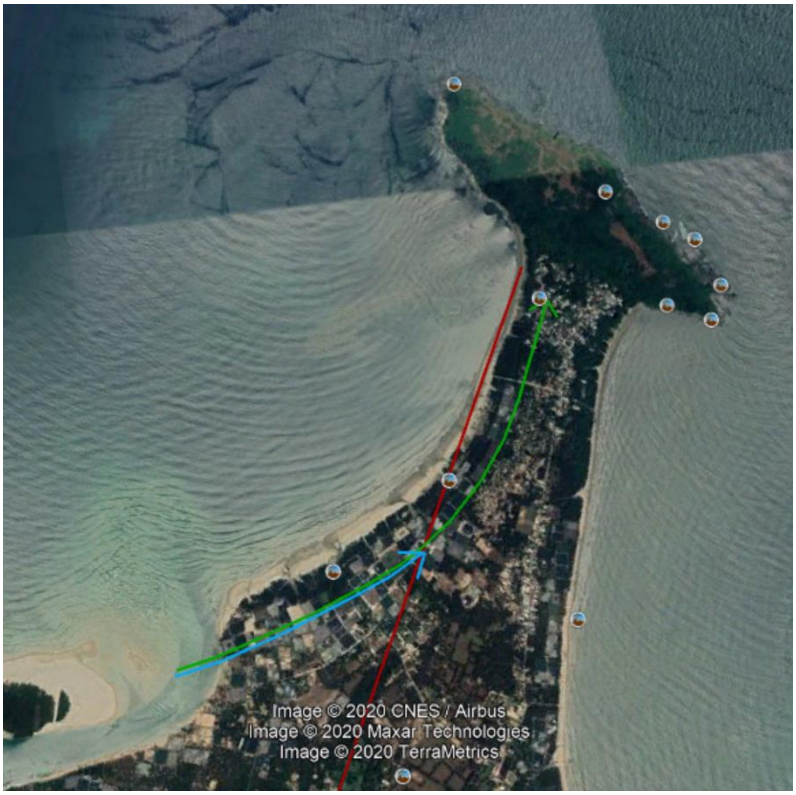

Figure 12. The two different modelled migration paths for the sand spit and the inlet. The red line represents the stop for the first scenario, which follows the blue line, and the green line represents the assumed migration path if An Hoa cape is the only hard boundary.

A summary of all constants which are used as input parameters in the modelling process is depicted in Table 3 below. The four columns in the table contains the name of the constant, the value including the unit, a short description of the constant, and if it was calibrated or measured.

Table 3. A collection of constants used in the equations and models, and the corresponding values.

Constant	***Value (unit)***	***Description***	***Calibrated (Yes/-)***
A_{L1}	13 (km^2)	Area of lagoon 1	-
A_{L2}	18 (km^2)	Area of lagoon 2	-
A_{I1}	588 (m^2)	Area of inlet 1	-
A_{I2}	2571 (m^2)	Area of inlet 2	-
A_{12}	400 (m^2)	Area of interconnecting inlet	Yes
k_{f1}	26	Loss coeff. inlet 1	Yes
k_{f2}	15	Loss coeff. inlet 2	Yes
k_{f12}	35	Loss coeff. interconnecting inlet	Yes
A_s	3000 (m^2)	Spit cross-sectional area	-
W	165 (m)	Initial inlet width	-
ρ	1000 (kg/ m^3)	Water density	-
g	9.81 (m/s^2)	Gravitational const.	-
k_L	0.195	Empirical transport coefficient	-
ρ_s	2660 (kg/ m^3)	Sediment density	-
p	0.4	Sediment porosity	-
γ_b	0.78	Breaker parameter	-
k_w	0.8	Sediment transport coefficient	Yes
f_D	0.03	Darcy friction	-
θ_{cr}	0.299	Shield's number	-
D_{50}	0.00015 (m)	Median sediment diameter	-
γ_w	1	Specific weight of water	-
γ_s	2.66	Specific sediment weight	-
α	7.47	Shape coefficient	-
W_S	280 (m)	Spit Width	-

5.2 Model Implementation

Below (Figure 13), a schematized diagram of the modelled processes and input/output values is illustrated. The illustration serves as a guidance for better understanding of the modelling sequence and the general principles around it. All the parts of the model were built in the programming language Python. Details about the implementation of each process can be found in the following paragraphs.

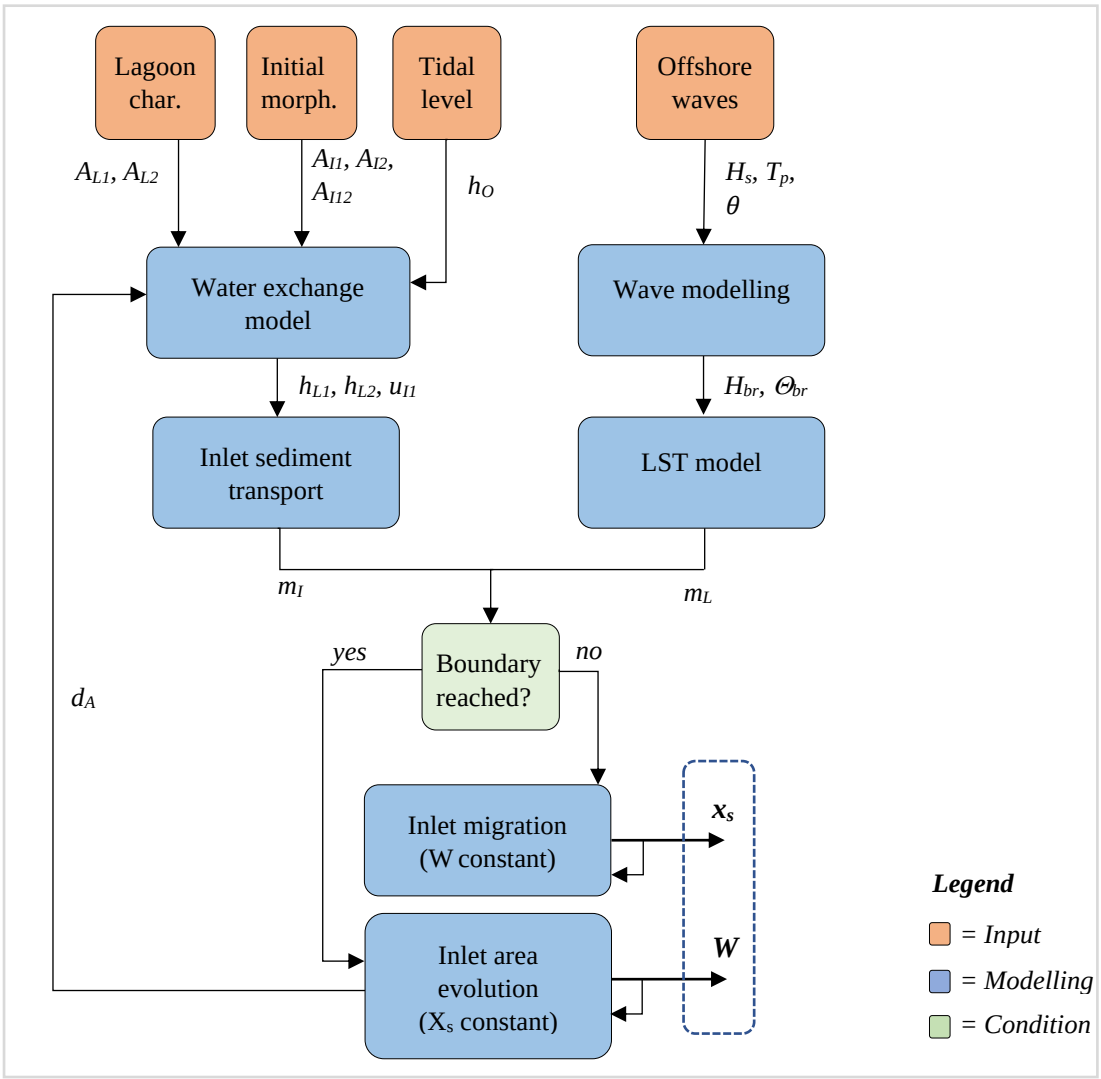

Figure 13. Schematized figure of the modelling process. Orange boxes include input parameters, blue boxes represent modelling steps, and green boxes includes a condition.

The final equations used to calculate the water levels for each time step in lagoon 1 and 2 were Equation 21a and 21b, respectively. The term which included the river flow (Q_R) was removed, the former river is instead included in the area of estuary 1 (A_{L1}).

$$h_{L1}{}^{k+1} = h_{L1}{}^{k} + \frac{\Delta t}{A_{L1}} \left\{ \begin{array}{l} \left(A_{I1} \sqrt{\frac{2g}{k_{f1}}} \right) \left(\frac{(h_o{}^{k} - h_{L1}{}^{k})}{\sqrt{|h_o{}^{k} - h_{L1}{}^{k}|}} \right) + \\ A_{12} \sqrt{\frac{2g}{k_{f12}}} \left(\frac{(h_{L2}{}^{k} - h_{L1}{}^{k})}{\sqrt{|h_{L2}{}^{k} - h_{L1}{}^{k}|}} \right) \end{array} \right\} \qquad (21a)$$

$$h_{L2}{}^{k+1} = h_{L2}{}^{k} + \frac{\Delta t}{A_{L2}} \left\{ \begin{array}{l} \left(A_{I2} \sqrt{\frac{2g}{k_{f2}}} \right) \left(\frac{(h_o{}^{k} - h_{L2}{}^{k})}{\sqrt{|h_o{}^{k} - h_{L2}{}^{k}|}} \right) + \\ A_{12} \sqrt{\frac{2g}{k_{f12}}} \left(\frac{(h_{L2}{}^{k} - h_{L1}{}^{k})}{\sqrt{|h_{L2}{}^{k} - h_{L1}{}^{k}|}} \right) \end{array} \right\} \qquad (21b)$$

Since the cross-sectional area of inlet 2 is large, and much larger than that of inlet 1, it was assumed that the water level in estuary 2 increases faster. This causes water to flow from estuary 2, through the connecting inlet, to estuary 1 to even out the water levels and achieve equilibrium. Therefore, the reference system was defined so that the positive direction for the velocities is from the ocean, through the inlets and into the estuaries, and from estuary 2 to estuary 1.

For the two calibration periods, measured ocean levels (SMS01) were resampled into 1 min intervals and interpolated linearly before using them as input to the model. The initial ocean water levels at time *t = 0* together with measured values for estuary surface area and initial guessed values for the loss coefficients acted as initial model input. The model was then run for subsequent ocean water levels for each time step of 60 s over the entire

measured period. The resulting modelled lagoon water levels were compared to the measured lagoon levels (TGR02) for calibration.

Inlet 2 has a crucial impact on the water levels in the estuaries. Since the cross-sectional area of inlet 2 is larger than the one in inlet 1, the water level increases at a higher rate in estuary 2. Therefore, the inlet interconnecting the estuaries acts to limit the impact from inlet 2 on estuary 1. Without the division of the total estuary and introduction of the connecting inlet, the effect from inlet 2 on the water levels in estuary 1 becomes too large in comparison with the impact on the lagoon water levels from inlet 1. The impact from inlet 2 is reduced by choosing an appropriate cross-sectional area and loss coefficient of the interconnecting inlet. Larger loss coefficient results in smaller influence from inlet 2 on lagoon 1.

For the validation period 2019-2020 the calibrated parameters set in the calibration period were used together with the simulated ocean water levels using a time step of 10 min. This specific time step was used since the model was fast enough to handle it, and a much larger time step for the lagoon measurements gave a somewhat unstable behaviour of the model (Figure 46 and 47, Appendix A5).

For the simulation period of 2020-2049, inlet sediment transport and the preceding processes were calculated with a timestep of 10 min. For every time step, the simulated ocean water level for the actual and consecutive time step was used in Equation 30 (section 5.2) to obtain the inlet velocity. The velocity was then used in the final equation for the inlet sediment transport (Equation 31) below:

$$m_I = \frac{k_w u_{I1} W_{I1}}{\rho g}\left(\frac{1}{8}\rho f_D u_{I1}^2 - \Theta_{cr} D_s(\gamma_s - \gamma_w)\right) \tag{31}$$

For six consecutive time steps, i.e. one hour, the inlet sediment transport was stored in a list. Every sixth time step, the median value of this list was calculated and used in the morphological model.

The final equation used to calculate the longshore sediment transport can be seen below, Equation 43.

$$m_L = k_L\left(\frac{\rho\sqrt{g}}{16\sqrt{\gamma_b}(\rho_s - \rho)(1-p)}\right) H_{br}^{2.5}\sin(2\theta_{br}) \tag{43}$$

Offshore wave data from 1988-2017 containing; date, significant wave height, wave period and the wave direction was used as input. The waves were sorted for right and left boundary conditions, related to the shoreline orientation, and then transformed to the nearshore breaking wave point. To obtain the breaking wave properties, the energy flux conservation equation combined with Snell´s law was used. These properties were then used in the CERC equation to calculate the longshore sediment transport. The transport direction from northwest to southeast was determined as the positive transport direction. The approximate method created by Larson et.al, (2010), was used.

The LST model returns the average annual positive, negative, net and gross longshore sediment transport for each year. In addition, it also returns the LST for every 3 h expressed as m^3/3 h for the entire period. Since the values from 2015-2017 were collected at an hourly interval, these were summed into three-hour values.

To use the models for predictions of future morphological changes of the inlet and the sand spit, a simplification had to be done. Both elongation of the sand spit and change in the inlet width takes place at the same time. A certain amount of sediment is depositing on the tip of the spit, leading to the erosion on the downdrift side. A certain amount is adding to the ebb shoal, and a portion is transported past the inlet as described in (2.1.7.3 Sediment bypassing). The relation between these quantities and the exact amounts are varying and are unknown since it is very difficult to measure and determine. To be able to take this into consideration in the models it is necessary to know the relations, which was outside the scope of the project. It was therefore assumed that the sand spit is initially elongating with a constant inlet width, an assumption deemed reasonable from the calibration of the model (section 5.3.3). This implies that the deposition of sediment on the north side of the inlet is balanced by the amount of erosion on the downdrift side of the inlet.

Hourly mean values from the three-hour LST values, and the absolute value of the hourly median of the inlet sediment transport was used in the final sand spit migration equation (Equation 49) to calculate the longshore sand spit migration. If the LST was negative for a certain time step, the migration was set to zero for the same time step. The background for this is that no observation was made in the validation where the inlet moves “backwards” over a period on an annual basis, which would happen if these events are not excluded.

$$x_s^{k+1} = \frac{m_L \Delta t}{A_s} - \frac{|m_I| \Delta t}{A_s} + x_s^k \tag{49}$$

This model is based on the assumption that the inlet width is constant, and the morphological changes with time occurs due to elongation of the sand spit. The elongation occurs due to longshore sediment transport causing deposition of sediment at the tip of the sand spit, northwest of the Cua Lo inlet. It is assumed that the elongation occurs until the sandspit and inlet reaches the boundary of the scenario that is run (either 980 m or 2000 m).

Before every hourly update of the spit migration, a check in the program was performed to see if the spit had reached its boundary. If not, the model process continued to use the spit migration routine. However, if it had, the equation describing the inlet width variation (Equation 52) was initiated and the migration model sequence was terminated.

$$W^{k+1} = \sqrt{\left(\frac{\alpha^2 \Delta t}{W_s}\left(\left|m_I^k\right| - m_L\right) + W^{k^2}\right)} \tag{52}$$

The model describes how the inlet width is changing via narrowing and widening due to the inlet sediment transport and the LST. Both the inlet transport and the LST are changing during the year, which in term affects the inlet in different ways and results in different morphological changes.

If the wave and water level conditions were assumed to be constant, the cross-sectional area of the sand spit could be assumed to approach an equilibrium over long time perspectives. Further, the spit growth is restricted, and the effect of the cross-shore transport was assumed negligible in the long term. It was therefore reasonable to assume that the cross-sectional area for the sand spit had reached an equilibrium ($A_s = A_e$) (Larson et.al, 2015).

5.3 Calibration and validation

5.3.1 Water exchange model

Calibration of the water exchange model was done by comparing the final calculated water levels in the lagoon (h_L) with the water levels measured in the lagoon during the survey in August and November 2019. Loss coefficients for

each inlet and the area of the interconnecting inlet were calibrated, one factor at a time. The areas of the two subsections of the lagoon were also adjusted slightly in order to improve the model result. Small adjustments were considered to be justified since the boundary between the two areas was somewhat undefined. The relation between the two lagoon areas has a large effect on the velocity through inlet 1 and in turn the sediment transport through the inlet. Specifically, the relation between the area of lagoon 1 and the inlet cross-sectional area has the largest effect on the inlet velocity if the lagoon area is large and the inlet area is small, resulting in a large quotient. This relation together with a small quotient between the cross-sectional area of the interconnecting inlet and the cross-sectional area of inlet 1 results in the largest velocity through inlet 1, due to the area relations (see Equation 30).

Changes in the three loss coefficients were affecting the amplitude and the phase of the lagoon water levels. When the loss coefficients were changed, both the amplitude and the phase of the lagoon water levels changed. Although some level of priority was designated to the phase alignment, the fitting of the amplitude of the calculated water levels is also of high importance. When the velocity of inlet 1 was calculated (Equation 42) the lagoon level difference between the present and preceding time step, as well as the level differences between the two lagoons defines the velocity. The gradient between these level differences is both dependent on the phase and the amplitude. The amplitudes affect the level difference between the time steps in lagoon 1, whereas the phase has a higher effect on the level difference between the lagoons. Thus, both the amplitude and phase were taken into consideration but since these never fitted simultaneously, a compromise between the two was made.

The loss coefficient in the interconnecting inlet has a large effect on the inlet velocity. It is possible to see in Equation 30, which describes the velocity in inlet 1, that a larger friction coefficient (k_{f12}) results in a larger velocity through inlet 1 and in turn a larger transport though the inlet. This causes the effect from lagoon 2 on inlet 1 to become reduced. The calibration of the model was considered acceptable when the calculated and the measured lagoon water levels were as close as possible.

Hoi An, the station at which the tidal constituents were derived was the closest location to Cua Lo with a complete harmonic analysis. Ocean water levels based on simulated values of h_o for a different location may not be optimal, but since the measuring stations outside Cua Lo were only temporary, a complete and accurate harmonic analysis could not be performed there.

Since the ocean water levels used in the modelled future scenario were simulated from tidal constituents some distance away from Cua Lo, a comparison between simulated and measured ocean water levels was made. Figure 14 shows both measured and simulated ocean water levels during a week in August year 2019. The blue line represents measured ocean water levels outside Cua Lo inlet (at measuring station SMS01), and the black line represents simulated ocean water levels in Hoi An. Variations of the water level over time are similar, both with mixed diurnal tidal variations. The peaks of the blue line are higher, with local maxima of 0.6 m compared to the peaks of the black line which reach local maxima of around 0.2 m. The local minimum values are lower for the simulated sea water levels, with a magnitude of around -0.6 m. The black line is phase shifted to the right.

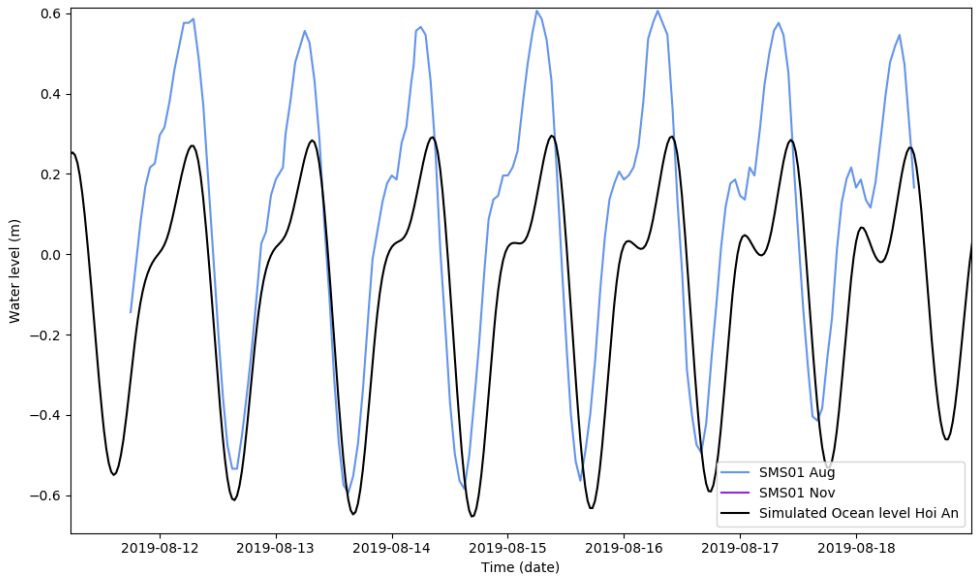

Figure 14. Measured and simulated water levels during a week in August 2019. The blue line represents measured ocean water levels outside Cua Lo inlet, the black line represents simulated sea water levels in Hoi An.

Figure 15 depicts the same as Figure 14, but during a week in November 2019. Measured ocean water levels outside Cua Lo inlet (at measuring station SMS01) are shown by the purple line, while the black line represents simulated ocean water levels in Hoi An. The appearance in terms of the water level variations with time are similar to August, both with mixed diurnal tidal variations. The peaks of the purple line are higher, with local maxima above 0.8 m whereas the peaks of the black line reach a local maximum of about 0.6

m. The local minimum values coincide rather well, with a magnitude between -0.3 m and -0.4 m. The graphs coincide well in terms of phase.

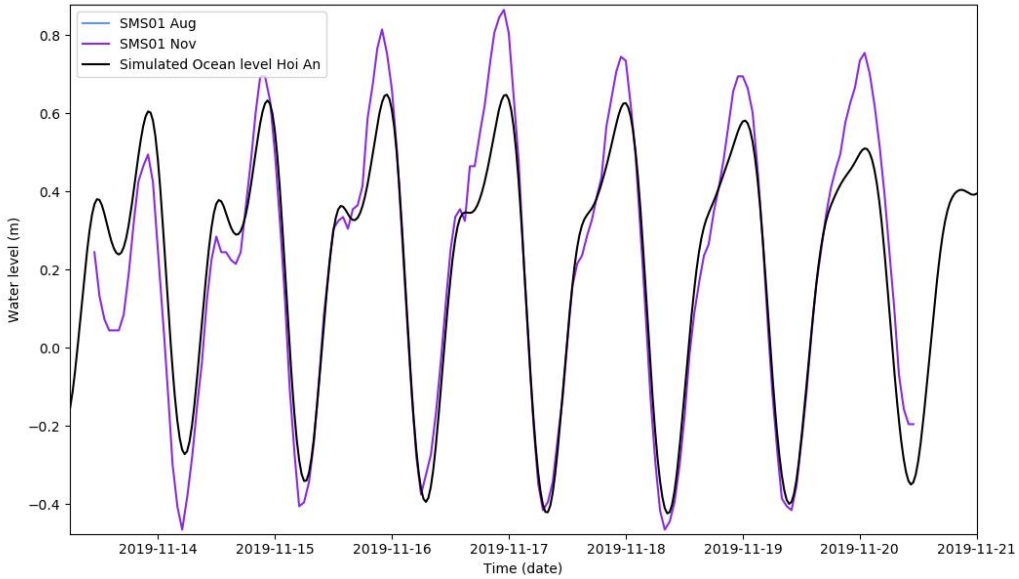

Figure 15. Measured and simulated water levels during a week in November 2019. The purple line represents measured ocean water levels outside Cua Lo inlet, the black line represents simulated sea water levels in Hoi An.

An aspect that should be considered when discussing the details of the water levels is short term water level variation. When performing the harmonic analysis, local irregular water level fluctuations such as storm surges or non-tidal wave action are excluded. Such effects could have influence on SMS01, leading to some of the observed differences. Altogether, the general pattern of the ocean water level variation is represented by the simulated data and was considered to be representative as input data for the long-term simulations.

Simulated lagoon water levels, based on the simulated ocean data, were validated towards the data set from TGR02 for 2019-2020. A randomly selected period with the behaviour of the water exchange model for lagoon 1, when substituting measured ocean levels for simulated ones, can be seen in Figure 16. The graph shows lagoon levels during the whole month of November 2019, including the week earlier presented in Figure 15 (2019-11-12 to 2019-11-19).

Observable is that the peaks of the lagoon levels based on measured ocean water levels (SMS01) are higher compared to the lagoon levels based on simulated ocean water levels in Hoi An. For the lagoon levels based on SMS01

data the troughs are also lower, suggesting that these water levels are less dampened. The calculated lagoon water levels (blue line) are initially oscillating around a lower baseline in comparison with the measured lagoon levels (red line), but later the graphs coincide rather well in terms of mean base level. The calculated values also have a small (minutes) phase shift to the right in comparison with the measured. The small phase shift could cause a difference in inlet velocity and consequently the inlet sediment transport. The difference was considered small, and the effects were not further investigated.

This said, it is not fully accurate to compare the measured levels with the simulated, since the point where the lagoon levels are measured (red line) is situated almost in the inlet channel and not in the centre of the lagoon. This may influence the results since the channel is more dynamic compared to the lagoon. During the ebb-tide cycle, the flow of water causes a lowering of the water level in the channel. When the tide shifts, the inertia of the two water bodies connected to the inlet causes a compression effect in the channel, raising or lowering water levels more compared to the estuary. Thus, water levels in this area can deviate significantly from those further into the estuary and ideally the water level measurements should have been taken further into the estuary to better represent the model assumptions. It is therefore reasonable that the two lines below do not coincide completely, but they should have a similar appearance, which is the case.

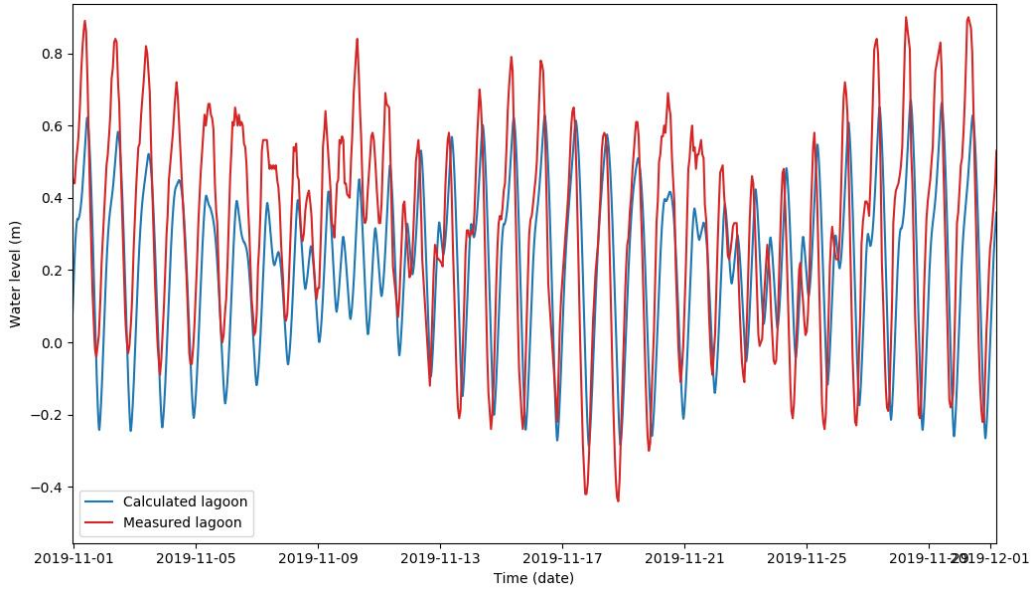

Figure 16. Calculated (blue line) and measured (red line) water levels during whole November year 2019. The calculated water levels in lagoon 1 are based on ocean water levels simulated at a point north of the inlet, in Hoi An.

5.3.2 Longshore sediment transport

Previously determined values of the longshore sediment transport in the area were used to validate the LST model. Nguyen et al. (2018 (b)) calculated the longshore sediment transport in the area and along the whole coast of Quang Nam, from Cua Dai inlet to Cua Lo. The LST was calculated from deep water offshore wave climate and the transport was divided into eight profiles with different transport, along the coast. The LST calculations were performed during the period 01 January 2011 to 31 December 2016 with a coastline orientation of 60-35 degrees. They obtained, in the profile closest to Cua Lo, an average longshore sediment transport of 100 000 m^3/year. This value was used to compare with and validate the calculated LST. Noteworthy is that the LST used here is estimated further away from the inlet compared to their estimates. The method by Larson et al. (2010) estimates the general LST in the area rather than for a specific location. Keeping this in mind, their results are still considered comparable with the ones used here. The results were similar (Table 5) and the LST calculated in this project was deemed representative for the location of the inlet position.

5.3.3 Morphological model

Satellite imagery from Google Earth dating back to 1988 was used to calibrate the inlet migration model. Visual measurements of the updrift side of the main channel, the tip of the spit constantly above water, and the downdrift side of the inlet bank were plotted for every year between 1988-2019 (Figure 17). For the years 2017 and 2019 more than one image was used since the resolution was better and morphological changes were observed. In addition, a linear fit to the sand spit migration 1988-2017 approximated by Duy et al. (2018) was also used in the calibration. Their linear fit was in turn also approximated from satellite imagery of the spit elongation from the same period, but with some different images. Except for the unsubmerged spit migration, the same spatial reference points were investigated in their study.

Table 4. Satellite image resolution for the calibration period. A summary of the years including image resolution from which satellite images were used for model calibration.

Year	*Resolution*
1988 - 2001, 2003 - 2009, 2012, 2013	30 m/pixel
2002, 2010, 2011, 2014 - 2019	2.1 m/pixel

The sand spit migration model (Equation 49) was run with the simulated ocean water levels from 1988 to 2017 as input and plotted together with the positions described above, and the linear fit. The empirical transport coefficient (k_w) and Darcy's friction factor (f_D) in the inlet sediment transport equation (31) were then adjusted to calibrate the model towards the updrift and downdrift positions. Thus, this step included both calibration of the inlet sediment transport and the model which describes the sand spit elongation. Figure 17 (b) (blue line) depicts the result of this calibration. Here, the blue crosses represent the unsubmerged part of the spit, the orange triangles the downdrift bank, and the blue triangles the updrift bank.

In a similar way, the validity of the assumption that the inlet width will remain constant until it reaches its boundary was investigated. This by plotting a visually measured inlet width measured at the narrowest section of the inlet channel, closest to the ocean, for the same time period as the migration. Figure 17 (a) illustrates these estimated inlet widths (blue dots), together with the assumed constant width (blue line).

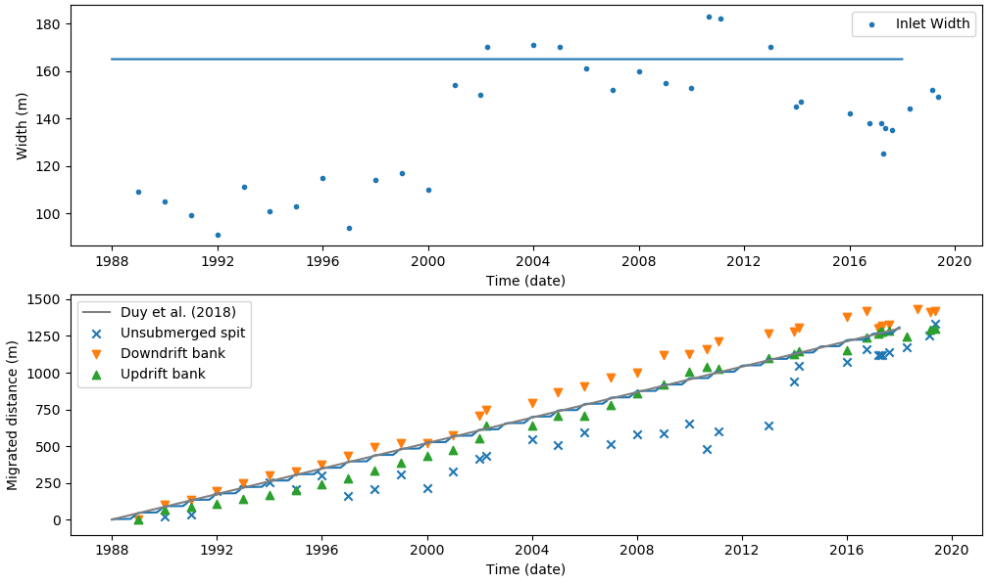

Figure 17. The upper part of the figure (a) shows measured inlet width from 1988 to 2019 measured in satellite images. The line at 165 m shows the constant width used in the inlet migration model. The lower part of the figure (b) shows migrated distance (blue line), where the orange triangles mark the right side of the inlet. The green triangles mark the most southwestern point under water on the left side of the spit. The blue crosses mark the left side on land on the spit.

It should be highlighted that the difference between the downdrift (orange) and the updrift (green) measurements does not equal the inlet width in the upper figure section. This derives from that the measurement points for the updrift and downdrift points differ spatially between years due to morphological changes of the spit appearance. The inlet width in turn is measured at the narrowest section where the spit, from a visual point of view, remains above the tidal range. With these definitions, the updrift and downdrift side can only in general terms be related to each other and should be interpreted individually.

With a pixel resolution of 30 m/pixel for the majority of the years, and a previously predicted migration of about 43 m/year, the measured positions are rough estimates. Although hard to analyse small changes due to the low resolution of large parts of the data, the validation measurements give rise to a couple of interesting observations. Over the years 2000-2004 the inlet width increased rapidly from about 110 to 150 m, but the migration of the up- and downdrift positions did not deviate much from the overall pattern. The

imagery revealed that the cause of the width increase was the loss of a tooth formation at the narrowest part of the channel, where the width was measured. A likely cause of such an event could be a riverine flood, eroding the inlet. The event coincides with a slower migration of the downdrift measurement point which could be deposition of the lost sediment from the tooth formation, but no causal connection can be made. Past the widening event the inlet width remained at a higher level for the rest of the period, possibly with a slight decreasing trend. Over this period, a large submerged spit platform formed and emerged in 2013-2014, seen as the steep pattern of the blue crosses for that period (Figure 17 (b)). This new unsubmerged area became the new narrowest section and thus changed the measurement point, leading to the observed width reduction.

A couple of events where the spit and inlet exhibited regression were also observed when performing the satellite imagery analysis of the spit and inlet migration. These events could however not be linked to a seasonal regression. Rather, they were more similar in appearance to a sand bypassing mechanism. More specifically, the spit platform breaching, or possibly ebb tidal delta breaching discussed in "2.1.7.3 Sediment bypassing" fitted the appearance of the regression behaviour, as well as the time scale. Formation of secondary channels on the submerged inlet platform were the background to this linkage. Although, since it is somewhat outside of the scope of this report, the exact nature of the bypassing is not analysed past the remark that the observed regression could be due to sand bypassing.

In general, the modelled spit migration follows both the updrift and the downdrift movement pattern of the inlet, as well as the linear approximation from previous research. The inlet width is varying rather much over long time periods, but a certain pattern could not be defined. With these considerations the migration model was deemed acceptable in terms of validation, and likewise the constant width assumption remained further in the modelling process.

In reality, single high river flow events could result in a sudden inlet widening and/or spit retraction. In fact, this could be a more representative scenario compared to a lower mean flow over two months. The mean flow during November, when the river reached its highest flows, was therefore also investigated but since the result did not differ much from the scenario above it was excluded in the report. Shorter events are difficult to include in the model due to their low predictability in terms of spatiality and magnitude. For

long modelled time periods, high flow events are necessarily not highly affecting the morphological end-result. Over the course of several years, sudden changes tend to be restored to the dynamical equilibrium state as discussed in “2.1.7.4 Seasonal evolution and morphological stability”.

6. Model results

6.1 Water exchange model

Figure 18 and 19 shows measured and calculated water levels during August and November 2019, respectively. Since the model has a "natural spin up time" before it behaves as it should, only the 3 - 4 last tidal cycles will be interpreted for results.

If the amplitudes are observed and compared for august, one can see that the amplitude difference is around 0.01 - 0.1 m. Out of the total 1 m tidal range for the period, this corresponds to an error of 2 - 20%. For November, the corresponding amplitude difference is 0.07 - 0.14 m, resulting in an error of 16 - 30%. Notable however is that for the last three tidal cycles, the entire graph for the calculated values is shifted upwards compared to the measured values. If the graphs were to be normalized for the offset for these cycles, the error would only be 0.05 - 0.03 m.

Comparing the phase difference between calculated and measured values in August; calculated levels exhibit a shift of 0.5 - 2 h towards the left. Corresponding values for November show a rightward shift of 0.3 - 0.75 h. For both periods, the phase of the measured values shows an uneven pattern, sometimes ahead and sometimes behind the calculated levels. This pattern can also be seen when comparing measured ocean levels to measured lagoon levels (Figure 46 and 47, Appendix A5).

The calculated lagoon water levels (blue line) have a smoother appearance in comparison to the measured lagoon water levels (red line). This is caused by the fact that the calculated levels are calculated with a shorter time interval, 10 min between each calculated value, in comparison with the measured which are measured each hour. Observing the cycles in August, the model also shows the semidiurnal component of the tidal cycle characterized by the flattening of the curve at Aug 15th to the second-high amplitude on the 18th, halfway into

the diurnal cycle. This semidiurnal part can also be seen in November, but since it lies in the first half of the modelling period it is a bare observation.

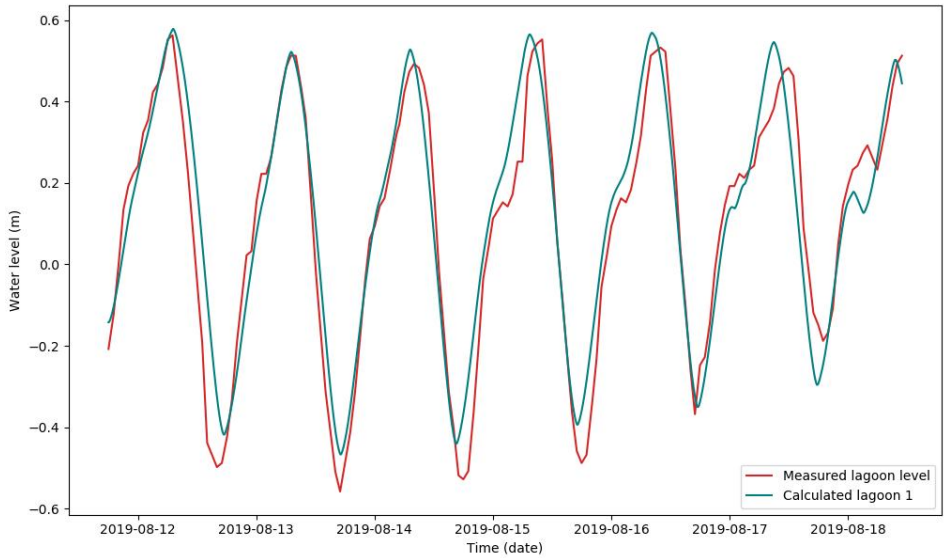

Figure 18. Water levels in lagoon 1 during August 2019, both measured and calculated. The red line represents the measured water levels and the blue line represents calculated water levels in the lagoon, based on recorded water levels in the ocean.

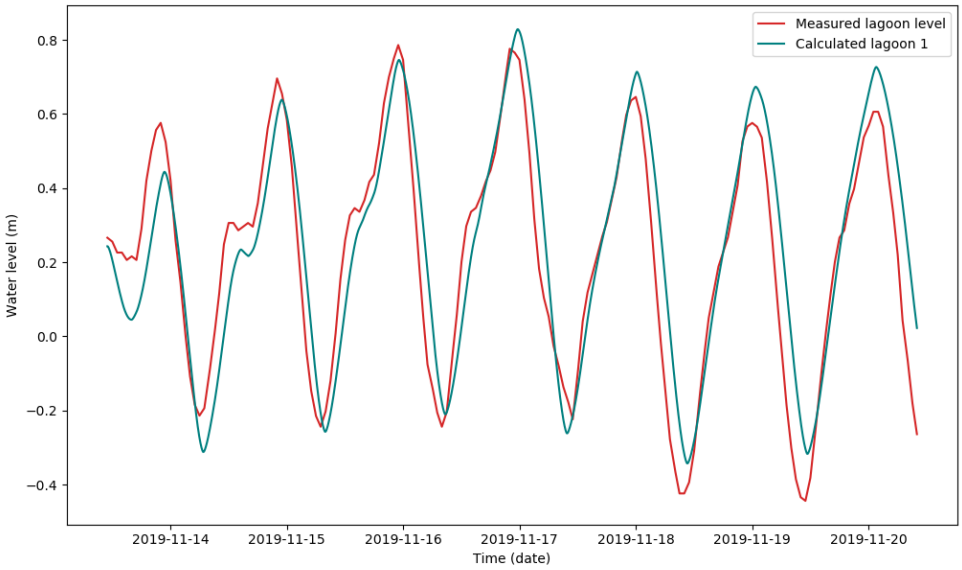

Figure 19. Water levels in lagoon 1 during November 2019, both measured and calculated. The red line represents the measured water levels and the blue line represents calculated water levels in the lagoon, based on recorded water levels in the ocean.

The measured and calculated water levels in lagoon 1 are more dampened in comparison with the ocean (Figure 46 and 47, Appendix A5). Lagoon 2, which has a larger lagoon area and a larger inlet cross-sectional area compared to lagoon and inlet 1, follows the ocean water levels well. The water levels in November have higher peaks in comparison with the water levels in August, but the troughs are lower in August. The water levels in lagoon 1 are phase shifted to the right in comparison with the ocean water levels and the water levels in lagoon 2.

6.2 Sediment transport

Offshore wave directions and wave heights during the dry season (left) and monsoon season (right) are depicted in Figure 20. The predominant wave direction is ENE during both seasons, but during dry season a large percentage of the waves are also approaching from E and ESE, and during monsoon season the waves approach more from NE. The wave heights are higher during the monsoon season, this is represented by the colours in the graphs. Dark blue represents smaller wave heights and red represents the largest recorded wave heights.

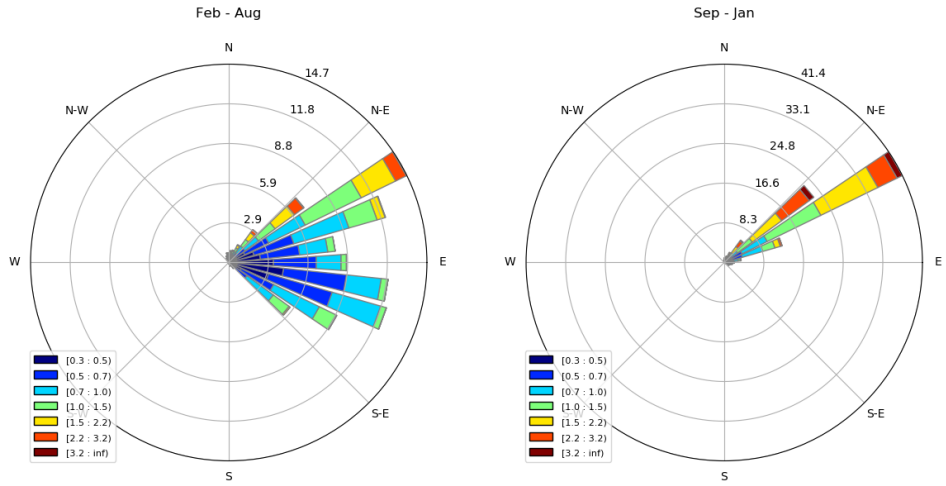

Figure 20. Graphs showing the incoming wave direction and the wave heights. The colours represent different wave heights, dark blue represents the smallest wave heights and red is the largest. The graph to the left is during dry season and the one to the right is monsoon season.

Figure 21 shows calculated mean values for each month of the positive LST (m_L) and the gross inlet sediment transport (m_I). LST is based on the wave climate 1988-2017 and calculated at a static point (Figure 10). The direction of the LST is defined with a positive direction towards the right (facing the ocean), resulting in positive values during the monsoon period from September to January and negative transport from February to August (dry season). The longshore transport is largest in November (about 50 000 m^3) and smallest in February (-2 000 m^3). The accumulated annual net LST in the area is estimated to 112 000 m^3/y, the annual positive to 270 000 m^3, and the corresponding gross LST is 420 000 m^3/y (Table 5).

Table 5. Accumulated mean values of the LST at Cua Lo for the period 1988-2017.

Mean LST	*Value (m^3/year)*
Annual positive	270 000
Annual Negative	-155 000
Annual Net	112 000
Annual Gross	421 000

There is a general trend in the inlet sediment transport, with two peaks and two troughs during an average year. The periods with lowest values of the inlet transport occur in March-April and August, and the larger transport occurs in May - July and September to January. During latter period, the inlet sediment transport is significantly higher than for the rest of the year. The inlet sediment transport is lower than the positive LST from September to April.

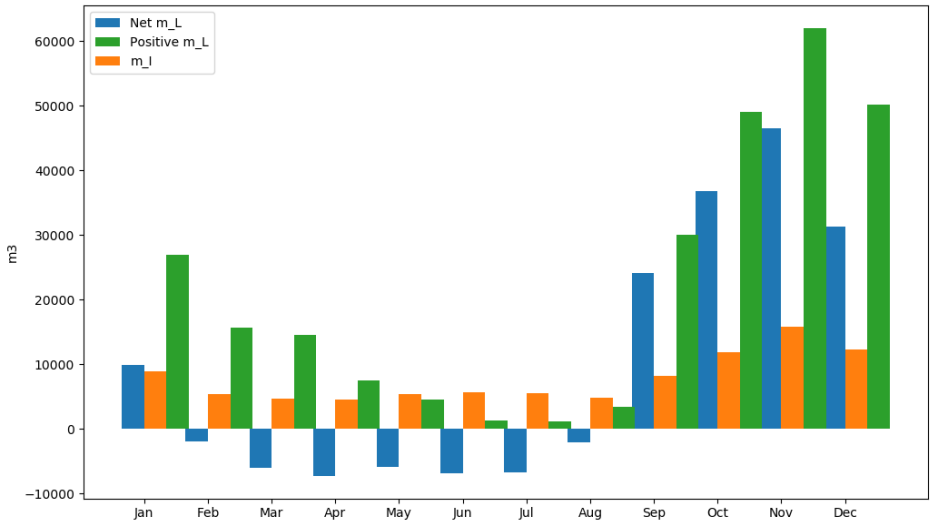

Figure 21. Calculated monthly mean net LST (blue bars) and positive mean LST (green bars), based on wave data from 1988 to 2017. Calculated mean values of the sediment transport in inlet 1 for each month during a year (orange bars, m_l), based on simulated ocean water levels for 2020-2049.

6.3 Inlet morphology

In scenario 1 (Figure 22) the inlet is allowed to freely migrate a maximum of 980 m before the width variation model is initiated. The blue line in the lower part of the figure shows the migration of the sand spit alongshore from 2020 to 2049. In November 2041 the inlet is predicted to reach the boundary. Up until then migration occurs in an annual cycle with little or no migration January-September and rather fast migration from mid September to end December. The black line in the same figure section represents an extrapolation of the satellite-based historical migration path by Duy et al. (2018) where the linear equation $x_S = 43.33 * Y_n$ (Y_n is the number of years) describing the migration of the sand spit was fitted to the observed spit location. Compared to the validation period for inlet migration (Figure 17,

Section 5.3) the migration rate is very similar, reaching about 120 m further over the corresponding time period.

Figure 22 (a) shows the changes in inlet width from November 2041, when the migration model is terminated, to year 2049. The net inlet width decreases between 2041 and 2042, reaching an apparent equilibrium state in December 2042. Seasonal variations occur, including little or no width change during the dry period and fast narrowing during the monsoon period. The width oscillates between peaks at about 30 m during dry season and values as low as 4 m during monsoon season. Two notable spikes occur after 2041. One in November 2043, with a width increase to 90 m, and one in the same month the following year with a width increase to 50 m.

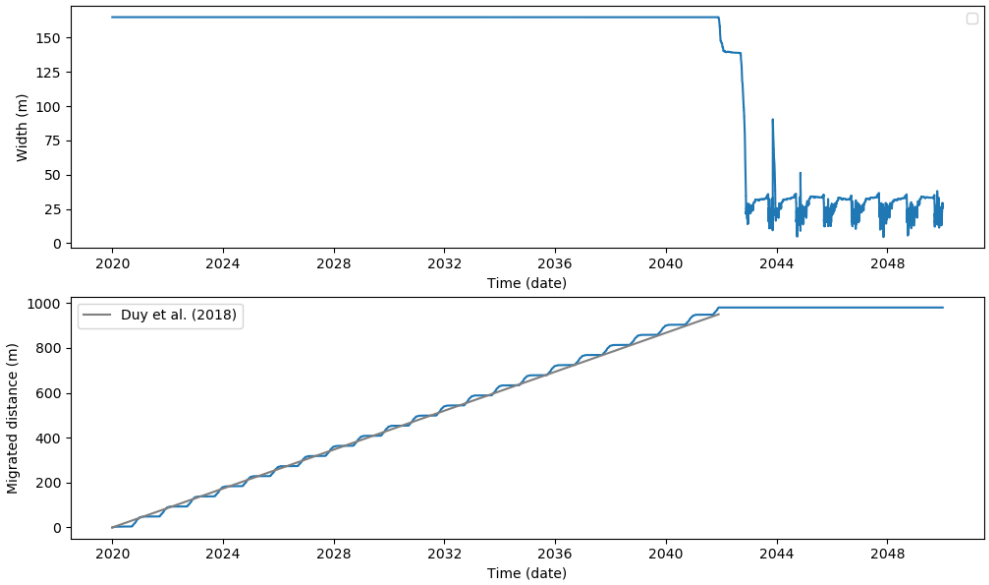

Figure 22. The upper figure (a) shows changes in the inlet width and the figure below (b) shows migration of the sand spit. Both graphs are modeled from year 2020 to year 2049. It is assumed that the sand spit elongates alongshore until it reaches the hard boundary at Tam Hai, then changes in the inlet width takes place. The grey line represents an extrapolation of previous research by Duy et al. (2018).

For Scenario 2 the downdrift side of the inlet does not reach An Hoa cape, 2000 m downdrift of the current position, within the modelled period (Figure 23). In the end of 2049, the total migrated distance is 1350 m. The migration pattern is very similar to that of Scenario 1.

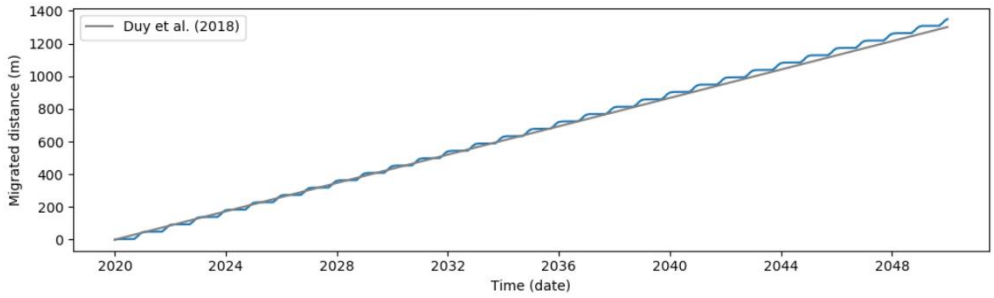

Figure 23. Modelled inlet migration 2020 – 2049, using 2000 m as boundary. Inlet width variation is excluded since the inlet does not reach its boundary.

6.4 Sensitivity analysis

When modelling over long time-perspectives, the stepping interval of which the model is run with has a large effect on the model runtime. To evaluate the time efficiency versus accuracy of the model, several different time steps were investigated. Figure 24 shows calculated water levels in lagoon 1 during one week in April 1998, when using two different time steps. The blue line was calculated with a time step of 60 min and the black line was calculated by using a time step of 10 min. It is possible to see that the black line generates a smoother curve, while the blue line has an edgy curve with local instability. It was highlighted e.g. by Nunes et al. (2018) that process-based models are good since they can handle larger time steps, but this does not seem like the case here. The effect on the end result of using large time steps was not further investigated due to that the model was still fast enough for that aspect of the purpose of the project to be fulfilled.

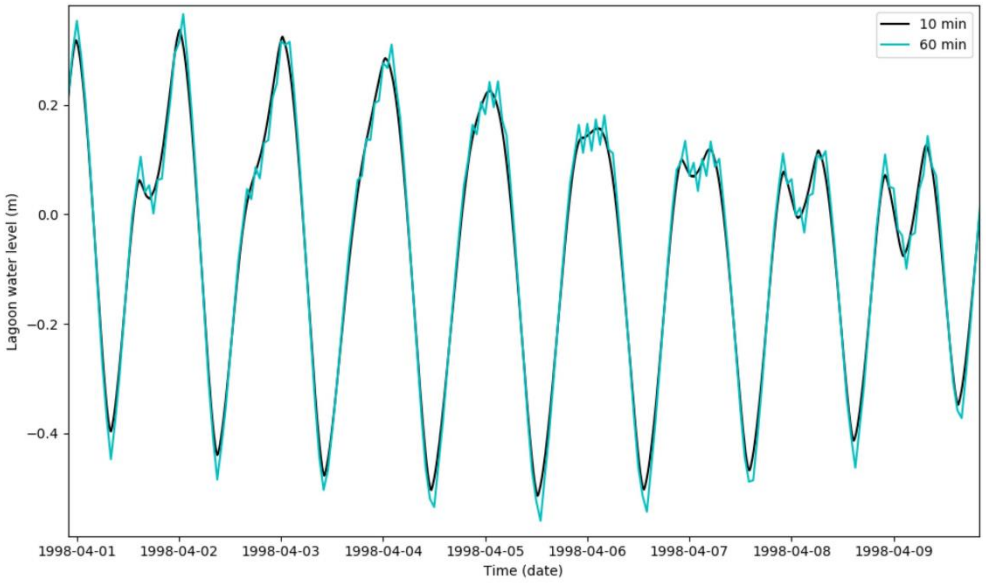

Figure 24. Water levels in lagoon 1 calculated with different time steps. The water levels are calculated during a week in April 1998. The blue line has a time step of 60 min and the black line have a time step of 10 min.

As discussed in section "5.1 Model input", the river inflow was excluded in the modelling process. For the majority of the year, no significant net flow occurs over the year except from in Nov and Dec (Figure 9, section 5.1.1) according to the obtained discharge data. Based on the data from Nov-Dec 2017 and Nov 2019, the mean flow in the river was calculated to 40 m^3/s. For the analysis, values of the river flow in the range 0 to 100 m^3/s, with a step of 20 m^3/s, was inserted into the preliminary water exchange model (Figure 25) and morphological model (Figure 26) to investigate the inlet migration and inlet width evolution. River flow was only included in the model for the months November and December.

In the modelled range, river flow does not have a large effect the lagoon water levels (Figure 25). The uppermost blue line is represented by the calculated lagoon water levels which has the highest river flow of 100 m^3/s, the lowest blue line represents lagoon levels with no river flow. At most the difference reaches 0.1m, during lagoon ebbtide. The additional inflow of water has its highest relative impact when water is flowing out of the lagoon and the two flows are counteracting each other. Then, the river acts to increase the lagoon levels, while the tidal flow is emptying the lagoon.

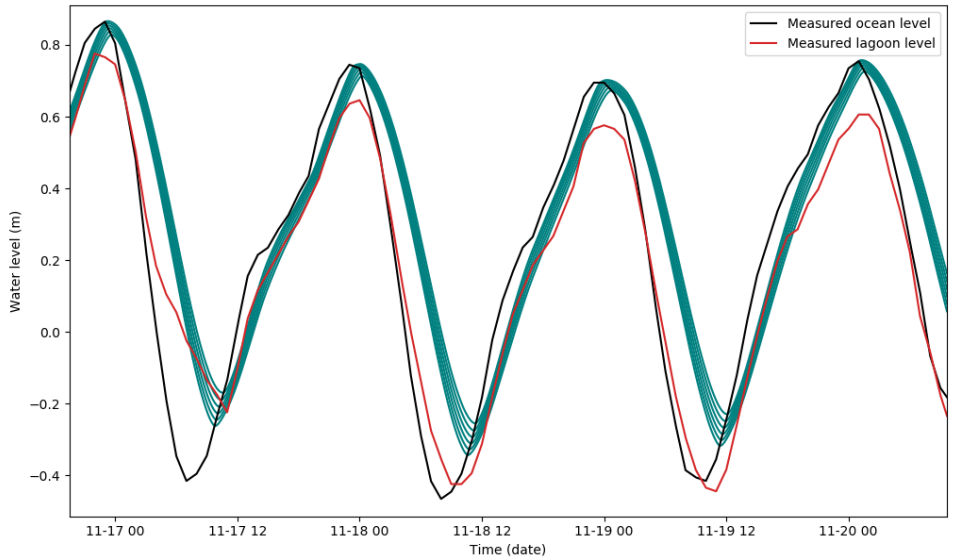

Figure 25. The black line represents measured ocean water levels, the red line represents measured lagoon levels, and the blue lines represents lagoon levels which includes river flows ranging from 0 to 100 m3/s with a step of 20 m3/s.

When the river flow variation propagates into the morphological model a small impact on both migration and width evolution can be seen (Figure 26). The graph in the top of Figure 26 (a) shows changes in the inlet width when the river flow is varied. If the river flow is large, the inlet width will be larger, represented by the upper line. Initially, when the inlet has reached the boundary and the width model initiates, the width is constant. This occurs since the boundary was reached in the start of a dry period. When the monsoon period begins, the width decreases rapidly and eventually finds an equilibrium state. The graph in the bottom, Figure 26 (b), shows how the inlet migration differs when the river flow varies. A large river flow will increase the scouring in the inlet and hinder migration, resulting in a smaller migrated distance represented by the lower line. The migrated distance will be larger if the river flow is zero, represented by the upper line. For comparison, the straight line represents an extrapolation of the linear fit to historical migration, performed by Duy et al. (2018). Two high spikes, one in Nov 2043 and one in Nov 2046, and several lower ones can be seen over the period. They are simply noted here and discussed further in “7.2 Model aspects and input data”.

Although some variation is observed, the net difference on the migration rate is less than one month over the entire period 2020-2049. When the migration has ended and the next monsoon period starts, there is an insignificant

difference in the narrowing rate and reached equilibrium level. Thus, the river flow in the observed flow range is not considered to affect the overall evolution.

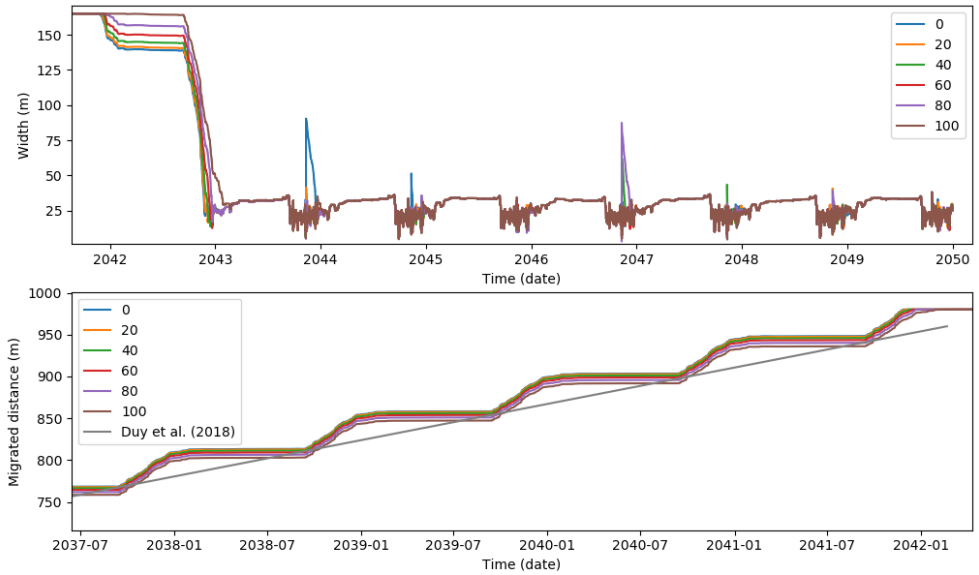

Figure 26. Sensitivity analysis of the river flow. The flow varies from 0 to 100 m^3/s with an interval of 20. The graph above (a) shows inlet width variations, the graph below (b) shows inlet migration.

Restricting the flow through the inlets, the loss coefficients influence the lagoon water levels and thus also the velocity and inlet sediment transport. In order to evaluate the magnitude of the effects, these were varied individually. Figure 27, 28 and 29 shows calculated water levels in lagoon 1 when the loss coefficients in the inlets are varying, represented by the blue lines. The most dampened blue line in each figure shows the line with the largest loss coefficient. The least dampened line is represented by the smallest loss coefficient. The red line shows the measured lagoon level, the black line shows measured ocean water levels. The three different cases which are represented in the below figures were chosen to see the impact on the water levels in lagoon 1 from varying one loss coefficient at the time according to Table 6.

Table 6. Description of how the different loss coefficients were varied in the sensitivity analysis for the water exchange model.

Figure	k_{f1}	k_{f2}	k_{f12}
29	1-100	1000	1000
30	1000	1-100	0.1
31	1000	0.1	1-100

The loss coefficients have a large impact on the lagoon water level and affects the amplitude and the phase. An increase in the loss coefficients decreases the amplitude and causes a phase shift to the right, a decrease causes the reversed situation. The loss coefficients are most sensitive for changes at small scales. The change from 1 to 10, represented by the two upper blue lines in the graph, has a larger effect on the water level compared to the change from 90 to 100 which is represented by the two most damped lines. Thus, the impact on the water levels from increasing the loss coefficients is not linear, which can be seen in the figures and Equation 21a. Figure 27 and 29 have a rather similar appearance, implying that case 1 and 3 have similar effects on the lagoon water levels. The biggest difference is that the lagoon water levels in Figure 29 (case 3) has a larger phase shift to the right compared to case 1.

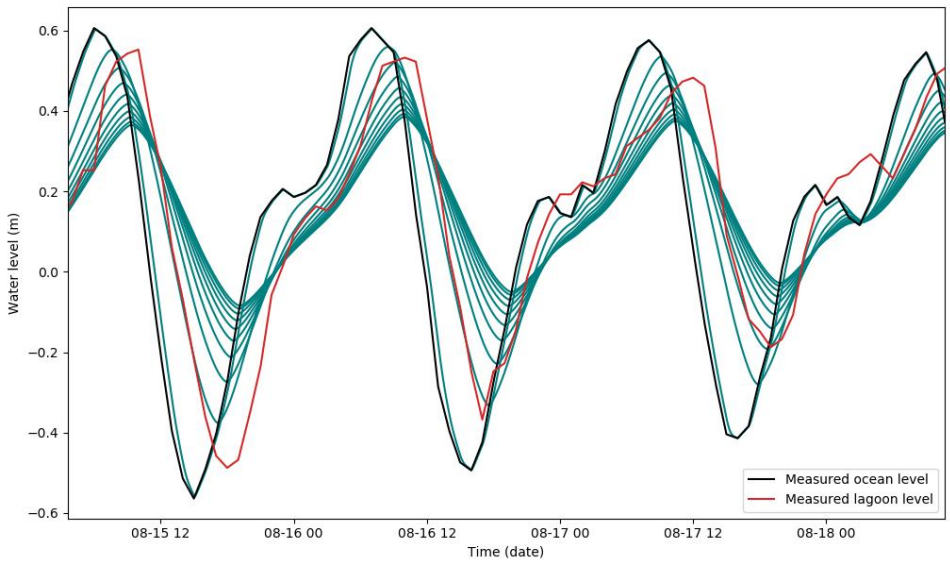

Figure 27. Water levels in the ocean and lagoon 1. The black line represents measured ocean water levels, the red line represents measured water levels in lagoon 1 and the blue lines represents calculated water levels in lagoon 1 when k_{f1} varies from 1 to 100.

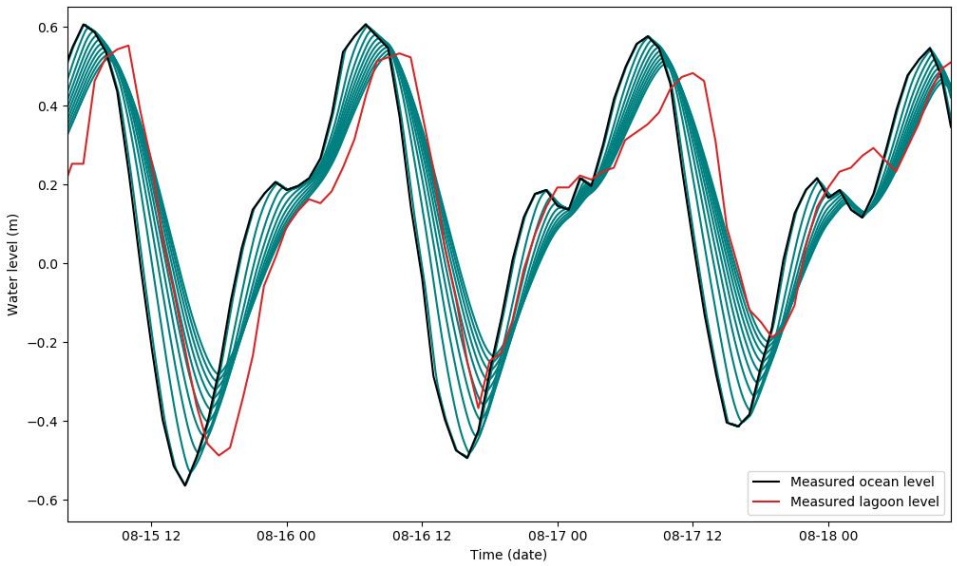

Figure 28. Water levels in the ocean and lagoon 1. The black line represents measured ocean water levels, the red line represents measured water levels in lagoon 1 and the blue lines represents calculated water levels in lagoon 1 when k_{f2} varies from 1 to 100.

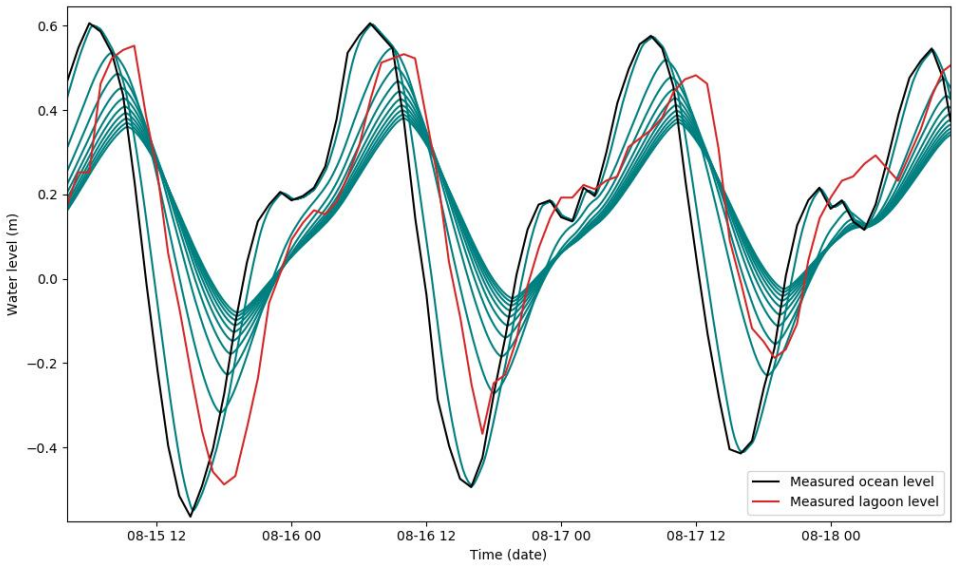

Figure 29. Water levels in the ocean and lagoon 1. The black line represents measured ocean water levels, the red line represents measured water levels in lagoon 1 and the blue lines represents calculated water levels in lagoon 1 when k_{f12} varies from 1 to 100.

Since the shoreline on which the inlet is migrating is curved, and LST is dependent on the beach orientation, uncertainty in the estimation of the LST is introduced. To investigate how this could affect the LST, a sensitivity analysis on the impact of a change in shoreline orientation was performed. By varying the shoreline orientation an estimation of its impact on LST can be illustrated (Figure 30). Here, the shoreline orientation is decreased from 60° to 50° with a step of 2°, while other input parameters in the LST model are held constant. Fifty-six degrees, the measured orientation used in the result, is represented by the red bars. A change to 54 degrees changes the annual average net from 112 000 to 20 000 m^3/year. For every consecutive 2° reduction the LST is reduced. The pattern is similar for every month except for June and July where the LST is more or less constant. Changes have the largest impact during Oct-Jan, which includes the monsoon period. This implies that the shoreline orientation largely affects the LST during the monsoon period.

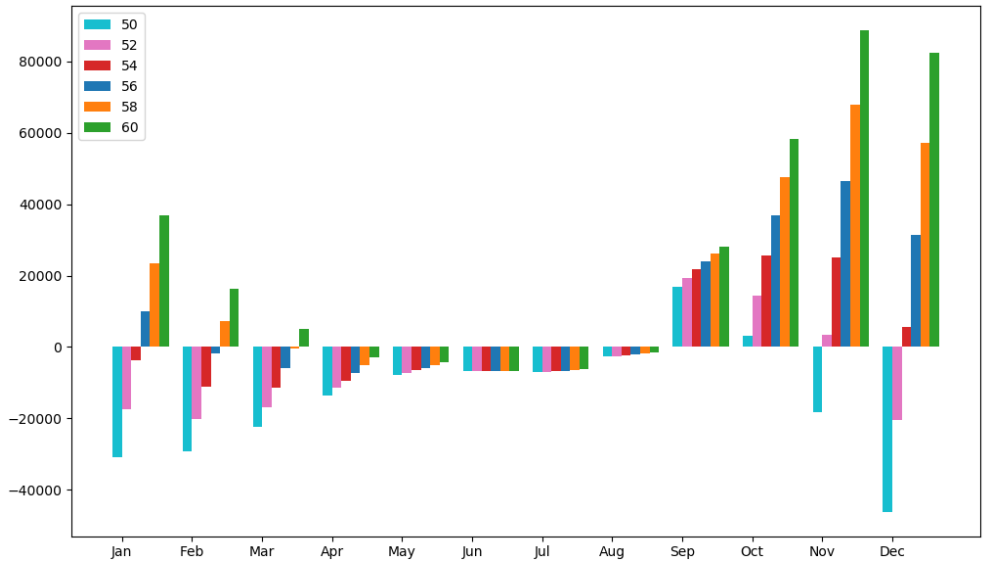

Figure 30. Changes in LST as a result of changing the shoreline orientation from 60 (highest values) to 50 degrees (lowest values).

Regarding inlet migration and inlet width evolution, several parameters involve approximations, and most importantly have an impact on the resulting migrated distance and changes in inlet width. These parameters are the spit area (A_s), the empirical transport coefficient (k_w), and the shape coefficient

for the inlet (α). Since the boundary was not reached in Scenario 2, Scenario 1 was used to illustrate the results of this sensitivity analysis.

In the figure below, Figure 31 (a) and (b), the changes in inlet width and inlet migration caused by variations in the spit area (A_s) are presented. The spit area varies from 2000 m^2 to 4000 m^2 with a step interval of 500 m^2. An increase in the spit area causes a decrease in the migration speed, together with an extended migration time until the boundary is reached. An increase in the spit cross-sectional area of 500 m^2 causes a decrease in the time it takes for the inlet to migrate and reach the boundary by about 4 years.

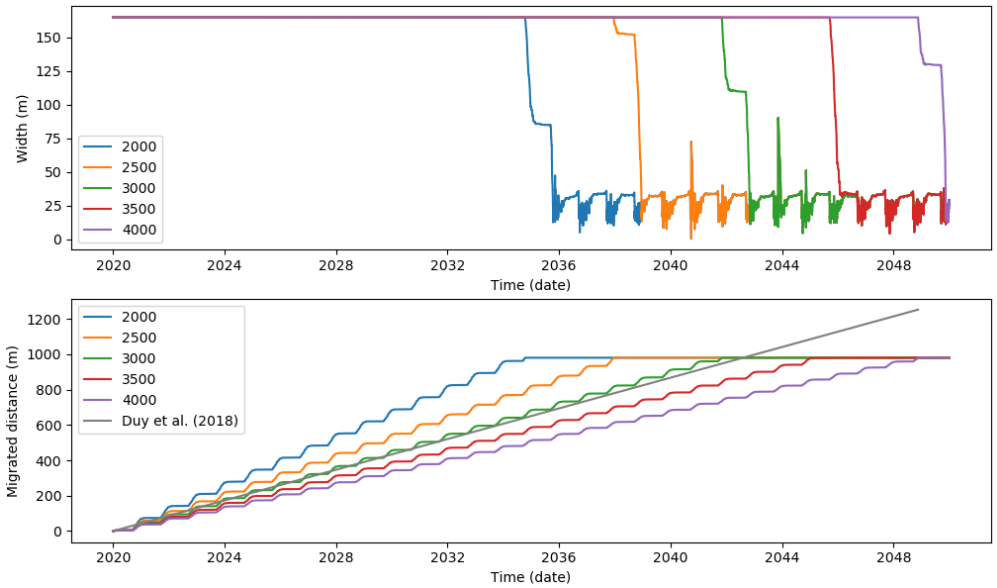

Figure 31. The upper graph (a) shows changes in inlet width and the lower graph (b) shows migrated distance, both graphs are influenced by a varying spit area which varies from 2000 m^2 to 4000 m^2 with a step of 500 m^2.

The empirical transport coefficient (k_w) affects the inlet sediment transport and thus also the inlet migration and inlet width changes. An increase in k_w will increase the transport in the inlet. If the inlet transport increases the inlet migration will decrease. In Figure 32 it is possible to see that if the transport coefficient is small, the inlet will migrate faster and sooner reach the boundary of when the width starts to vary. The dark blue line represents the results with a value of 0.2 on k_w, while the light blue line represents the model outcome with a value of 2.0 on k_w. For a value of 0.2 will the inlet reach the boundary

approximately in year 2040, with a value of 2.0 will the boundary be reached in year 2048.

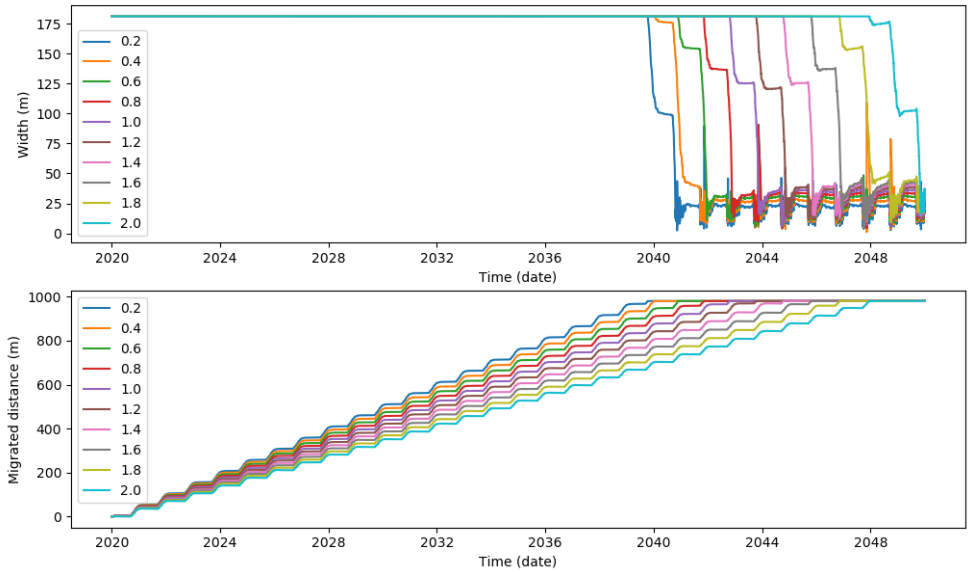

Figure 32. Changes in inlet migration and inlet width when k_w varies. k_w varies between 0.2 and 2.0 with a step of 0.2. The upper graph (a) shows width changes and the lower graph (b) shows migrated distance.

Inlet width and inlet cross-sectional area are related through the shape coefficient (α). It is assumed that geometric similarity prevails, which entails a constant value of the shape coefficient. The shape coefficient is a sensitive parameter for the inlet migration and width changes, which makes it reasonable to investigate how variations in the parameter affects the results. Changing α can also serve as an indication of how the model would behave if the inlet width was varied.

In Figure 33 (a) and (b) the effect on the inlet width and inlet migration caused by variations in the shape coefficient is evaluated. The parameter was varied between 5 and 10, with a stepping interval of 1. An increase in the shape coefficient of one step causes a delay in the migration rate by 1 year. Depending on which month of the year that the boundary is reached, different appearances can be seen in the upper figure graph. The light blue line which reaches the boundary first, experience two dry periods and one monsoon period before the last monsoon period causes a drastic decrease in the inlet width and an equilibrium state was reached. The brown line, which was the

last line to reach the boundary, only experience one monsoon period which immediately reduces the inlet width drastically and the equilibrium state was reached. Notably, a change in α has the largest effect on the equilibrium level for the width out of all the parameters in the sensitivity analysis.

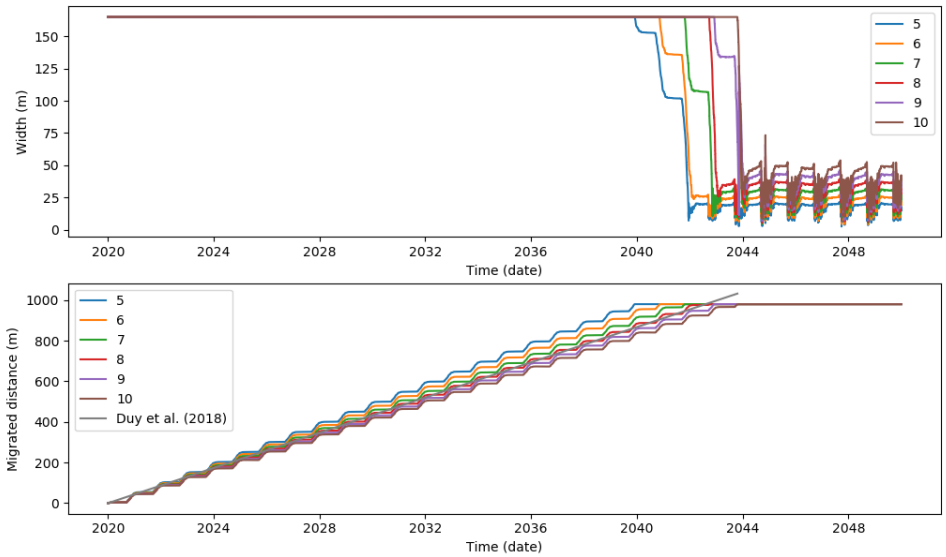

Figure 33. Changes in inlet migration and inlet width when α varies. α varies between 5 and 10 with a step of 1. The upper graph (a) shows width changes and the lower graph (b) shows migrated distance

Having varied the parameters considered to affect the model results, a sensitivity analysis was also performed on how the sediment dynamics would have to change to stabilize the inlet. The chosen method for this was to vary the LST by either a fixed annual value, or by a percentage reduction in the calculated values. The latter corresponds to a reduction in the sediment supply to the area. Such a scenario could be due to e.g. updrift sand mining or a reduction in the sediment supply from the Thu Bon river mouth as a result of damming or hydropower construction. Fixed annual LST changes are hard to relate to a real scenario other than large changes in the offshore wave climate. It is instead more related to the required overall LST for stabilization, and to investigate the model behavior.

In order to keep the inlet from having a net migration, the LST had to be reduced by 87% after which the inlet would only migrate back and forth about 1 m on an annual basis (Figure 34). This was found following an analysis of

reducing the LST between 90% and 10% (Figure 49, Appendix A6). A similar result, with a net zero long-term inlet migration, was obtained by increasing k_w to 6.1 (Figure 48, Appendix A6).

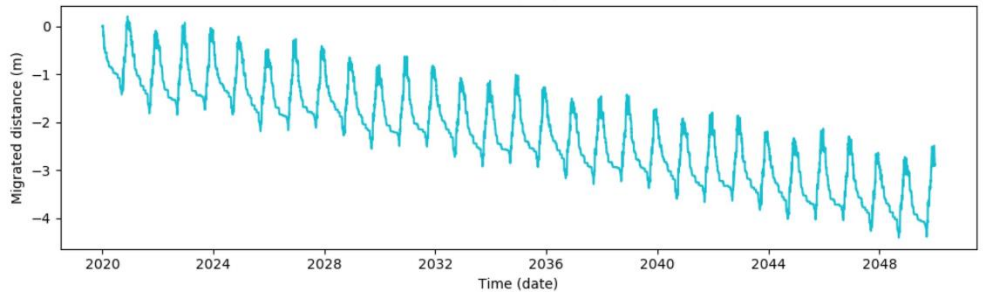

Figure 34. Predicted migrated distance of the sand spit during the period from year 2020 to 2049 when reducing the LST by 87%.

When varying the annual LST by fixed values, the resulting inlet migration and width changes turned out as in Figure 35 when running only the width variation model, and (b) when running only the migration model. The chosen values represent the annual positive LST. This since the negative LST values are disregarded in the migration model, and the negative LST during the summer months does not significantly affect the inlet width. An LST in the positive direction of 50 000 m^3/year would result in a stable inlet with regards to both inlet width and inlet migration if the models are run individually. A higher LST would result in a narrowing until a new equilibrium width is reached (Figure 35), or a positive migration (Figure 36). In turn, a smaller LST would result in a negative migration or a widening of the inlet until a new equilibrium is reached. Since it is known that the inlet is migrating, and not varying much in width in response on the seasonal variation in LST, the most realistic stable scenario is with an LST of 50 000 m^3/year.

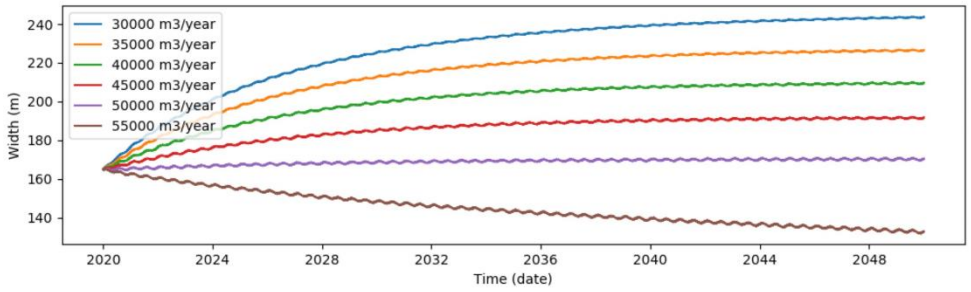

Figure 35. Inlet width changes when positive LST varies between 30 000 m^3/year and 55 000 m^3/year.

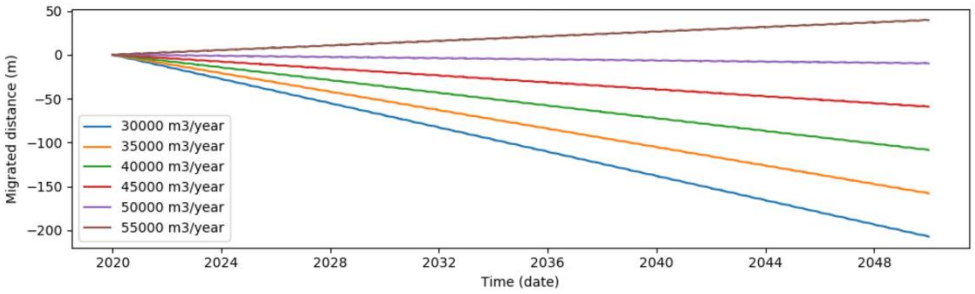

Figure 36. Inlet migration when positive LST varies between 30 000 m³/year and 55 000 m³/year.

As stated, when deciding the modelled scenarios, Scenario 1 is somewhat inconsequent. This with regards to the assumption in the second sub-scenario that LST no longer favors migration but is still kept constant for the inlet width model. A simplified case for the inlet at the boundary in Scenario 1 is that the LST is losing much of its annual variation due to shadowing effects and the change in beach orientation. Therefore, a constant LST scenario was also run with both the models run at the same time. This enables one to see how different equilibrium states could look like. The result, shown in Figure 37 below, suggests that several equilibrium states exists but the scenario of an LST of 50 000 m^3/year leads to no net migration or width variation.

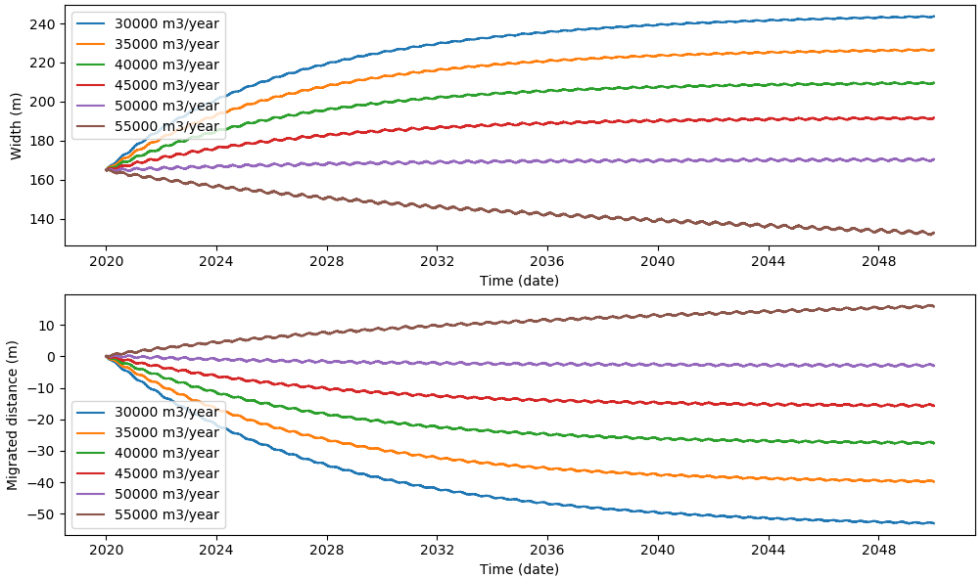

Figure 37. Inlet width changes in the upper part of the figure (a) and migration in the lower part (b), when positive LST varies between 30 00 m³/year and 55 000 m³/year. The models were run simultaneously.

7. Discussion

7.1 Effects on the estuary

Historically, the migration of the spit and inlet has already caused erosion into aquaculture ponds and residential houses (Duy et al., 2018, Nguyen et al., 2018 a,b). The results of this study do not indicate that the migration rate will slow down soon, and the erosion will continue into several more residential buildings (Figure 12). Protective measures, in the form of different hard structures, to reduce the riverbank erosion has already been implemented several times without success. Since the erosion rate is rather high, soft protective measures would have had to be renewed with short intervals and would not be cost-effective to implement. Construction of jetties to stabilize the inlet could be a solution, but the net gain in relation to the cost could be questionable. With a rather high LST during the monsoon period, sand bypassing on the updrift jetty could also occur, leading to sand infilling in the inlet. Dredging already occurs in inlet 1 according to some of the locals, but no official source supporting this was found or seen in the satellite imagery. Dredging would keep the inlet open and possibly slow down migration as sediment starts to fill in the channel again. It will however not solve the problem of the inlet migration.

It has not been mentioned much in the modelling process but inlet 2 (Ky Ha), with its much larger cross-sectional area, is the main channel for maritime transport in the estuary. This channel is already dredged (Figure 45, Appendix A4) to enable large ships to enter the ports of the estuary. Since the distance between the two inlets is short, a redirection of the traffic from inlet 1 to inlet 2 might not imply large changes for the locals. Even so, the locals should always be included in management plans since they are the frequent users of the area and will be the most affected people.

A cost-effective measure to deal with the erosion issues could be manual closure of the inlet via sand infilling, as also proposed by Duy et al. (2018). If such measures would be taken, the water quality in the affected area should also be considered. The applied water exchange model in this case suggests that the estuary is hydrodynamically separated into two sections (Figure 44, Appendix A2), one dependent on each of the inlets. If inlet 1 is filled in, attention to the intrinsic water exchange inside the estuary should be investigated. The section of the Troung Giang river connecting Cua Dai with Cua Lo, has a node and almost no net flow from the upstream sections during dry season. This implies that the section could be more dependent on the water

exchange through inlet 1 compared to previous estimations. This section of the river is also lined by aquaculture, amplifying the need of securing the water quality. Nevertheless, even if manual closure is not implemented the considerations of water quality still needs to be done as the inlet will probably close eventually on its own.

Cua Lo and Cua Dai are related in several aspects and are strongly dependent on each other. The main source of sediment supplied to Cua Lo inlet originates from Thu Bon river and Cua Dai inlet (Nguyen et al., 2018(b)). The littoral zone between Cua Dai inlet and Cua Lo inlet is controlled by the sediment supplied from Thu Bon river and the whole littoral system would be affected if the source of sediment would change or stop. The two inlets are also connected through the Truong Giang river channel which flows between Cua Dai estuary and Cua Lo estuary. Changes in Cua Dai inlet sediment supply could significantly affect Cua Lo inlet and estuary.

For long-time modelling and predictions on future morphology, changes in the climate could also affect the result. Sea level rise over the course of the modelled period could affect the estuary significantly and could therefore be of interest to include to increase its accuracy. The low-lying nature of the estuary makes it sensitive to increases in the mean sea level, and it is already affected by flooding events. Inclusion of sea-level rise can if deemed necessary be included in the model to increase its accuracy.

7.2 Model aspects and input data

Several datasets of the ones collected by the research group at Thuyloi University during the survey in 2019 were used as model input data. The fact that the data collection was not collected by the authors leads to some knowledge gaps in which decisions that were taken during the data collection. Although the impact may be small, the bathymetry lacks some precision since the bottom contours vary constantly due to tides and waves, which may cause shoaling in the channel and in the estuary. A probably larger source of error in the bathymetry data may be approximations when the data was interpolated in QGIS to get a complete description of the depth variations in the area. The measured water levels in lagoon 1 (TGR02) may also lack accuracy due to the measuring instrument or related to the reference system of the water levels. When the water levels had been collected, the values had to be corrected to the local mean sea level. Errors may have been introduced during this step. The same errors exist within the ocean water levels which were measured

outside Cua Lo river mouth (SMS01). The across-river profiling (ARP01) used to register river flows in Truong Giang river may also include sources of error. These could originate from the measurement instrument or the measuring method used. Sources of error with using the sampled data may be that unrepresentable conditions prevailed during the survey. Since the data only was collected during two separate weeks, the data is not representative for describing the full hydrodynamics of the river. The measured data could be used in combination with the simulated river flows to get a better understanding of the conditions in the river.

An aspect that Nunes et al. (2020) mentions is the fact that the inlet channel morphology is represented as the width. An advantage with using the width is that it is possible to compare and validate the result with easy-access satellite data. On the other hand, a disadvantage is the inaccuracy of measuring the inlet width in a satellite image since the width is seldom well-defined. This may introduce errors in the results. The same approach is used in this study thus the same problematic situation occurs.

LST is the quantity which has the least uncertainties related to input data and calculation steps, but some measurement deviations from reality might occur. Though, in general the uncertainties with the measuring instrument (wave buoy) and the recorded parameters are still very small in relation to other parameters and calculations in the models used in the project. By far, the largest uncertainty of the LST calculations is the location of the point where the transport is calculated as discussed further in section 7.5.

How the boundaries for wave shadowing are defined is also a sensitive parameter, especially since the inlet is moving towards one of the shadowing structures along a curved shoreline. Another fact that has a significant influence on the models is how the LST is used as input parameter. The decision to calculate average values for 1h intervals based on the measured 3h intervals for 1988-2014 is not an exact approach, but it was chosen as the most representative way to compare the LST in relation to the time step used for the inlet sediment transport.

The CERC equation, used to calculate the LST, is well established, reliable and has few unknown parameters. Some uncertainty is included in the density of water (ρ) since the environment is a mixture between freshwater and salt water is the density depending on the ratio of these. Most likely a dominance of salt water resides as the river inflow was low, which would increase the density slightly. The porosity of the sediment is also an average approximated

value since the used value is based on the assumption that the field site has a predominance of fine sand. The porosity was thus chosen from research as a common value for fine sand.

When estimating the inlet sediment transport, the most sensitive parameter is the velocity, which in term is driven by and depends on the gradient between the ocean water level and the lagoon water level. Within the equation itself (Equation 30), some input parameters and calculation steps present further uncertainties. Recommended values or intervals were not found for the empirical transport coefficient (k_w) from past research or modelling, this parameter is thus chosen freely as a calibration parameter. Darcy´s friction factor (f_D) is a constant which has recommended values from previous studies, which makes this parameter more reliable. Shield´s coefficient was calculated from an empirical formula produced from different studies. Since it is a well-known parameter, the number is considered reliable. The sediment diameter (D_s) was assumed to be represented by the median diameter (D_{50}) from sediment samples. Thus, this is an approximation and not an exact value.

The models containing the most error margins are the models describing the inlet migration and the width variation. This since these contain input from all the preceding model steps, thus all errors within the other models are gathered. In addition, the two models contain a few unique uncertainties as well. In the inlet migration model, the relation between inlet width and area assumes that geometric similarity occurs. In essence, the slopes are constant and the relation between the top width and bottom width is assumed to be constant. The cross-sectional area of the sand spit is approximated to have the shape of a trapezoid and is then calculated from bathymetry data.

The complex dynamics of inlet morphology was reduced to only depend on the balance between the inlet sediment transport, causing scouring, and the LST, causing channel infilling or updrift sediment deposition. The entire model, including plotting of the migration path and width evolution, takes only 100 seconds to run on a computer with a 2.5 GHz processor. This is with a 10 min time step for processes up until inlet sediment transport is calculated, and 1 h time step for the morphological changes. Noteworthy though is that the model seems to handle longer time steps for the water exchange model rather poorly, a fact of which an explanation was not found. That the ocean water levels were interpolated from 1 h to 10 min intervals should not have a large influence on the resulting lagoon water levels precisely since the data was just interpolated. As stated in “6.4 Sensitivity analysis” the computation times

were still short, so the consecutive effects later in the modelling process were not investigated. With such a short computation time several cases could still be tested rather fast, and the analysis and effectiveness of modelling results could be improved easier compared to other more complex models.

Nunes et al. (2020) performed a similar study where they constructed a numerical mathematical model to predict inlet width changes of an inlet in Brazil. A hydrodynamic model proposed by Hill (1994) was used in Nunes´s study but customized to their scenario. As in the current study, it was for them of high importance to have a good representation of the hydrodynamics as errors early in the model could amplify during the modelling process. For the modelled lagoon water levels in Cua Lo, the validation showed that the water levels in lagoon 1 corresponds satisfactory to the real situation. This indicates, as concluded in their study, that the inlet hydrodynamics model was acceptable. In the mentioned study, the result was compared with a previous study by MacMahan et al. (2014) who applied the same type of hydrodynamic model to the New River Inlet, NC in USA. It was then expected that the same approach applied to similar coastal lagoons would yield good performance. The two mentioned studies involved tidally choked inlets, which implies a large reduction of the wave amplitude. A somewhat different hydrodynamic situation exists in Cua Lo since the estuary is restricted rather than choked. However, the main differences between the types are less amplitude reduction and weaker phase shift for the restricted inlet, which the hydrodynamic model was able to describe. Thus, the approach should still be applicable and comparable for the Cua Lo lagoon.

By using a one-dimensional approach on modelling the water levels in the estuaries, spatial variations in water depth, water levels, lagoon area, and velocities are not accounted for. This could cause the inlet sediment transport results to be less accurate, especially since the estuary exhibits quite a large variation in bathymetry (Figure 45, Appendix A4). A measure to account for some of this variation was to define the estuary as two separate entities with an interconnecting channel restricting the exchange between them. Indeed, this alteration enabled the model to better fit the measured data. Without it, the loss coefficients for inlet 1 and 2 would have had to be set at an unrealistic level for a restricted estuary.

7.3 Water exchange model

Analysing the effect of the calibration parameters through the sensitivity analysis showed a large impact from the loss coefficients on the lagoon water levels. The impact on the water levels was rather similar from isolating the effect from inlet 1 as from isolating the effect from the interconnecting inlet (inlet 12) on the water levels in lagoon 1. Inlet 2 had a larger effect on the lagoon when the water levels were low, below the mean sea level. The impact from inlet 1 and inlet 12 was the same for both positive and negative lagoon levels. Although the effect was large on the lagoon water levels, the change in the morphological model was small in the estimated range (Appendix A6, Figure 50). Since the loss coefficients were considered reasonable, the error margin on the morphological evolution was considered low.

Despite the discrepancies in ability to characterize the measured highest water levels in lagoon 1, and alignment of the phase, the model was still capable of recreating the diurnal component in the tidal variation. The pattern arising from the fortnightly neap-tide was also reflected in the model results. This pattern is considered important when modelling over longer time perspectives as it has a high influence on the water exchange (MacMahan et al., 2014). With this taken into consideration, the water exchange model is considered to exhibit sufficient accuracy for long-term simulations.

7.4 Sediment transport

The sediment transport in inlet 1 is affected by water level gradients and variations, between lagoon 1 and the ocean, and between lagoon 1 and lagoon 2. A large gradient causes higher velocities and larger transport in the inlet. The floodtide and ebbtide are the largest factors influencing transport in the inlet. This likely explains the near-sinusoidal component of the curve that depicts the monthly inlet sediment transport in Figure 23. Why the pattern has the appearance it has is hard to conclude. It could be a result of that the period of one of the tidal constituents coincides with these months. It is somewhat unlikely though that the period is exactly aligned with the months of the year, which it almost must be given that the pattern is based on 29 years of data. A slight misalignment would erase or flatten the pattern otherwise. Moreover, the monsoon period seems to affect the inlet sediment transport more since it is much higher during this period. A concluding remark on this topic is still that tidal influence is a likely cause of the observed pattern.

Analyzing the annual variation in the LST and the wave rose (Figure 22), it is reasonable that the average net LST is positive during the monsoon period, as the wave direction changes. Then the waves originate mostly from NE or ENE which results in incoming angles from the fourth quadrant in relation to the shoreline orientation, leading to an LST in the positive direction (northwest to southeast). During the dry season, the incoming wave direction is mostly coming from ENE or ESE which in turn causes a negative longshore transport. During the monsoon, the wave heights are significantly higher, which also results in larger sediment transport.

In the vicinity of today's inlet position, the LST values were successfully validated but the changes in sediment transport along the curvature can be significant. From Figure 30 in paragraph 6.4, it was concluded that the shoreline orientation had a large effect on the LST. When moving downdrift, from west to east, the shoreline orientation decreases and so does the LST. A couple of degrees can change the LST in the scale of 10 000 m^3/y (Figure 30, paragraph 6.4). An increase in the angle of 2° increased the transport significantly. The magnitude of the increase differed between months and the impact was largest in December, implying that the sediment transport is most sensitive to the chosen shore orientation angle during the monsoon period. What can be said is that the position at which the inlet is located is a complex zone for determining the actual LST, situated at the end of the littoral cell. It introduces large uncertainty to the model and limits the certainty of the end result of the inlet morphology. This issue can be dealt with by modelling the LST in more detail, by including feedback processes from the inlet, refraction and cross-shore transport. Such modelling lies outside the scope of this project, but can be included if deemed necessary for future decision making of the migration issue. The LST calculated here might thus be more of a general indication, and detailed investigations and conclusions of the morphological model should be interpreted with care.

7.5 Spit migration and inlet morphology

A clear annual cycle is seen in the spit migration for both Scenario 1 and 2, where movement is halted in the dry season and accelerated during the monsoon period. By excluding the negative LST values when calculating the migrated distance, most of the otherwise observed regression of the inlet was eliminated. Some regression does still occur in the model as a result of a lower LST compared to inlet transport (Equation 49). As suggested in "5.3.3

Morphological model calibration" the regression does not seem to be related to a seasonal behaviour. Instead, a suggestion is that the small regression in the model is an artefact deriving from assuming that the inlet has a constant width when modelling migration. It is easy to forget that what is actually modelled is the spit migration, and the inlet migration implicitly follows the spit. In reality, scouring of the inlet is more likely to occur compared to a migration of both sides. Small width variations over the year would then occur instead, which this model cannot describe due to the complex interplay between sediment deposition, scouring and bypassing. In a larger perspective, the net migration of the spit and inlet did still coincide with the observed migration for the validation period, indicating that the model can sufficiently describe long-term migration on fairly straight shorelines.

From the sensitivity analysis it can be concluded that no isolated parameter will stabilize the inlet migration or possible later width variation if varied within the estimated error margins. An increase in the cross-sectional area of 500 m^2 increased the time it took for the inlet to reach the boundary by about 4 years. With an estimated area of 3000 m^2, this would result in 8 years earlier or later reaching of the boundary. A 1000 m^2 error in the estimation is rather much (30%), and with the used method the error is thought to be lower.

Similarly, an increase of k_w by 1 increased the transport in the inlet which in turn could better withstand the LST resulting in a delay of 4 years in the migration time it took to reach the boundary. k_w is a calibrated parameter for the model, so the purpose of the sensitivity analysis for it was more to investigate the overall impact on the model. Plus or minus 1 unit from the used value is considered a large error as the deviation from the validation period is large and no indication was found that the transport coefficient would change significantly for the prediction period.

Geometric similarity in the inlet channel is expressed mathematically with the shape coefficient (α). This parameter caused, in the sensitivity analysis, a 1-year delay in the migration rate when it was increased by a step of 1. In comparison with the impact from the transport coefficient and the spit cross-section area, the shape coefficient had a smaller impact and is thus a less sensitive parameter for the model. The estimation of the parameter itself is based on the inlet shape for one instant moment, and since the inlet is migrating the shape could change over time. With only four years difference in total migration rate when varying α by 5 units, the maximum effect is still considered low.

Altogether, the considered “worst case scenario” is that the migration rate has an error of 15 years. An error of this magnitude is considered rather unlikely with respect to the calibration and validation results. Realistically, the migration rate is believed to differ more in the magnitude of one or two years. That is if the LST changes little over the migration path, which appears to be a crude simplification.

Overcoming the complications related to the curvature of the migration path and the subsequent changes in LST are the largest challenges when describing the long-term evolution. The linear appearance of the inlet migration might have been accurate for the past, but for the prediction period perhaps a decreasing migration rate would be expected due to a decreasing LST. This in turn would lead to that the inlet will migrate slower and reach its endpoint later. The modelled time to reach the boundary can thus be considered as a worst case scenario, timewise. Considering the limitations in the LST model with respect to the curvature, such scenarios were not modelled. However, the situation of a changing LST was briefly investigated in Figure 35 and 36 paragraph 6.4 by assigning different constant values to LST and look at the response on inlet migration and width variation. An average annual positive LST of 50 000 m^3/year both kept the inlet from migrating and changing width when the models were run individually. At the time of modelling, the annual average positive LST was roughly 270 000 m^3/year which corresponds to more than five times the transport. Even though the current LST is large, the curvature, changes in the sediment supplied from Thu Bon river and Cua Dai inlet could drastically decrease the LST in the vicinity of Cua Lo. Sediment is also deposited along the entire stretch on which the inlet is migrating, leaving less and less to drive the inlet migration.

That the LST is changing along the profile and that it will affect the morphology is rather certain. The issue is to characterize the change in a representative way. By modelling both the width and migration at the same time for fixed LST intervals, equilibrium for both width and migration was achieved at a positive annual LST of 50 000 m^3/year. A reduction of the calculated LST by 87%, close to one fifth, also lead to that the inlet ceased to migrate. However, such an equilibrium can be obtained for several different widths and further or less migrated distances (Figure 35 and 36, section 6.4). The chosen point for Scenario 1 was only estimated from the curvature of the beach, and a possibility that a rocky boundary exists under the sand formation attached to An Hoa cape. Knowing these limitations in the model result, the discussion of result from Scenario 1 below can be considered more as an

indication of what could happen. Either when the inlet reaches An Hoa cape, or the 980 m boundary.

Over the course of one year after the inlet reaches its boundary in Scenario 1, all but 30 m of the original inlet width is left. The large difference in LST between seasons (Figure 23) is the likely explanation of both the rapid narrowing and the oscillatory behaviour of the inlet width variation after the inlet reaches its boundary point. Narrowing is a result of large LST in comparison with the inlet sediment transport during monsoon season. Widening likely occurs when the LST is weaker during the dry period. Weaker LST in turn is caused by the weaker wave-driven currents and by the fact that Tam Hoa cape causes dissipation of the wave-driven currents since the waves partly originates from an ESE direction during this period. A couple of spikes are seen in the period after the boundary is reached. These are thought to be modelling artefacts which occur when the width is very narrow, the velocities large, and the LST low. Such a scenario seems to cause the model (Equation 52) to go beyond realistic width values.

The inlet width in the study of Nunes et al. showed similar behavior as the inlet in the study of Larson et al. (2020), the inlet width either stabilized at equilibrium or closed. The outcome depended on the magnitude of the constant input value of the longshore transport (m_L). This situation is similar to the one in this study, where inlet width depends highly on the relation between the inlet transport and the LST.

From end-2041 and onwards, a seeming dynamical equilibrium of the inlet width is reached. However, as the inlet reaches as narrow as 4m during monsoon closure will most likely occur. It is possible that the inlet moves towards permanent closure, or that temporary seasonal closure occurs during monsoon periods as with several other inlets in Vietnam (Tung, 2011). Historical satellite images do not show that the inlet exhibits closure, but as the inlet is still migrating it is not possible to visually conclude that closure will not occur (Duy et al., 2018). In the work of Nguyen et al. (2018), closure is suggested to occur during neap tide in the monsoon period based on Delft 3D simulations. This pattern would not be seen on satellite images unless the time of neap tide is caught precisely. Another factor supporting that closure might occur is that inlets, as discussed in 2.1.7, with similar (small) cross-sectional areas and small tidal prism commonly close on a seasonal basis.

An important factor to consider is that the developed model does not take into account events such as storm surges or floods. Even if a more permanent

closure would occur a single storm could reopen it, possibly enabling at least one more annual cycle to occur before another narrowing or closure. In turn, closure may also occur following a large storm during the monsoon period even before the inlet has reached its boundary.

Yet another factor affecting the lagoon dynamics is the presence of the larger inlet 2. Flooding events which could otherwise reopen or widen inlet 1 may be hydrodynamically favoured to be directed to inlet 2 due to a larger flow area when water levels are high, and the larger size of the inlet. Even before the inlet reaches its final destination, inlet 2 could affect the morphology of inlet 1. This is believed to be mainly through alterations such as dredging of inlet 2 or the passage between the Troung Giang river branch and the upper parts of the lagoon, and the lower part. Changes in the hydrodynamics would follow such implementations, which could favour narrowing or closure of inlet 1.

8. Conclusion

The objective of the project was to investigate the morphological dynamics of the sand spit and the Cua Lo inlet in the central parts of Vietnam and describe its long-term development, the subsequent effects on inlet-associated erosion and possible water exchange effects in the connecting estuary. It was of priority to keep the model simple in terms of input data, and fast in terms of computational times but still capable of describing important concepts of reality.

Two scenarios were investigated. One where the inlet was assumed to stop after 980 m due to either hitting a rock boundary, or changes in the longshore transport. Another, where the inlet was allowed to migrate up to 2000 m after which it reaches a hard rock boundary.

Following the assumptions of Scenario 1, the inlet is expected to reach the boundary around 2041. After that the inlet width is suggested to narrow and stabilize around 4-20 m with a seasonal variation. As the inlet becomes very narrow, it points towards that the inlet will exhibit seasonal or permanent closure. Uncertainties in the result mainly depend on how the LST changes along the curved coastline. If the LST is reduced by around 80-85%, from e.g. the shoreline curvature, an equilibrium where the inlet stops migrating and remains open could take place earlier, both spatially and timewise. The decreasing LST along the curvature could also retard the migration rate, making the inlet reach its boundary later.

When allowing the spit and inlet to migrate up to 2000 m, disregarding possible changes in the LST, it does not reach the boundary within the modelled period. This scenario, but also Scenario 1, will lead to loss of properties for local citizens along the migration path. One possible measure to eliminate this is to manually close the inlet by sediment infilling.

A finding when constructing the water exchange model related to the water quality of the northwestern areas of the lagoon is that the exchange between this area and the parts closer to the larger inlet seem to have a restricted water exchange. Closure of inlet 1, either as a consequence of migration to a hard boundary, or manually performed could therefore lead to changes in water quality for the northwestern areas of the lagoon. This is also the area with most aquaculture and the situation should be further investigated.

Although some discrepancies existed, the water exchange model was capable of describing the main characteristics of the lagoon water level variations.

These included the amplitude, phase, diurnal and fortnightly spring-neap tidal patterns. The migration model was successfully calibrated towards satellite data for the period 1988-2017.

A runtime of about 100 s was required for running simulations on morphological change from 2020 to 2049 when using a 10 min time step for the water exchange model and 1 h for the morphological model. This allowed for an analysis on the effects from several of the input parameters on the morphological evolution. Future model accuracy can be increased by modelling the LST in more detail.

9. References

Airy, G. B. (1845). Tides and waves. B. Fellowes.

Asplund, E., & Malmström, H. (2018). Coastal erosion in the region of Thu Bon River mouth, Vietnam. TVVR18/5007.

Bruun, P. & Gerritsen, F. (1959). Natural bypassing of sand at coastal inlets. Journal of Waterways, and Harbors Division, ASCE, 85(4):75–107.

Bruun, P., & Gerritsen, F. (1960). Stability of coastal inlets. Coastal Engineering Proceedings, (7), 23-23.

Bruun, P. (1966). Tidal inlets and littoral drift: Vol. 2, Universitelsforlaget, Oslo.

Bruun, P., Mehta, A. J., & Johnson, I. G. (1978). Stability of Tidal Inlets: Theory and Engineering. Developments in Geotechnical Engineering. Elsevier Science, Amsterdam.

Bruun, P. (2005). Bypassing at littoral drift barriers. In Schwartz, M. L., editor, Encyclopedia of coastal science, pages 210–216. Springer, Dordrecht, NL.

Cayocca, F. (2001). Long-term morphological modeling of a tidal inlet: the Arcachon Basin, France. Coastal engineering, 42(2), 115-142.

Couture, S. (2008). River Dynamics and Erosion. Great Bay Siltation Commission, December, 1.

De Alteris, J. T. and Byrne, R. J. (1975). The recent history of Wachapreague Inlet, Virginia. In Cronin, L. E., editor, Estuarine Research, volume 2, pages 167–181. Academic Press, New York.

Dissanayake, D. M. P. K., Ranasinghe, R., & Roelvink, J. A. (2009). Effect of sea level rise in tidal inlet evolution: A numerical modelling approach. Journal of Coastal Research, 942-946.

Duy, D. V., Tanaka, H., Mitobe, Y., & Viet, N. T. (2016). Observation of sand spit development at Cua Lo River mouth, Central Vietnam.

Duy, D. V., Tanaka, H., Mitobe, Y., Viet, N. T., & Binh, L. T. (2017). Analysis of erosion and accretion waves on Cua Dai Beach in Central Vietnam. Tohoku journal of natural disaster science, 53, 53-58.

Duy, D. V., Tanaka, H., Mitobe, Y., Anh, N. Q., & Viet, N. T. (2018). Sand Spit Elongation and Sediment Balance at Cua Lo Inlet in Central Vietnam. Journal of Coastal Research, 81(sp1), 32-39.

Elwany, M. H. S., Flick, R. E., & Aijaz, S. (1998). Opening and closure of a marginal southern California lagoon inlet. Estuaries, 21(2), 246-254.

Escoffier, F. F. (1940). The stability of tidal inlets. Shore and Beach, 8:111–114.

Evans, O. F. (1942). The origin of spits, bars, and related structures. The Journal of Geology, 50(7), 846-865.

FitzGerald, D. M. (1982). "Sediment bypassing at mixed energy tidal inlets," Proceedings 18th CoastalEngineering Conference, ASCE, 1094-1118.

FitzGerald, D. M. (1988). Shoreline erosional-depositional processes associated with tidal inlets. In Aubrey, D. G. and Weishar, L., editors, Lecture Notes on Coastal and Estuarine Studies, Vol.129, Hydrodynamics and Sediment Dynamics of Tidal Inlets, pages 186– 225. Springer, Verlag, New York.

Glaeser, D. J. (1978). Global distribution of barrier islands in terms of tectonic setting. Journal Geology, 86:283–297.

Hughes, S. A. (2002). Equilibrium cross sectional area at tidal inlets. Journal of Coastal Research, 160-174.

Imran, M., Nakashima, K., & Kawasaki, S. (2017). Combination technology of geotextile tube and artificial beachrock for coastal protection. International Journal, 13(39), 67-72.

Inman, D., & Harris, R. W. (1966). Oceanographic and Engineering report on investigation of sedimentation silting and dredging requirements. Saigon: Daniel Mann Johnson & Mendenhall.

Jarrett, J. T. (1976). Tidal prism-inlet area relationships (Vol. 3). US Department of Defense, Department of the Army, Corps of Engineers, Experiment Station.

Johnson, D. W. (1919). Shore processes and shoreline development. John Wiley & Sons, Incorporated.

Keulegan, G.H., (1967). Tidal Flow in Entrances. Water-Level Fluctuations of Basins in Communication with Seas. US Army Corps of Engineers, Vicksburg, MS. Technical Bulletin No. 14.

Kjerfve, B. (Ed.). (1994). Coastal lagoon processes. Elsevier.

Kraus, N. C. (1999). Analytical model of spit evolution at inlets. Proc. Coastal Sediments 99, ASCE, 1739 – 1754.

Kraus, N. C. (2010). Engineering of tidal inlets and morphologic consequences. In Handbook of coastal and ocean engineering (pp. 867-900).

Larson, M., Wikramanayake, N., Hanson, H., & Ranasinghe, R. (2009). Seasonal closure of Chilaw Inlet, Sri Lanka: physical processes and mathematical modeling. In Proceedings Of Coastal Dynamics 2009: Impacts of Human Activities on Dynamic Coastal Processes (With CD-ROM) (pp. 1-11).

Larson, M., Hoan, L. X., & Hanson, H. (2010). Direct formula to compute wave height and angle at incipient breaking. Journal of waterway, port, coastal, and ocean engineering, 136(2), 119-122.

Larson, M., Palalane, J., & Hanson, H. (2015). Sandy Spits and Their Mathematical Modeling. In Sand and Gravel Spits (pp. 217-245). Springer, Cham.

Larson, M., Nunes, A., & Tanaka, H. (2020). Semi-analytic model of tidal-induced inlet flow and morphological evolution. Coastal Engineering, 155, 103581.

Leatherman, S. P. (1988). Barrier island handbook. University of Maryland Press, College Park.

MacMahan, J., van de Kreeke, J., Reniers, A., Elgar, S., Raubenheimer, B., Thornton, E., & Brown, J. (2014). Fortnightly tides and subtidal motions in a choked inlet. Estuarine, Coastal and Shelf Science, 150, 325-331.

Murray, A. B. (2003). Contrasting the goals, strategies, and predictions associated with simplified numerical models and detailed simulations. Geophysical Monograph-American Geophysical Union, 135, 151-168.

Montanari, A., Beach protection strategies and structures, 2017-03-21, 2020-05-11, [https://distart119.ing.unibo.it/albertonew/?q=node/100]

Nauditt, A., & Ribbe, L. (Eds.). (2017). Land use and climate change interactions in central Vietnam. Springer.

Nguyen, Q. D. A. et al. (2018a). Numerical modeling of the sand spit elongation at Cua Lo inlet. Proceedings of the 8th International Conference on Fluid Mechanics (ICFM8) September 25-28, 2018, Tohoku University, Sendai, Japan

Nguyen, Q. D. A. et al. (2018b). Determination of the longshore sediment transport along the beach from Cua Dai to Cua Lo estuaries in Quang Nam, Vietnam. Proceedings of the 8th International Conference on Fluid Mechanics (ICFM8) September 25-28, 2018, Tohoku University, Sendai, Japan

Nunes, A., Larson, M., & Fragoso Jr, C. R. (2020). Morphological modeling of long-term inlet channel evolution with an application to the Mundaú Lagoon inlet, Brazil. Estuarine, Coastal and Shelf Science, 235, 106618.

Ranasinghe, R., Pattiaratchi, C., & Masselink, G. (1999). A morphodynamic model to simulate the seasonal closure of tidal inlets. Coastal Engineering, 37(1), 1-36.

Rijn, L. C. (2011). Coastal erosion and control. Ocean & Coastal Management, 54(12), 867-887.

State of New Hampshire. (2007). Final Report of the Comission to Study the Causes, Effects, and Remediation of Siltation in the Great Bay Estuary. HB 216, Chapter 31, Laws of 2007.

Palalane, J., Larson, M., & Hanson, H. (2014). Analytical model of sand spit evolution. Coastal engineering, 2.

Parker, B. B. (2007). Tidal analysis and prediction.

Pernetta, J. C., & Milliman, J. D. (1995). Land-ocean interactions in the coastal zone: implementation plan. Oceanographic Literature Review, 9(42), 801.

Quang, D (2020). River Simulations of the VGTB (Vu Gia Thu Bon) river basin, Unpublished work.

Siegle, E., & Asp, N. E. (2007). Wave refraction and longshore transport patterns along the southern Santa Catarina coast. Brazilian Journal of Oceanography, 55(2), 109-120.

Stive, M. J., & Wang, Z. B. (2003). Morphodynamic modeling of tidal basins and coastal inlets. In Elsevier oceanography series (Vol. 67, pp. 367-392). Elsevier.

Stive, M. F. J., de Vriend, H. J., Dronkers, J., van Dongeren, A., and B.,W. Z. (2006). Coastal inlets and Tidal basins. Delft University of Technology, Delft.

Stive, M., Ji, L., Brouwer, R. L., van de Kreeke, C., & Ranasinghe, R. (2010). Empirical relationship between inlet cross-sectional area and tidal prism: A re-evaluation. Coastal Engineering Proceedings, (32), 86-86.

Tanaka, H., Takahashi, F., & Takahashi, A. (1997). Complete closure of the Nanakita River Mouth in 1994. In Coastal Engineering 1996 (pp. 4545-4556).

Tang, C. F., Tan, B. W., & Ozturk, I. (2016). Energy consumption and economic growth in Vietnam. Renewable and Sustainable Energy Reviews, 54, 1506-1514.

Tung, T. T., Stive, M. J., van de Graaff, J., & Walstra, D. J. R. (2007). Morphological behavior of seasonal closure of tidal inlets. In Coastal Sediments' 07 (pp. 1589-1600).

Tung T. T. (2011). Morphodynamics of seasonally closed coastal inlets at the central coast of Vietnam.

Turner, R. K., Subak, S., & Adger, W. N. (1996). Pressures, trends, and impacts in coastal zones: interactions between socioeconomic and natural systems. Environmental management, 20(2), 159-173.

US Army Corps of Engineers. (1984). Shore Protection Manual, Washington D.C.: US Army Corps of Rngineers, Coastal Engineering Research Center.

van de Kreeke, J. (1996). "Morphological changes on a decadal time scale in tidal inlets: modeling approaches." Journal of Coastal Research 73-81.

van de Kreeke, J., & Brouwer, R. L. (2017). Tidal inlets: hydrodynamics and morphodynamics. Cambridge University Press.

Van der Wegen, M., Dastgheib, A., & Roelvink, J. A. (2010). Morphodynamic modeling of tidal channel evolution in comparison to empirical PA relationship. Coastal Engineering, 57(9), 827-837.

Yin, Y., Karunarathna, H., Reeve, D.E. (2019). Numerical modelling of hydrodynamic and morphodynamic response of a meso-tidal estuary inlet to the impacts of global climate variabilities. Mar. Geol. 407, 229–247. https://doi.org/10.1016/j. margeo.2018.11.005.

Walton Jr, T. L., & Adams, W. D. (1977). Capacity of inlet outer bars to store sand. In Coastal Engineering 1976 (pp. 1919-1937).

A. Appendix

A1 Complete equation for inlet width

The complete equation for changes in the inlet width is described in the following section.

The below equation describes how the inlet width changes with time. The equation for u_{I1} is inserted into m_I, and the shape factor is included to express the inlet cross-sectional area (A_{I1}) in terms of the inlet width (W_{I1}). The water level in lagoon 1 (h_{L1}^{k+1}) is also affected by changes in the inlet cross sectional area. This is taken into consideration in the calculations, but it is not included in the formula below since the equation would be too long. The equation was solved numerically in Python.

$$
\begin{aligned}
&W_{I1}^{k+1} \\
&= \left(\frac{\alpha^2 \Delta t}{B} \left(\frac{k_w W_{I1}^k}{\rho g} \left(\frac{(h_{L1}^{k+1} - h_{L1}^k)}{\Delta t} A_{L1} \left(\frac{\alpha}{W_{I1}^k} \right)^2 - Q_R X \left(\frac{\alpha}{W_{I1}^k} \right)^2 \right.\right.\right. \\
&\left.\left.\left. - A_{12} \left(\frac{\alpha}{W_{I1}^k} \right)^2 \sqrt{\frac{2g}{k_{f12}}} \frac{(h_{L2}^k - h_{L1}^k)}{\sqrt{|h_{L2}^k - h_{L1}^k|}} \right) \left(\frac{1}{8} f_D \rho \left(\frac{(h_{L1}^{k+1} - h_{L1}^k)}{\Delta t} A_{L1} \left(\frac{\alpha}{W_{I1}^k} \right)^2 \right.\right.\right.\right. \\
&\left.\left.\left.\left. - Q_R X \left(\frac{\alpha}{W_{I1}^k} \right)^2 - A_{12} \left(\frac{\alpha}{W_{I1}^k} \right)^2 \sqrt{\frac{2g}{k_{f12}}} \frac{(h_{L2}^k - h_{L1}^k)}{\sqrt{|h_{L2}^k - h_{L1}^k|}} \right) - \theta_{cr} D_s (\gamma_s - \gamma_w) \right) - m_L \right) \\
&\left. + W_{I1}^k \right)^{\frac{1}{2}}
\end{aligned}
$$

A2 Model input

Figure 38 and 39 shows measured river flow each hour in Truong Giang river in August and November 2019. The data collection was performed by the research team at Thuyloi University during the surveys in 2019. The mean and median values in August were -41 m^3/s and -104 m^3/s, in November were the

mean and median values 50.72 m^3/s and 27.25 m^3/s. In other words, the flow direction in August is from SE to NW, from the estuary into the river channel. In November is the flow direction from NW to SE, from the river channel into the estuary.

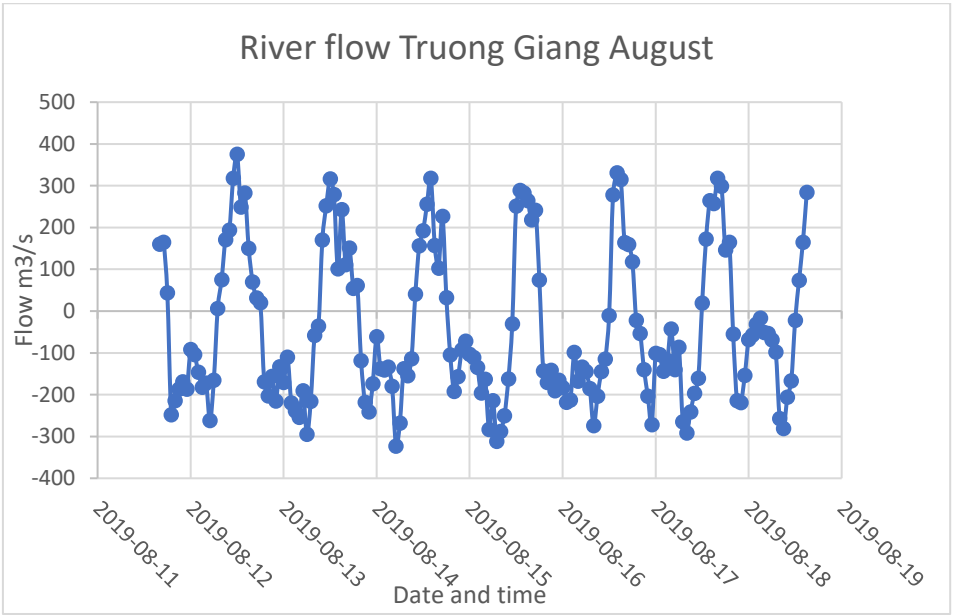

Figure 38. Measured flow in Truong Giang river, each hour, during a week in August 2019.

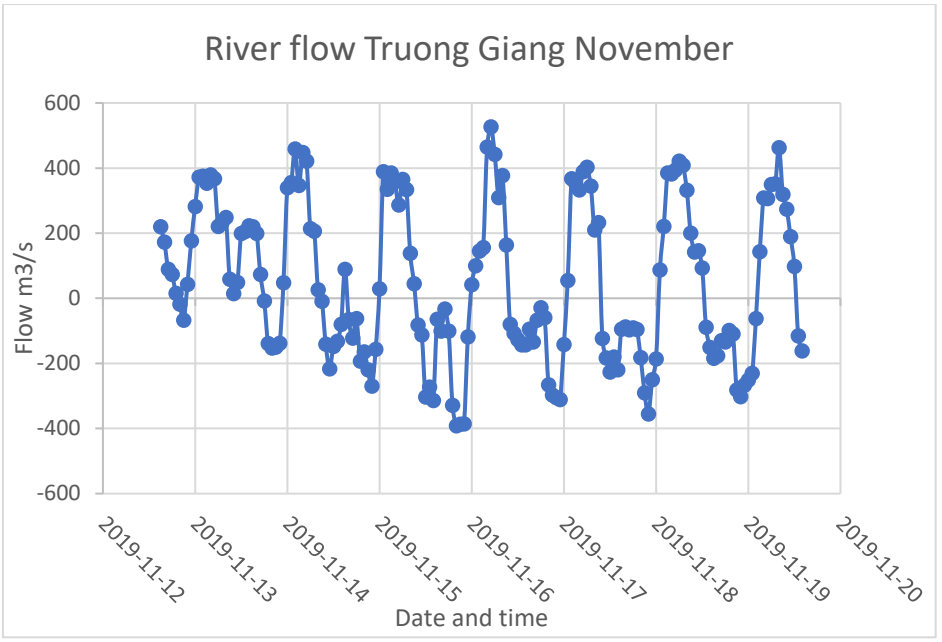

Figure 39. Measured flow in Truong Giang river, each hour, during a week in November 2019.

Figure 40 and 41 shows the flow (m^3/s) in Truong Giang river simulated for year 2017 during dry- and flood season, respectively. The figures show the flow from Cua Dai estuary, left side of the figures, to Cua Lo estuary, right side of the figures. The thick, dashed red line marks the line of zero flow. The thin, dashed red line represents the median flow. The blue bars show the median flow above and below zero, respectively. During dry season the median flow is almost zero. During flood season the median flow is about 30 m^3/s.

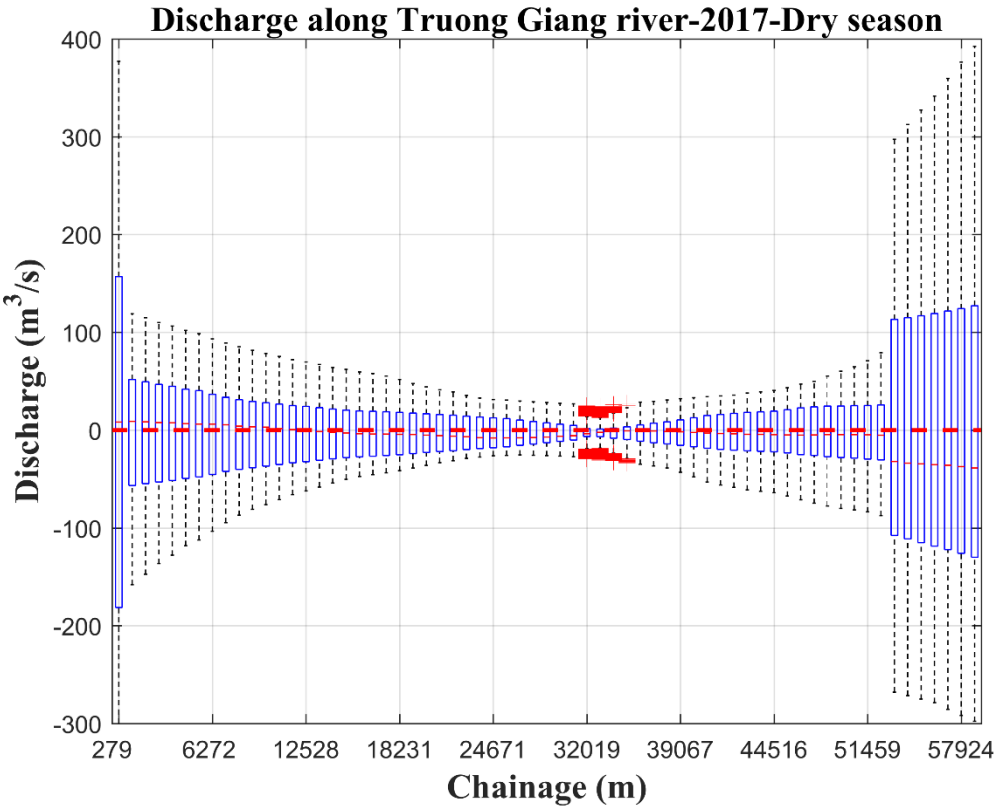

Figure 40. Box whisker plot of the flow in Truong Giang river during dry season. The thick, dashed red line marks the line of zero flow. The thin, dashed red line represents the median flow. The blue line shows median flows above and below zero in the river (Quang, 2020).

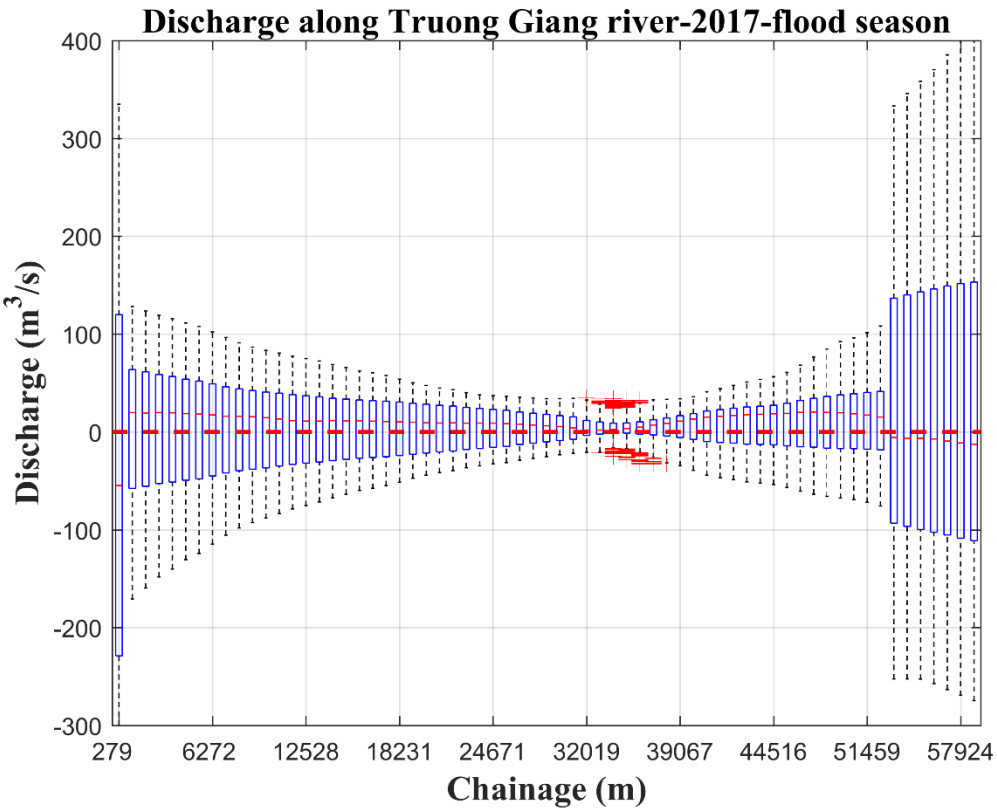

Figure 41. Box whisker plot of the flow in Truong Giang river during flood season. The thick, dashed red line marks the line of zero flow. The thin, dashed red line represents the median flow. The blue line shows median flows above and below zero in the river (Quang, 2020).

Figure 42 and 43 shows the cross-sectional area at the narrowest part for inlet 1 and 2, respectively. The cross-sectional areas were approximated with trapezoidal shapes. The red line represents the actual cross-sectional area, the blue line represents the approximated trapezoidal area.

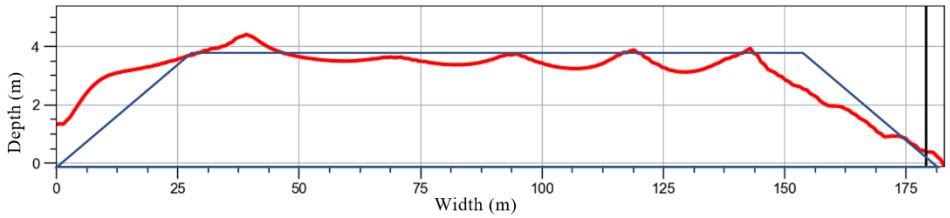

Figure 42. A cross-sectional profile of inlet 1, the red line. The blue line is an approximated trapezoidal shape of the cross-sectional profile.

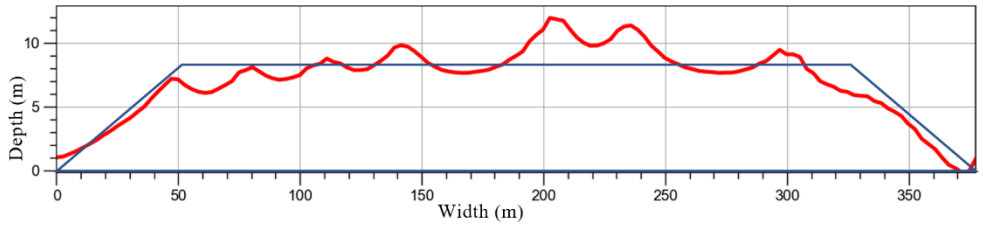

Figure 43. A cross-sectional profile of inlet 2, the red line. The blue line is an approximated trapezoidal shape of the cross-sectional profile.

The figure below (Figure 44) shows the defined lagoon areas. The green area represents lagoon 1, the blue area represents lagoon 2.

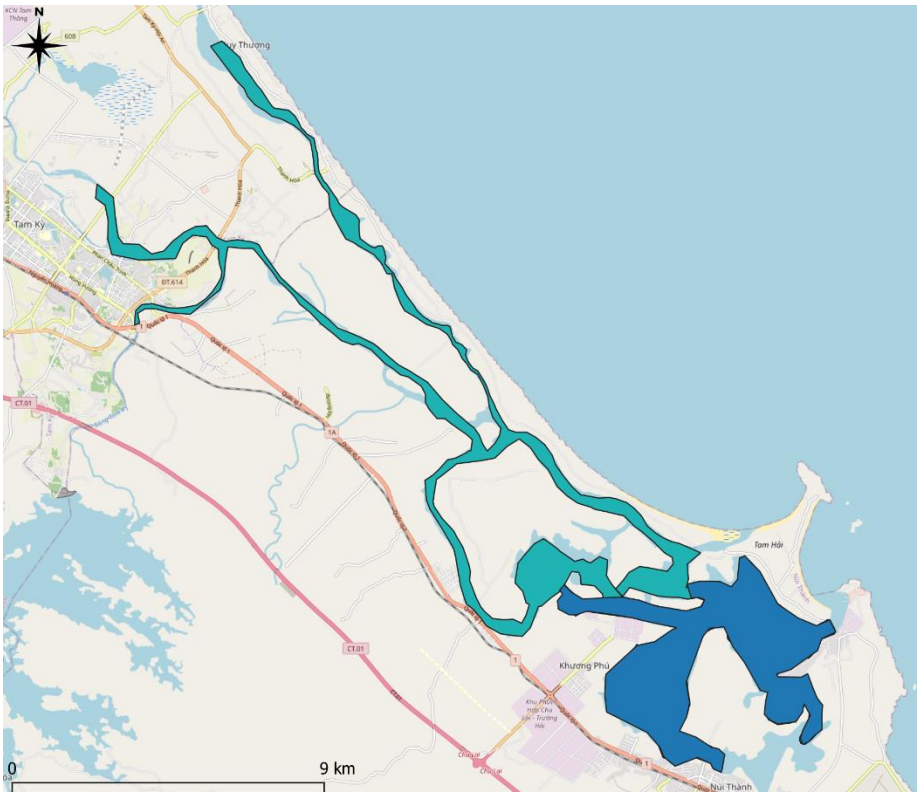

Figure 44. Schematic illustration of the lagoon area split into the two modelled lagoon areas. The green area represents lagoon 1 and the blue area represents lagoon 2.

A3 Tidal constituents

Table 7 includes information on the tidal constituents which were used for ocean water level predictions at Hoi An. The tidal constituents have a number, a name, an amplitude in centimetres, and a phase in degrees.

Table 7. Tidal constituents for ocean water level predictions at Hoi An. The table includes the number of each tidal constituent, the name, the amplitude in centimeters, and the phase in degrees.

Num	*Name*	*Amplitude (cm)*	*Phase (deg)*
1	K1	24.189	183.9
2	SA	17.106	249.1
3	M2	17.098	98.4
4	O1	17.952	141.6
5	S2	5.906	127.3
6	P1	7.807	182
7	N2	3.855	77
8	SSA	5.009	67.1
9	MM	0.554	138
10	Q1	3.287	129.5
11	K2	1.67	139.7
12	MF	2.791	68.5
13	M1	0.97	170.6
14	NU2	0.638	90.7
15	J1	1.084	212.2
16	MS4	0.284	241.4
17	MSF	1.432	69.1
18	L2	0.2	146.6
19	MU2	0.81	53.4
20	M4	0.415	180.1
21	T2	0.357	115.8
22	R2	0.093	358.9
23	2SM2	0.06	133.4
24	S1	0.294	0.7
25	M3	0.307	352.5
26	M6	0.184	330.9
27	S4	0.053	26.6

A4 Bathymetry

Bathymetry data is represented in Figure 45. The bright areas are the deepest while the darker blue are more shallow. The dark blue areas also defines the land-water intersection.

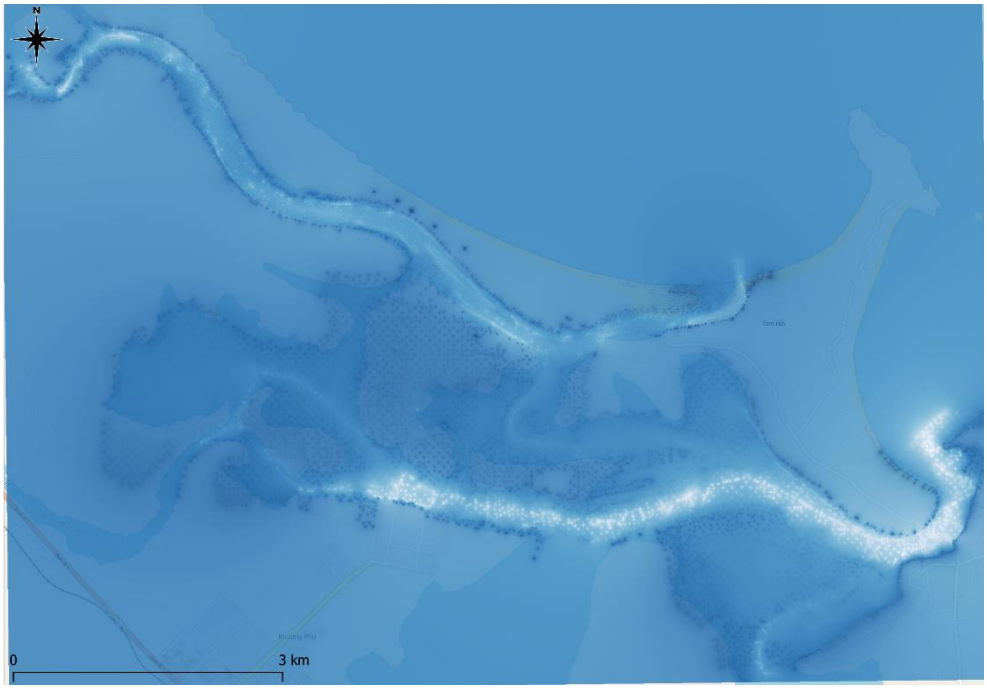

Figure 45. Bathymetry data measured in the Cua Lo estuary and it´s vicinity. The bright areas are the deepest.

A5 Lagoon water levels

Figure 46 and 47 are extended versions of Figure 20 and 21, respectively. The calculated water level in lagoon 2 and the measured ocean water level are also added in the below figures. It is possible to see that the measured and calculated water levels in lagoon 1 are more damped in comparison with the ocean (the black line). Lagoon 2, the green line, which has a larger lagoon area and a larger inlet cross-sectional area compared to lagoon- and inlet 1, follows the ocean water levels well. The water levels in November have higher peaks in comparison with the water levels in August, but the valleys are lower in

August. The water levels in lagoon 1 are phase shifted to the right in comparison with the ocean water levels and the water levels in lagoon 2.

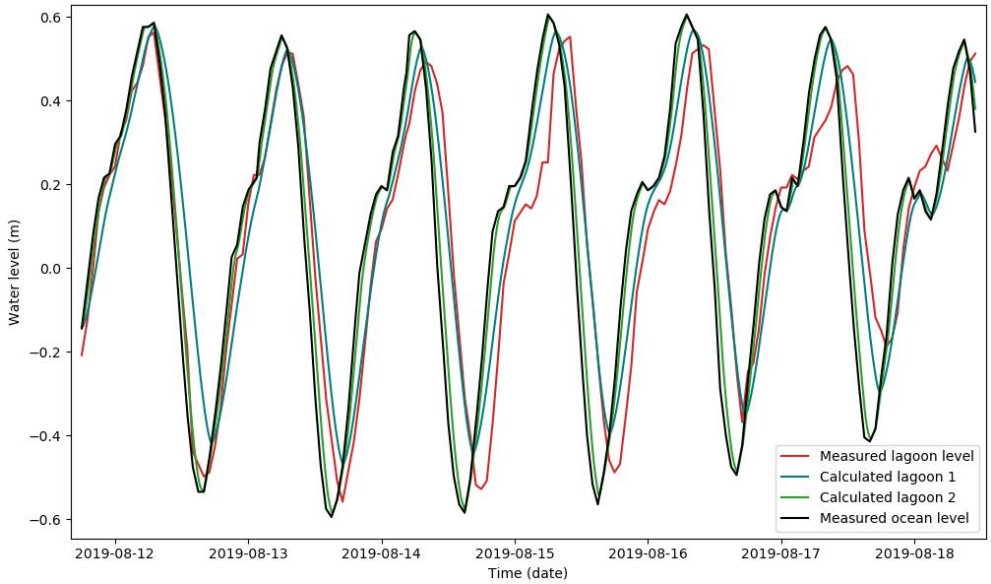

Figure 46. Measured and calculated water levels during one week in August 2019. The red line represents measured levels in lagoon 1, the blue line is calculated levels in lagoon 1, the green line is calculated levels in lagoon 2, and the black line is measured water levels in the ocean.

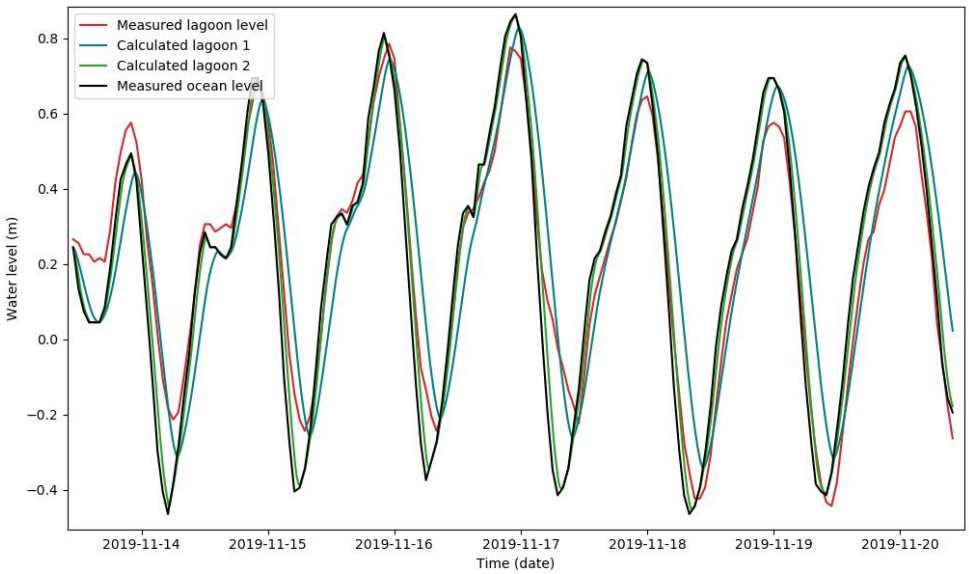

Figure 47. Measured and calculated water levels during one week in November 2019. The red line represents measured levels in lagoon 1, the blue line is calculated levels in lagoon 1,

the green line is calculated levels in lagoon 2, and the black line is measured water levels in the ocean.

A6 Morphology

The migrated distance of the inlet with a transport coefficient of 6.1 is shown in Figure 49. With a transport coefficient of 6.1, no long-term migration was observed.

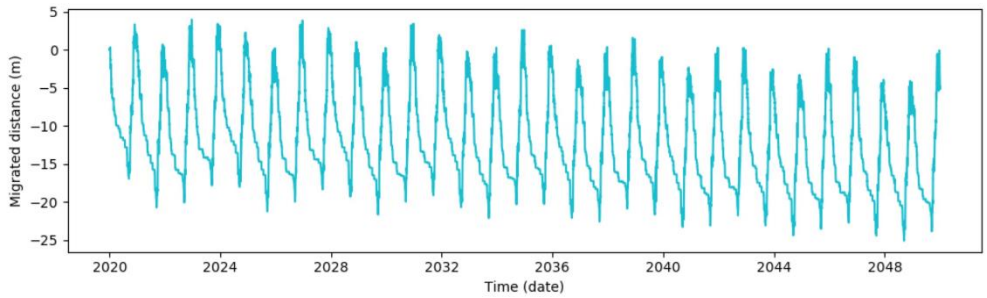

Figure 48. Migrated distance of the inlet when the transport coefficient is set to 6.1, resulting in no long-term net migration.

Migrated distance at reduced LST is represented in Figure 49. LST was reduced from 10 % to 90 % with a step of 10 %. Migration occurred until LST was reduced with around 80 % (orange line), then the inlet migration stopped.

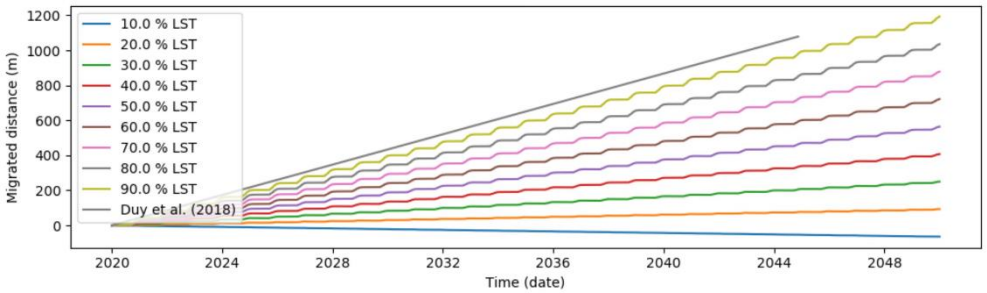

Figure 49. Migrated distance at reduced LST, ranging from 10 % to 90 % of the calculated LST. The grey line represents the predicted migrated distance from Duy et al. (2018).

Figure 50 shows width changes and migrated distance at different values of the loss coefficient in inlet 1 (k_{f1}). k_{f1} ranged from 10 to 100 with a step of 10. A large value decreased the inlet transport which increased the migration rate (light blue line). The reversed situation occurred for small values of k_{f1}

(dark blue line). A value of 100 reduced the migration rate enough to hinder the inlet from finding an equilibrium state for width variations. The inlet managed to arrive to the boundary during the simulation period, but the width variations were only just initiated.

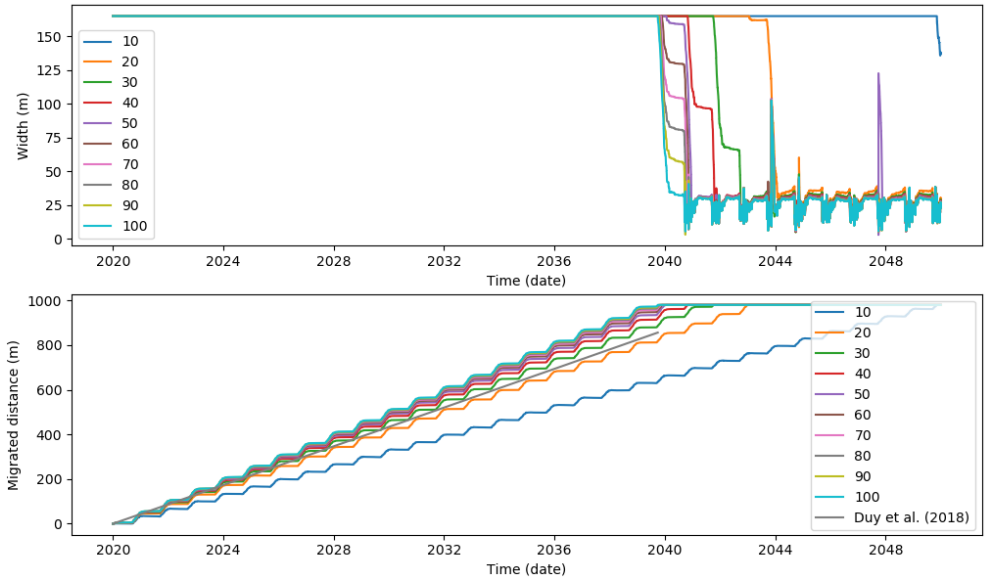

Figure 50. Inlet width changes (upper graph (a)) and inlet migration (lower graph (b)) at different values of the loss coefficient in inlet 1 (kf1). Kf1 ranged from 10 to 100 with a step of 10.

A7 Python code

```
1.  # LST program made from Magnus Larson's LST calculator in Fortran
2.
3.  # Program to analyze the offshore wave data and generate values of l
    ongshore
4.  # sediment transport.
5.
6.  import os
7.  import matplotlib.pyplot as plt
8.  from windrose import WindroseAxes
9.  import matplotlib.cm as cm
10. import math
11. from datetime import datetime
12. from collections import defaultdict
13. import numpy as np
14. import csv
15.
16. DEPTH = 56
```

```
MULTIPLIER = 1
SHORE_ORIENTATION = -38
LEFT_LIMIT = -15
RIGHT_LIMIT = 11
YEARS = 27
GAMBR = 0.78


def get_wave_file(filename):
    """opens the wave climate file"""
    infile = open(filename)
    lines = infile.readlines()
    wave_data_list = []
    for line in lines[1:]:
        line.rstrip()
        lista = line.split()
        date = lista[0]
        date = datetime.strptime(date, '%Y%m%d')
        lista = [float(i) for i in lista[1:]]
        [hour, hs, ts, direction] = [lista[0], lista[1], lista[2], l
ista[3]]
        wave_data_list.append([date, hour, hs, ts, direction])
    return wave_data_list


def filter_waves(SHORE_ORIENTATION, LEFT_LIMIT, RIGHT_LIMIT, i):
    if i[4] > 270:
        i[4] = i[4] - 360
    if (i[4] < float(LEFT_LIMIT)) or (i[4] > float(RIGHT_LIMIT)):
        i[4] = 0
    else:
        i[4] = float(SHORE_ORIENTATION) - i[4]


def remove_off_range(i):
    if i[4] > 90 or i[4] < -90:
        i[4] = 0


def convert_to_radians(i):
    i[4] = math.radians(i[4])


def get_valid_waves(wave_data):
    for i in wave_data:
        filter_waves(SHORE_ORIENTATION, LEFT_LIMIT, RIGHT_LIMIT, i)

        remove_off_range(i)
        convert_to_radians(i)
    return wave_data


def use_disp_eqn(period_in):
```

```
    """THIS ROUTINE SOLVES THE DISPERSION EQUATION USING A PADE APPROXIMATION"""

    Y = (2 * math.pi / period_in) ** 2 * DEPTH / 9.82
    F = Y + 1.0 / (1.0 + Y * (0.66667 + Y * (0.3555 + Y * (0.16084 + Y * (0.06320 + Y * (0.02174 + Y * (0.00654 + Y * (0.00171 + Y * (0.00039 + Y * 0.000111)))))))))
    w_length_in = 2 * math.pi / math.sqrt(Y * F / DEPTH ** 2)
    C = 4 * math.pi * DEPTH / w_length_in

    if C < 15.00:
        CN = 0.5 * (1 + C / math.sinh(C))
    else:
        CN = 0.5

    group_velocity = CN * w_length_in / period_in
    return [w_length_in, group_velocity, CN]


def calc_wave_br_prop(wave_height_in, period_in, angle_in):
    """CALCULATE WAVE PROPERTIES AT INCIPIENT BREAKING
    (USING APPROXIMATIVE METHOD BY LARSON ET AL.)"""
    radian_angle_in = angle_in
    CNIN = use_disp_eqn(period_in)[2]

    celerity_in = use_disp_eqn(period_in)[0] / period_in
    alpha = ( celerity_in / math.sqrt(9.82 * wave_height_in)) ** 4 * GAMBR ** 2 / CNIN
    lambda_a = (math.cos(radian_angle_in) / alpha ) ** 0.4
    epsilon = (math.sin(radian_angle_in)) ** 2 * lambda_a
    delta = 1.0 + 0.1649 * epsilon + 0.5948 * epsilon ** 2 - 1.6787 * epsilon ** 3 + 2.8573 * epsilon ** 4
    lambda_corr = lambda_a * delta
    breaker_depth = lambda_corr * celerity_in ** 2 / 9.82
    breaker_height = breaker_depth * GAMBR # This is the breaking wave height

    if abs(math.sin(radian_angle_in) * math.sqrt(lambda_corr)) > 1.0:
        print('NO SOLUTION')
        breaking_wave_angle = 0.0
        breaker_height = 0.0
    else:
        breaking_wave_angle = math.asin(math.sin(radian_angle_in) * math.sqrt(lambda_corr))
    return [breaker_height, breaking_wave_angle]


def calc_LST(sorted_wave_data):
    LST= []
    HBR = []
    ABR = []
    j = 0
    for i in sorted_wave_data:
```

```
        if i[3] > 0.00 and i[2] > 0.00:
            breaking_wave_height = calc_wave_br_prop(i[2], i[3], i[4])[0]
            breaking_wave_angle = calc_wave_br_prop(i[2], i[3], i[4])[1]
            # cerc_const = 60 * (0.39 * ( 1000 / (16 * math.sqrt(GAMBR) * ( 2660 - 1000) * (1 - 0.4))))
            if j > 78895:
                TIME_FACTOR = 1
            else:
                TIME_FACTOR = 3
            Q = 50.166 * TIME_FACTOR * math.sqrt(9.82) * breaking_wave_height ** 2.5 * math.sin(2 * breaking_wave_angle) * MULTIPLIER
        else:
            Q = 0
        j += 1
        LST.append(Q)
        HBR.append(breaking_wave_height)
        ABR.append(breaking_wave_angle * 57.3)
    return LST #[LST, HBR, ABR]


def append_lst(wave_data, LST):
    j = 0
    for i in wave_data:
        i.append(LST[j])
        j += 1
    return wave_data

def sort_into_dates(lst_list):
    wave_data_list = []
    for date in lst_list:
        wave_data_list.append([date[0], date[5]])
    hour_values = []
    three_hour_dates = []
    [three_hour_dates.append(day[0]) for day in wave_data_list[78896::3]]
    [hour_values.append(day[1]) for day in wave_data_list[78896:]]

    three_hour_values = list(np.add.reduceat(hour_values, np.arange(0, len(hour_values), 3)))
    three_hour_list = []
    i = 0
    for line in three_hour_dates:
        three_hour_list.append([three_hour_dates[i], three_hour_values[i]])
        i += 1
    new_lst_list = wave_data_list[:78896]
    new_lst_list.extend(three_hour_list)
    return new_lst_list


def write_to_csv(lst_list):
    filename = "lst_list_19882017_2.csv"
    fields = ['Date', 'lst']
```

```
163.     with open(filename, 'w', newline='') as csvfile:
164.         csvwriter = csv.writer(csvfile)
165.         csvwriter.writerow(fields)
166.         csvwriter.writerows(lst_list)
167.
168. def plot_wave_rose(wave_climate, breaking_waves):
169.     """plots the general wave climate during flood and dry season""
     "
170.
171.     wave_direction_dry = []
172.     wave_direction_wet = []
173.     wave_height_dry = []
174.     wave_height_wet = []
175.     i = 0
176.     for time in wave_climate:
177.         if time[0].month in range(9, 13):
178.             wave_direction_wet.append(breaking_waves[2][i] + 56)
179.             wave_height_wet.append(breaking_waves[1][i])
180.         else:
181.             wave_direction_dry.append(breaking_waves[2][i] + 56)
182.             wave_height_dry.append(breaking_waves[1][i])
183.         i += 1
184.
185.     fig=plt.figure()
186.     rect=[0.05, 0.1, 0.4, 0.8]
187.     ax_1=WindroseAxes(fig, rect)
188.     fig.add_axes(ax_1)
189.     ax_1.bar(wave_direction_dry, wave_height_dry, normed=True, open
     ing=0.8, edgecolor='grey', bins=np.logspace(-
     0.5, 0.5, 7), nsector=32)
190.     ax_1.set_legend()
191.     ax_1.set_title("Dry season", position=(0.5, 1.1))
192.
193.     rect=[0.55, 0.1, 0.4, 0.8]
194.     ax_2=WindroseAxes(fig, rect)
195.     fig.add_axes(ax_2)
196.     ax_2.bar(wave_direction_wet, wave_height_wet, normed=True, open
     ing=0.8, edgecolor='grey', bins=np.logspace(-
     0.5, 0.5, 7), nsector=32)
197.     ax_2.set_legend()
198.     ax_2.set_title("Wet season", position=(0.5, 1.1))
199.
200.
201.
202. def lst_main():
203.     wave_data = get_wave_file("wavesum19882017.txt")
204.     sorted_wave_data = get_valid_waves(wave_data)
205.     LST = calc_LST(sorted_wave_data)
206.     lst_list = append_lst(sorted_wave_data, LST)
207.     date_lst = sort_into_dates(lst_list)
208.     write_to_csv(date_lst)
209.     #plot_wave_rose(wave_data, LST)
210. lst_main()
```

```
def get_wave_file(filename):
    """opens the wave climate file"""
    infile = open(filename)
    lines = infile.readlines()
    wave_data_list = []
    for line in lines[1:]:
        line.rstrip()
        lista = line.split()
        value = lista[1].split(";")
        date = lista[0]
        date = datetime.strptime(date, '%Y-%m-%d')
        [hour, lst] = [date, float(value[1])]
        wave_data_list.append([date, lst])
    return wave_data_list


def create_date_dict_1(lst_appended_1):
    date_dict_1 = {}
    for date in lst_appended_1:
        date[0] = '{:%m-%d}'.format(date[0])
    for line in lst_appended_1:
        if line[0] in date_dict_1:
            date_dict_1[line[0]].append(line[1])
        else:
            date_dict_1[line[0]] = [line[1]]
    return date_dict_1

def create_date_dict_2(lst_appended):
    date_dict = {}
    for line in lst_appended:
        if line[0] in date_dict:
            date_dict[line[0]].append(line[1])
        else:
            date_dict[line[0]] = [line[1]]
    return date_dict

def calc_three_hour_averages(lst_dict):
    net_lst = 0
    for key in lst_dict.keys():
        lst_dict[key] = sum(lst_dict[key]) / len(lst_dict[key])
        net_lst += lst_dict[key]
    return lst_dict


def group_as_years(long_date_dict):
    newdict = defaultdict(lambda: [])
    for key in sorted(long_date_dict):
        newdict[(key.year)][:] += long_date_dict[key][:]
    return newdict


def annual_avg_summation(wave_dict):
    annual_lst = []
    annual_pos = 0
    annual_neg = 0
```

```
    for key in wave_dict:
        annual_lst.append(sum(wave_dict[key]))
        for value in wave_dict[key]:
            if value > 0.00:
                annual_pos += value
            else:
                annual_neg += value

    annual_avg_net = sum(annual_lst) / len(wave_dict)
    annual_gross = (annual_pos - annual_neg) / len(wave_dict)
    return [annual_pos / len(wave_dict) , annual_neg / len(wave_dict),
            annual_avg_net, annual_gross]


def monthly_avg_Q(lst_dict):
    n_years = len(group_as_years(lst_dict))
    newdict = defaultdict(lambda: [])
    monthly_avg = {}
    months = ['1', '2', '3', '4', '5', '6', '7', '8', '9', '10', '11', '12']
    i = 0
    for key in sorted(lst_dict):
        newdict[(key.month)][:] += lst_dict[key][:]
    for key in newdict:
        monthly_avg[months[i]] = sum(newdict[key]) / (n_years)
        i += 1
    return monthly_avg

def plot_monthly_averages(lst_dict):
    plt.bar(*zip(*lst_dict.items()))
    plt.ylabel('LST (m3/month)')
    plt.xlabel('Month')
    plt.show()


def lst_main():
    lst_date_list = get_wave_file("lst_list_19882017.csv")
    lst_dict_2 = create_date_dict_2(lst_date_list)
    lst_dict_1 = create_date_dict_1(lst_date_list)
    three_h_averages_dict = calc_three_hour_averages(lst_dict_1)
    annual_sorted_waves = group_as_years(lst_dict_2)
    annual_avg_lst = annual_avg_summation(annual_sorted_waves)
    print(('Annual average positive: {:.2f} \nAnnual average negative: {:.2f} \nAnnual avergare net: {:.2f} \nAnnual gross: {:.2f}')
          .format(annual_avg_lst[0], annual_avg_lst[1], annual_avg_lst[2], annual_avg_lst[3]))
    monthly_dict = monthly_avg_Q(lst_dict_2)
    #plot_monthly_averages(monthly_dict)
    #plt.bar(*zip(*monthly_dict.items()))
    #return monthly_dict
    return [three_h_averages_dict, monthly_dict]
```

```
# Orio Johansson Spring 2020
# Master's thesis in water resource management, LTH, Lund.
# Program to model the morphological evolution of the sand spit in Cua Lo, Vietnam, using longshore
# sediment transport and a simple water exchange model

import os
import math
import matplotlib
import matplotlib.pyplot as plt
from datetime import datetime, timedelta
import itertools
import LST_model
from LST_model import lst_main
import statistics as stat
from collections import defaultdict
import numpy


# Global constants, used in numerous equations:
LAGOON_AREA_1 = 13000000 # m2
LAGOON_AREA_2 = 18000000 # m2
TIME_STEP = 600 # Seconds
TIME_STEP_2 = 3600 * 1 # Seconds
FRICTION_1 = 26 #10
FRICTION_2 =  15 #8
FRICTION_3 =  35 #20
INLET_1 = 0.5 * 3.8 * ((156.25 - 28) + (181)) # m2
INLET_2 = ( 0.5 * 8.5 * ((325 - 50) + (330))) # m2
INLET_3 = 400 # m2
#RIVER_1 = 40 #m3/s
SHAPE = 7.47



def read_records_from_file(filename):
    """Reads the data records and compiles a list of the necessary data"""
    all_data = open(filename)
    lines = all_data.readlines()
    water_levels = []
    date_list = []
    for line in lines[1:]:
            split = line.split(";")
            date = split[0]
            try:
                local_date = datetime.strptime(date, '%Y-%m-%d %H:%M:%S') + timedelta(hours=7)
            except ValueError:
                local_date = datetime.strptime(date, '%Y-%m-%d %H:%M') + timedelta(hours=7)
            hoi_an = float(split[1]) / 100
            water_levels.append([local_date, hoi_an])
    all_data.close()
    return water_levels
```

```
52.
53.
54.
55. def read_records_from_file_2(filename):
56.     """Reads the data records and compiles a list of the necessary d
    ata"""
57.     all_data = open(filename)
58.     lines = all_data.readlines()
59.     water_levels = []
60.     date_list = []
61.     for line in lines[1:]:
62.             split = line.split(";")
63.             date = split[0]
64.             date = datetime.strptime(date, '%Y-%m-%d %H:%M:%S')
65.             tam_hai  = float(split[1]) / 100
66.             water_levels.append([date, tam_hai])
67.     all_data.close()
68.     return water_levels
69.
70.
71. def read_records_from_file_3(filename):
72.     """Reads the data records and compiles a list of the necessary d
    ata"""
73.     all_data = open(filename)
74.     lines = all_data.readlines()
75.     water_levels = []
76.     date_list = []
77.     for line in lines[1:]:
78.             split = line.split(";")
79.             date = split[0]
80.             try:
81.                 date = datetime.strptime(date, '%Y-%m-
    %d %H:%M:%S')
82.             except ValueError:
83.                 date = datetime.strptime(date, '%Y-%m-
    %d %H:%M')
84.
85.             tam_hai  = float(split[1])
86.             water_levels.append([date, tam_hai])
87.     all_data.close()
88.     return water_levels
89.
90.
91.
92. def calc_level_diff_term_1(row, lagoon_level_1, inlet_area):
93.     """level difference factor calculation"""
94.     level_diff_1 = inlet_area / LAGOON_AREA_1 * math.sqrt(2 * 9.81 /
     FRICTION_1) * ((row[1] - lagoon_level_1)
95.
                / math.sqrt(abs(row[1] - lagoon_level_1)))
96.     return level_diff_1
97.
98.
99.
100. def calc_level_diff_term_2(row, lagoon_level_2):
```

```
101.     """level difference factor calculation"""
102.     level_diff_2 = INLET_2 / LAGOON_AREA_2 * math.sqrt(2 * 9.81 / F
    RICTION_2) * ((row[1] - lagoon_level_2)
103.
                    / math.sqrt(abs(row[1] - lagoon_level_2)))
104.     return level_diff_2
105.
106.
107.
108. def calc_second_lagoon_term(Lagoon_area, lagoon_level_1, lagoon_lev
    el_2):
109.     """calculates the water level in the second, fictive, lagoon"""

110.     if lagoon_level_2 - lagoon_level_1 != 0:
111.         lagoon_term = INLET_3 / Lagoon_area * math.sqrt(2 * 9.81 /
    FRICTION_3) * ((lagoon_level_2 - lagoon_level_1) / math.sqrt(abs(lag
    oon_level_2 - lagoon_level_1)))
112.     else:
113.         lagoon_term = 0
114.     return lagoon_term
115.
116.
117.
118. def calc_river_term(water_level, RIVER_1):
119.     """Calculates the term dependent on the river inflows"""
120.     if water_level[0].month in range(11, 13):
121.         river_term = (RIVER_1/LAGOON_AREA_1)
122.     else:
123.         river_term = 0
124.     return river_term
125.
126.
127.
128. def calculate_lagoon_level(lagoon_level_1, lagoon_level_2, water_le
    vel, RIVER_1, inlet_area=INLET_1):
129.     """formula for calculating the lagoon water levels"""
130.     lagoon_level_2 += TIME_STEP * (calc_level_diff_term_2(water_lev
    el, lagoon_level_2)
131.                                    - calc_second_lagoon_term(LAGOON
    _AREA_2, lagoon_level_1, lagoon_level_2))
132.
133.     lagoon_level_1 += TIME_STEP * (calc_level_diff_term_1(water_lev
    el, lagoon_level_1, inlet_area)
134.                                    + calc_second_lagoon_term(LAGOON
    _AREA_1, lagoon_level_1, lagoon_level_2) + calc_river_term(water_lev
    el, RIVER_1))
135.     return [lagoon_level_1, lagoon_level_2]
136.
137.
138.
139. def calculate_inlet_velocity(lagoon_levels, i, water_level, RIVER_1
    , inlet_area=INLET_1):
140.     """Calculates the inlet velocity for a timestep by using the en
    ergy and volume conservation
141.     equations"""
```

```
    if (lagoon_levels[i][1] - lagoon_levels[i][0]) != 0:
        inlet_velocity = (((lagoon_levels[i + 1][0] - lagoon_levels[i][0]) / TIME_STEP)
                          * (LAGOON_AREA_1 / inlet_area) - (INLET_3 / inlet_area) *
                          math.sqrt(2 * 9.81 / FRICTION_3) *
                          ((lagoon_levels[i][1] - lagoon_levels[i][0]) / math.sqrt(abs((lagoon_levels[i][1] - lagoon_levels[i][0])))) - ((calc_river_term(water_level, RIVER_1) * LAGOON_AREA_1) / inlet_area))
    else:
        inlet_velocity = (((lagoon_levels[i + 1][0] - lagoon_levels[i][0]) / TIME_STEP)
                          * (LAGOON_AREA_1 / inlet_area) - ((calc_river_term(water_level, RIVER_1) * LAGOON_AREA_1) / inlet_area))
    return abs(inlet_velocity)


def calc_inlet_transport(lagoon_levels, i, water_level, RIVER_1, inlet_width=165, inlet_area=INLET_1):
    """ Calculates the inlet transport in m3/s"""
    transp_coeff = 0.8 # Calibrated
    darcy_f = 0.03
    rho_g = 9.81 * 1000
    sed_dens = 2.66
    water_dens = 1
    d_50 = 0.15 * 10 ** (-3)
    d_star = (9.81 * (sed_dens - 1) / 1.002 ** 2 ) ** (1 / 3) * d_50
    shields = (0.3 / (1 + 1.2 * d_star)) + 0.055 * (1 - math.exp(-0.02 * d_star))
    inlet_velocity = calculate_inlet_velocity(lagoon_levels, i, water_level, RIVER_1, inlet_area)
    inlet_transport = (transp_coeff * inlet_velocity * inlet_width / rho_g) * (
        (1000 / 8) * darcy_f * inlet_velocity ** 2 - shields * d_50 * (sed_dens - water_dens))
    return [inlet_transport, inlet_velocity]


def calc_inlet_width(inlet_transport, LST, width):
    """Calculates the inlet width assuming that the inlet downdrift position
    remains fixed. Based on the work of Almir et al. """
    spit_width = 280
    shape_term = (SHAPE ** 2 * TIME_STEP_2 / spit_width)
    inlet_area = (width / SHAPE) ** 2
    if LST >= 0:
        width = math.sqrt((shape_term * (inlet_transport  - abs(LST)) + width ** 2 ))
    return width


```

```
182.
183. def calc_inlet_morphology(longshore_transp, water_level_list, RIVER
    _1):
184.     """Calculates the inlet position and width over time"""
185.     lagoon_level_list = [[water_level_list[1][1], water_level_list[
    1][1]]]
186.     k_alpha = 1 / math.tan(1.8 * math.pi / 180) + 1 / math.tan(2.3
    * math.pi / 180)
187.     spit_area = (1.4 + 6) * 280 * (1 + k_alpha * (6 - 1.4) / (2 * 2
    80))
188.     inlet_pos = 0
189.     inlet_morph_list = []
190.     i = 0
191.     inlet_width = 165
192.     inlet_area = INLET_1
193.     avg_transp = []
194.     inlet_transport_list = []
195.     inlet_velocity_list = []
196.     inlet_sum = 0
197.
198.     for step in water_level_list:
199.         lagoon_levels = calculate_lagoon_level(lagoon_level_list[i]
    [0], lagoon_level_list[i][1], step, RIVER_1, inlet_area)
200.         lagoon_level_list.append(lagoon_levels)
201.         LST = longshore_transp['{:%m-
    %d}'.format(step[0])] / (3 * 3600)
202.         inlet_transport, inlet_velocity = calc_inlet_transport(lago
    on_level_list, i, step, RIVER_1, inlet_width, inlet_area)
203.         inlet_transport_list.append(inlet_transport)
204.         inlet_velocity_list.append(inlet_velocity)
205.         avg_transp.append(abs(inlet_transport))
206.         inlet_sum += abs(inlet_transport)
207.
208.         if i % ((1/(TIME_STEP/3600))* (TIME_STEP_2 / 3600)) == 0:
209.             inlet_transport_1 = stat.median(avg_transp)
210.
211.             if inlet_pos < 980 and LST >= 0:
212.                 inlet_pos += (LST * TIME_STEP_2 / spit_area) - (inl
    et_transport_1 * TIME_STEP_2 / spit_area)
213.             else:
214.                 inlet_pos += 0
215.             if inlet_pos >= 980: # and LST >= 0:
216.                 try:
217.                     inlet_width_1 = calc_inlet_width(inlet_transpor
    t_1, LST, inlet_width)
218.                     if inlet_width_1 > 180:
219.                         inlet_width = inlet_width
220.                     else:
221.                         inlet_width = inlet_width_1
222.                 except ValueError:
223.                     inlet_width = inlet_width
224.             avg_transp = []
225.
226.         i += 1
227.         inlet_area = (inlet_width / SHAPE) ** 2
```

```
228.         inlet_morph_list.append([step[0], inlet_pos, inlet_width, i
    nlet_transport])
229.     print(inlet_sum)
230.     return [inlet_morph_list, lagoon_level_list]
231.
232.
233.
234.
235. def dates_for_plot(water_level_list):
236.     date_list = []
237.     for timestep in water_level_list:
238.         date_list.append(timestep[0])
239.     dates = matplotlib.dates.date2num(date_list)
240.     return dates
241.
242.
243.
244. def plot_model(lagoon_levels, water_level_list_4, water_level_list_
    1, water_level_list_2, water_level_list_3):
245.     """plots the calculated and the measured water levels in the
246.     lagoon"""
247.     hoi_an = []
248.     ocean_level = []
249.     SMS_01_aug = []
250.     SMS_01_nov = []
251.     online_tgr_02 = []
252.     #measured_lagoon_nov = []
253.     #measured_lagoon_aug = []
254.
255.     for minute in lagoon_levels:
256.         hoi_an.append(minute[0])
257.         #lagoon_2.append(minute[1])
258.
259.     for minute in water_level_list_1:
260.         ocean_level.append(minute[1])
261.
262.     for minute in water_level_list_3:
263.         SMS_01_nov.append(minute[1])
264.         #measured_lagoon_aug.append(minute[2])
265.
266.     for minute in water_level_list_2:
267.         SMS_01_aug.append(minute[1])
268.
269.     #for minute in water_level_list_4:
270.         #online_tgr_02.append(minute[1])
271.
272.     dates_1 = dates_for_plot(water_level_list_1)
273.     dates_2 = dates_for_plot(water_level_list_2)
274.     dates_3 = dates_for_plot(water_level_list_3)
275.     dates_4 = dates_for_plot(water_level_list_4)
276.     #plt.figure(2)
277.     plt.plot_date(dates_1, hoi_an[:-
    1], 'tab:blue', label='Calculated lagoon')
278.     plt.plot_date(dates_2, SMS_01_aug, 'cornflowerblue', label='SMS
    01 Aug')
```

```
    plt.plot_date(dates_3, SMS_01_nov, 'blueviolet', label='SMS01 Nov')
    #plt.plot_date(dates_1, ocean_level, 'black', label='Simulated Ocean level Hoi An')

    plt.ylabel('Water level (m)')
    plt.xlabel('Time (date)')
    plt.legend(loc="best")
    plt.show()


def plot_inlet_morphology(inlet_morphology, inlet_migration, channel_migration, downdrift_channel_migration, width_history, RIVER_1):
    """plots the inlet position and width over time from
    the reference position (2019)"""
    dates = []
    position = []
    duy_line = []
    width = []

    pos = 0
    for time in inlet_morphology:
        dates.append(time[0])
        position.append(time[1])
        width.append(time[2])

    i = 0
    while position[i] <= 980 and i <= len(dates)-100:
        pos += 43.33 / (365 * 24 * 6)
        duy_line.append(pos)
        i += 1

    downdrift_side = [i[1]*100 for i in downdrift_channel_migration]
    updrift_side = [i[1]*100 for i in channel_migration]


    plt.subplot(211)
    plt.plot(dates, width)#, label=RIVER_1)
    plt.legend()
    plt.ylabel('Width (m)')
    plt.xlabel('Time (date)')

    plt.subplot(212)
    plt.plot(dates, position)#, label=RIVER_1)
    #if RIVER_1 == 100:
    plt.plot(dates[:len(duy_line)], duy_line, 'grey', label='Duy et al. (2018)')
    plt.legend()
    plt.ylabel('Migrated distance (m)')
    plt.xlabel('Time (date)')
    #plt.show()


```

```
329.
330.
331.def group_as_months(inlet_morphology):
332.    """Sums the inlet sediment transport accumulated accross all ye
    ars"""
333.    date_dict = {}
334.    i=0
335.    for line in inlet_morphology:
336.        if line[0] in date_dict:
337.            date_dict[line[0]].append((line[3] * TIME_STEP))
338.        else:
339.            date_dict[line[0]] = [(line[3] * TIME_STEP)]
340.        i += 1
341.    newdict = defaultdict(lambda: [])
342.    for key in sorted(date_dict):
343.        newdict[(key.month)][:] += date_dict[key][:]
344.    return newdict
345.
346.
347.
348.def plot_lst_vs_inlet(lst, inlet_morphology):
349.    """Plots the accumulated monthly average lst and inlet transpor
    t"""
350.    print('It has begun!')
351.    monthly_inlet = group_as_months(inlet_morphology)
352.    for key in monthly_inlet.keys():
353.        monthly_inlet[key] = sum([abs(i) for i in monthly_inlet[key
    ]] ) / 29
354.    montly_inlet_list = [*zip(*monthly_inlet.items())]
355.    lst_list = [*zip(*lst.items())]
356.    N = 12
357.    fig, ax = plt.subplots()
358.    ind = numpy.arange(N)    # the x locations for the groups
359.    width = 0.35         # the width of the bars
360.    p1 = ax.bar(ind, lst_list[1], width)
361.    p2 = ax.bar(ind + width, montly_inlet_list[1], width)
362.
363.    ax.set_xticks(ind + width / 2)
364.    ax.set_xticklabels(('Jan', 'Feb', 'Mar', 'Apr', 'May', 'Jun', '
    Jul', 'Aug', 'Sep', 'Oct', 'Nov', 'Dec'))
365.    ax.legend((p1[0], p2[0]), ('m_L', 'm_I'))
366.    ax.ylabel('m3')
367.    ax.autoscale_view()
368.    plt.show()
369.
370.
371.
372.def main():
373.    import time
374.
375.    t0 = time.time()
376.    filename_1 = "TIDAL LEVEL 2020-2049_10min_interpolate.csv"
377.    water_level_list_1 = read_records_from_file(filename_1)
378.
379.    three_h_avg_lst, monthly_lst = lst_main()
```

```
    RIVER_1 = 0
    inlet_morphology_1, lagoon_levels_1 = calc_inlet_morphology(three_h_avg_lst, water_level_list_1, RIVER_1)
    plot_inlet_morphology(inlet_morphology_1, RIVER_1)
    plt.show()
    #plot_lst_vs_inlet(monthly_lst, inlet_morphology)
    #plot_model(lagoon_levels_1, water_level_list_4, water_level_list_1, water_level_list_2, water_level_list_3)

    t1 = time.time()

    total = t1-t0
    print(total)

main()
```